Calibration Under Uncertainty for Finite Element Models of Masonry Monuments

Mode 5 elevation.
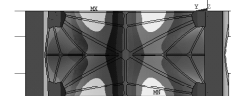
Mode 5 plan view.

(a) Mode 5 Correlation

Edited by Hector Hinojosa, Group IRM-CAS.

About the Cover:
The figures on the cover illustrate three aspects of the validation of a computational model developed to predict the vibration response of historic masonry monuments. Top right: The National Cathedral, Washington, DC, where vibration response of vaults is experimentally measured to assess the effect of structural damage. The measurements provide acceleration time series used to verify and validate predictions of the numerical simulation. Top left: The computational finite element model is shown to illustrate the mesh discretization of a vault. The model is analyzed to simulate the vibration response. Colors represent different material properties whose uncertainties are propagated through the calculation. Bottom: The measurement of a vibration mode shape of the structure (solid line) is compared to the prediction of the finite element model (dashed line). Crosses illustrate the uncertainty of predictions due to variability of the boundary conditions and material properties. Statistical tests are implemented to quantify the accuracy of the finite element model, given measurement variability and prediction uncertainty.

Calibration Under Uncertainty for Finite Element Models of Masonry

Sezer Atamturktur*
François Hemez
Cetin Unal

* Clemson University, Civil Engineering Department, 110 Lowry Hall, Clemson,
  South Carolina 29634-0911

Los Alamos
NATIONAL LABORATORY
— EST.1943 —

Contents

List of Figures

List of Tables

List of Acronyms

ANOVA   analysis of variance
DR   Douglas-Reid
EMA   experimental modal analysis
ERA   eigensystem realization algorithm
FE   finite element
FFT   Fast Fourier Transform
FRF   frequency response function
FRP   fiber-reinforced polymers
GCI   grid convergence index
GPM   Gaussian process model
IEM   Inverse Eigensensitivity Method
LSCE   least squares complex exponential
MAC   Model Assurance Criteria
MCMC   Markov Chain Monte Carlo
PIRT   Phenomenon Identification and Ranking Table

x

CALIBRATION UNDER UNCERTAINTY FOR FINITE ELEMENT MODELS OF MASONRY MONUMENTS

by

Sezer Atamturktur,[1] François Hemez,[2]
Cetin Unal[3]

ABSTRACT

Historical unreinforced masonry buildings often include features such as load bearing unreinforced masonry vaults and their supporting framework of piers, fill, buttresses, and walls. The masonry vaults of such buildings are among the most vulnerable structural components and certainly among the most challenging to analyze. The versatility of finite element (FE) analyses in incorporating various constitutive laws, as well as practically all geometric configurations, has resulted in the widespread use of the FE method for the analysis of complex unreinforced masonry structures over the last three decades. However, an FE model is only as accurate as its input parameters, and there are two fundamental challenges while defining FE model input parameters: (1) material properties and (2) support conditions. The difficulties in defining these two aspects of the FE model arise from the lack of knowledge in the common engineering understanding of masonry behavior. As a result, engineers are unable to define these FE model input parameters with certainty, and, inevitably, uncertainties are introduced to the FE model.

As the complexity of the building increases, as is the case for historical unreinforced masonry buildings, the errors and uncertainties in the analysis also increase. In the presence of high and numerous uncertainties originating from multiple sources, deterministic approaches in which parameters are defined as constant values assumed to be known with certainty cannot be implemented reliably. Probabilistic methods, however, provide a rigorous and rational means in treating the uncertainty present in the FE analysis of historical unreinforced masonry buildings. The way in which uncertainty in

---

[1] Assistant Professor, Civil Engineering Department. Mailing: Clemson University, Civil Engineering Department, 110 Lowry Hall, Box 340911, Clemson, South Carolina 29634-0911. Phone: 864-656-3000. Fax: 864-656-2670. E-mail: sez@clemson.edu. Currently, long-term visiting faculty staff member at the Los Alamos National Laboratory, Los Alamos, New Mexico 87545.

[2] Technical Staff Member in X-Division. Mailing: Los Alamos National Laboratory, XCP-1, Mail Stop F644, Los Alamos, New Mexico 87545. Phone: 505-667-4631. Fax: 505-667-3726. E-mail: hemez@lanl.gov. Manager of the verification project element of the Verification and Validation program for Advanced Scientific Computing.

[3] Technical Staff Member in CCS-Division. Manager of the Nuclear Energy Advanced Modeling and Simulation program for fuels modeling. Mailing: Los Alamos National Laboratory, CCS-DO, Mail Stop B297, Los Alamos, New Mexico 87545. Phone: 505-665-2539. Fax: 505-665-0120. E-mail: cu@lanl.gov.

historical unreinforced masonry construction is treated is one of the novel and main contributions of this dissertation.

While building FE models, sometimes it is advantageous to model only a smaller portion of a larger structure. This substructure modeling approach not only reduces the computational time of FE analysis but also reduces required preliminary work for the model development. In this dissertation, substructure FE models of vaulted sections of two Gothic churches are calibrated using a Bayesian statistics-based procedure against physical evidence collected through experimental modal analysis. During calibration both the FE calculations and experimental measurements are treated probabilistically. The probabilistic nature of the FE calculations stems from the fact that several FE model parameters, which are determined to introduce significant analysis uncertainty, are treated probabilistically. The probabilistic nature of experimental measurements stems from the fact that a large number of repeated experiments are compiled to determine experimental uncertainty. The fact that uncertainty in both numerical calculations and experimental measurements are accounted for is one of the novelties of this dissertation. The modal parameters measured on the vault are statistically compared to the predictions of the FE model during calibration. According to the automated Bayesian statistics-based calibration procedure, the posterior distributions for the appropriately selected calibration parameters, such as modulus of elasticity of the vault material and support spring constants of the vaults, are obtained. This stochastic procedure is applied to the substructure FE models of the choir vaults of the National Cathedral, Washington, DC, and to the nave vaults of Beverley Minster, Beverley, UK.

Chapter 1

INTRODUCTION

A computer lets you make more mistakes faster than any invention in human history—with the possible exceptions of handguns and tequila.

Mitch Radcliffe

1.1 Introduction to the Problem

Growing interest in the preservation of architectural heritage has created a need for tools capable of reliably analyzing unreinforced masonry structures. The versatility of finite element (FE) analyses in incorporating various constitutive laws, as well as practically all geometric configurations, has made the FE analysis a more generally applicable method for masonry systems compared to graphical or semigraphical analysis methods initially proposed by Heyman (1966). Over the last three decades, FE methods became a widely applied tool for the analysis of unreinforced masonry structures. However, the success of the FE model depends on the accuracy of its input parameters.

As the complexity of the problem increases, as is the case for historic masonry structures, the ability to fully incorporate the physical reality in the FE model decreases. The difficulties routinely faced during the FE model development of unreinforced masonry structures are primarily in obtaining physical dimensions and material properties. While defining these two aspects, uncertainty and error arise from numerous sources:

- Aside from natural variability between masonry units, the variable and time-dependent properties of mortar add uncertainty to the analysis. Even in cases where material coupons or spare stone units can be obtained from the structure, the limited number of tests provides statistically insignificant information. Even when these tests are considered representative, the properties of stone units alone are not sufficient to define the material behavior, as the behavior of masonry heavily relies on mortar properties (De Stefano 2007).
- Determining material properties of mortar is also problematic because extraction of an intact mortar specimen from an existing structure is a very challenging task. On the other hand, tests to measure mortar properties of young laboratory mortar specimens yield unrealistic results due to the age-dependent hardening of mortar.

- The mechanical properties of a homogenized masonry assembly are strictly anisotropic due to the presence of mortar joints. However, these anisotropic material properties are difficult to determine due to the highly variable mortar joint thickness, hidden material defects, nonuniform dimensions of the stone units, and irregular layout of units and joints.

- The interior constitution of masonry construction, especially historic construction, often includes empty or roughly filled volumes and material discontinuity. Although an inspection of the interior constitution may be possible through thermal- or radar-based methods, incorporating this information into an FE model is not straightforward.

- The geometry of masonry construction is almost always imperfect, even when built in laboratory conditions; for an example see the arch specimen of Ramos (2007). Moreover, the out-of-plane rotation of vertical members due to lateral loads, the flattening of arches and vaults due to the formation of cracks, and the geometric deformation due to the movement of supports induce further variability to the geometry of these structures. Typically, in the FE analysis, the geometry is idealized. This aspect unavoidably introduces uncertainties in the analysis.

- The environmental conditions, such as temperature, are known to affect the behavior of masonry structures. Ramos (2007) noted another very important but less obvious environmental factor: the effect of moisture on a masonry system. Absorbed moisture increases the mass of stone units and reduces the stiffness of mortar joints. As a results, an increase in moisture results in a decrease in natural frequencies. As seen, environmental effects must be included in the analysis. However, unless the FE analysis incorporates probabilistic methods, it is difficult to include environmental variability.

- Effects of accumulated structural damage and past repairs or interventions on a historic masonry structure are often poorly documented. These aspects increase the number of unknown factors and, likewise, increase the complexity of FE modeling.

- The effect of workmanship on the masonry structural behavior is known to be an important factor. However, it is very difficult to quantify the effects of this factor for a large-scale historic structure and even more difficult to incorporate in the FE model.

To reduce the problem to a manageable size, it is crucial to establish appropriate assumptions and simplifications for each of these aspects related to the material behavior and physical geometry of masonry construction. Moreover, further uncertainties are introduced to the analysis while representing the support conditions in the FE model due to the complicated soil-structure interaction at the base of the structure. Accurate boundary condition representation also becomes a problem when the FE model is built to analyze a substructure of the entire system. Substructure modeling is feasible when (1) structural analysis is necessary only for a small portion of a larger structure, for instance, when analyzing one of the spans of a multispan system (Brencich and Sabia 2008), (2) the structure of interest has a complex interaction with an adjacent structure which is not

of interest, for instance, when analyzing a tower that has a common wall with an adjacent building (Gentile and Saisi 2007, Bayraktar et al. 2008, and Júlio et al. 2008), or (3) the structure has self-repetitive components, in which analysis of one will be sufficient, for instance, when analyzing a church with multiple nominally identical vaults (Erdogmus 2004 and Atamturktur 2006).

When building a substructure model, boundary conditions between components involve factors depending on contact pressure, surface friction, existing cracks, and load path, as well as the elastic behavior of each masonry unit and mortar. However, the connectivity options in general-purpose FE packages typically include translational and rotational restraints without providing any options to implement the more complex underlying physics such as joint friction, inelastic deformation, rigid body motion, etc. On the other hand, an attempt to include these relevant physical phenomena further complicates the problem due to the unknown parameters of these phenomena. For macro-models, this additional complication is hardly justified. Thus, implementing the admittedly approximate boundary conditions available in the FE package still remains the option commonly selected by the engineer.

Many similar instances routinely experienced during FE model development of an existing masonry system limit the analysis capabilities to represent the physical reality. As a result, the burden of appropriate implementation of FE tools lies entirely on the skill and intuition of the engineer. When called upon to analyze an existing masonry structure, engineers are also confronted with a lack of analysis guidelines. Therefore, engineers are forced to choose an FE model, which, according to their best engineering judgment, will yield satisfactory results. An example of this common confusion regarding masonry behavior was recently reported subsequent to the Catoctin Creek Aqueduct elliptical arch restoration. The consulting engineers reported that the numerical model resulted in unrealistically high stresses within the stone arch (Biemiller 2006). When developing masonry structure FE models, particularly for historic structures, there are numerous opportunities to misinterpret the actual system, to build an unsuitable model, and to obtain erroneous solutions.

Over the last three decades, progress has been made in correlating FE solutions with physical evidence for civil structures with corresponding measurements (i.e., bridges, frame buildings, towers, stadiums, etc.), a procedure commonly known as model correlation. As the need for structural assessment of historic buildings increased, the model correlation concept has been applied to the masonry structure analysis such as masonry towers (e.g., bell towers, minarets), buildings (e.g., residential, public), and monuments (e.g., churches, mosques, basilicas, arch bridges,). Typically, when the FE solutions compare favorably with the corresponding measurements, this is accepted as a sign of accuracy of the model. However, if the comparison does not yield an acceptable match, the discrepancy is attributed to the deficiencies in the model due either to imprecise model parameters or to erroneous modeling decisions.

Following the advancements in model correlation, researchers in other fields investigated the use of physical evidence to reduce FE model deficiencies, a process commonly known as model calibration. During the calibration process uncertain parameters are either manually or automatically adjusted until the resulting FE model reproduces acceptable agreement with the physical evidence. In this context, physical

evidence is obtained through experimental measurements that are relevant to the identified deficiencies in the model. The relevancy of physical evidence to the model deficiencies is typically decided based on engineering judgment.

Calibration of masonry structure FE models requires considerations about the large uncertainty in masonry construction. This topic has not been fully addressed in the pertinent literature. To address this topic, this dissertation brings together the aspects of model calibration under uncertainty and outlines a probabilistic framework applicable to historic masonry structures. The study ultimately aims to obtain calibrated FE models with calculated uncertainty bounds on the input parameters. Such models will provide engineers the ability to predict masonry monument structural behavior with increased confidence where experimental technology is not readily available.

1.2 Problem Statement and Objectives

This study formulates a Bayesian calibration approach suitable for complex vaulted historic masonry structures and probabilistically characterizes the poorly known FE model input parameters. The choice of the structure type is motivated by the high uncertainties associated with historic masonry systems as discussed in the previous section. The procedure outlined below may ultimately be applied to analysis of other civil engineering structures with high parameter uncertainties originating from numerous sources. Specific objectives of the study are outlined below:

Objective 1: Develop FE Models of a Historic Masonry Structure. A model intended for calibration must be parameterized appropriately. The first objective is to present an FE modeling approach suitable for calibration activities.

The FE models in this study are developed based on observed geometry and construction of the selected case study structure. The models are representations of a substructure of the overall building and they include the ribs and webbing of a masonry vault, the adjacent nave walls, and the fill. The boundary conditions, representing the structural interaction between the modeled elements and those that are excluded from the model, are to be abbreviated in the FE model. The boundary conditions that are difficult to represent through fixed or hinged connections are defined with linear elastic springs. This study is devoted to the determination of appropriate boundary conditions and material property values to be used in analysis.

Objective 2: Conduct *In Situ* Calibration Experiments of Historic Masonry Structures. Inherent in their definition, calibration experiments are tied to the deficiencies in the FE model. As the aim of this study is to improve the quality of the FE model by calibrating parameters that are directly related to the stiffness and mass distribution in the system, nondestructive dynamic test results are used to obtain relevant physical evidence. This study devotes attention to the particular aspects of dynamic testing as applied to complex vaulted masonry monuments.

Objective 3: Calibrate the FE Models of Historic Masonry Structures Based on *In Situ* Dynamic Measurements. The spring constant and material property values, parameterized in Objective 1, are poorly known; therefore, they are calibrated with the

help of physical evidence, obtained in Objective 2. The calibration procedure implemented in this study goes beyond a deterministic method that ignores the presence of uncertainty to one that relies on the definition and propagation of parameter uncertainty. With this step, an improved, quantitative knowledge is gained about the material property values for each structural component, as well as about the restraining forces applied by adjacent components to each other, for instance, from buttresses to the nave walls.

Objective 4: Validate the Calibrated Model Parameters. The aim of this objective is to validate the results of the calibration study. In the absence of refined knowledge about the material properties, the probability distributions of the material property values obtained through calibration in Objective 3 cannot be validated. However, it is possible to estimate the boundary condition spring constants by modeling the remainder of the structure and to judge the acceptability of the calibration exercise completed in Objective 3.

1.3 Research Hypothesis

This study starts with the hypothesis that the FE solutions to predict phenomena of interest (A, in Figure 1-1) can be improved by calibrating the appropriately selected model parameters according to the physical evidence that is provided by experimental measurements (B, in Figure 1-1). When the calibration is completed, a separate and independent information set can be used to judge the calibrated model (C, in Figure 1-1).

1.4 Model Verification, Validation, and Calibration

Also of far-reaching importance is defining model calibration in a larger context and emphasizing its role in relation to model verification and validation. The terms calibration, validation, and verification are used interchangeably in the literature, hindering the adequate communication of these principles. To provide clarity, this section describes what model calibration is and is not. For this clarification, the factors to which the accuracy of the FE solutions is dependent are listed below:

a) the adequacy of the governing equations involved in the analysis, i.e., mathematical definitions for dynamic behavior of shells,

b) the precision of numerical solution, i.e., fineness of discretization,

c) the accuracy of the physical parameters, i.e., values for material properties and definitions for boundary conditions, and

d) the adequacy of the constitutive element models, i.e., assuming linearity only when the response is predominantly linear.
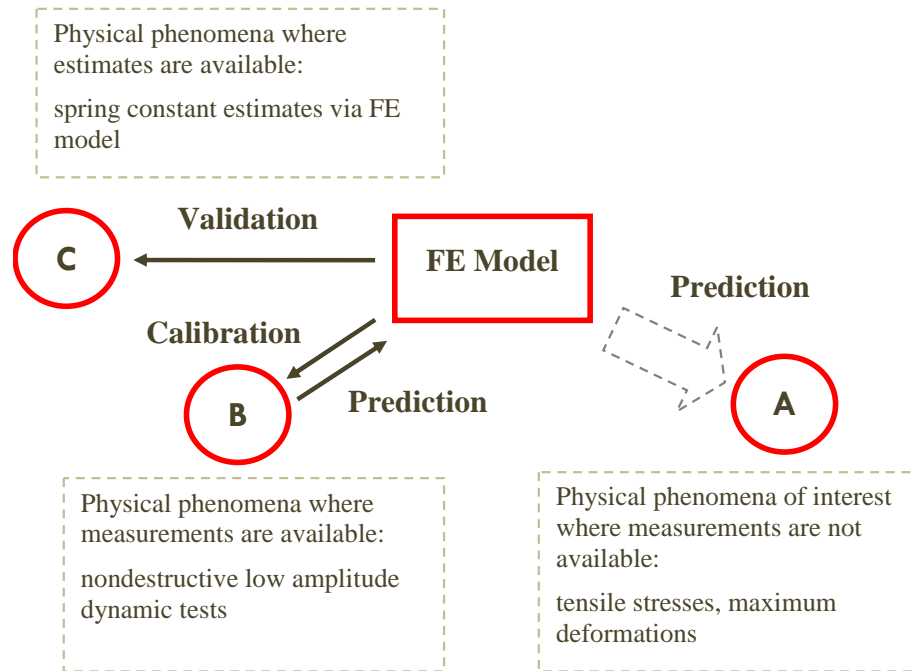
Figure 1-1: Calibration of the imprecise input parameter of the numerical model by the use of comparative features.

The first two factors are purely mathematical and are the topic of model verification. As Roache (1998) states, model verification aims to answer the question: "Are we solving the equations right?" When disagreement between model predictions and measurements are believed to be the result of inadequate mathematical representation or imprecise numerical solution, verification activities must be initiated. Verification is a prerequisite to validation activities. Although the crucial role of verification is acknowledged, only a very limited attention is paid to the verification procedures in this dissertation.

The last two factors are based on physical phenomena and the assessment relates to the model validation. According to Roache's definition, model validation aims to answer the question: "Are we solving the right equations?" When an FE analysis reproduces a match to a set of physical evidence, the model is typically considered validated. However, when there is disagreement between model predictions and physical evidence, the numerical model can be calibrated as discussed earlier. When the first set of physical evidence is used to calibrate a model, a separate and independent set of physical evidence must be gained to validate the FE model. Therefore, calibration can be considered as a subcomponent of validation. An extensive discussion about the semantics of verification and validation has been provided by Trucano et al. (2006).

1.5 Scope of the Research

This study is confined to linearly elastic analyses based on the FE method. This is a necessary step that needs to be successfully completed before nonlinear and inelastic characteristics of masonry can be incorporated into an FE analysis.

The study will be accomplished through investigation of records of an experimental program and simulations of a monumental, unreinforced masonry building: The National Cathedral (Washington, DC, USA). This building contains characteristics of stone masonry monuments, e.g., piers, walls, buttresses, and vaults.

Chapter 2

LITERATURE REVIEW

Papers focused on building vaults tend to be more general, more conjectural, and have less opportunity to introduce positive confirming evidence (although several redundant masonry bridges have been available for destructive testing, one hardly expects to see testing of redundant cathedrals).

Thomas E. Boothby

2.1 Introduction

In the early 1980s, computer-based finite element (FE) methods were first seriously applied to the analysis of masonry structures. Because an FE model is only as accurate as its input parameters, questions regarding the validity of the FE solution were immediately raised. Mark (1982) initiated one of the earliest efforts to validate masonry structure behavior predictions. In Mark's studies, photoelastic tests on small-scale plastic samples of Gothic vaults were conducted to identify internal stress distributions under wind load (Figure 2-1). These internal, scaled stresses were compared to the FE model predictions to confirm the applicability of the FE analysis. Although the adapted test technique was primarily limited to wind loads, Mark's early studies illustrated the accuracy concerns of historic masonry monument FE analysis.

Today, the application of the FE method to various structural analysis problems has been widely accepted. Commercially available FE software delivers accurate analyses that are limited by the accuracy of the user-defined inputs. However, the current challenge is in implementing physically substantiated input parameters for the analysis. For typical masonry structures, FE model inaccuracies primarily arise when defining the complicated boundary conditions between structural components and the complex mechanical behavior of masonry and mortar assemblies. To remedy these FE model inaccuracies, researchers have devoted decades of consistent attention to model calibration. This chapter provides a review of the extent of these prior studies' success and identifies the remaining technical challenges.
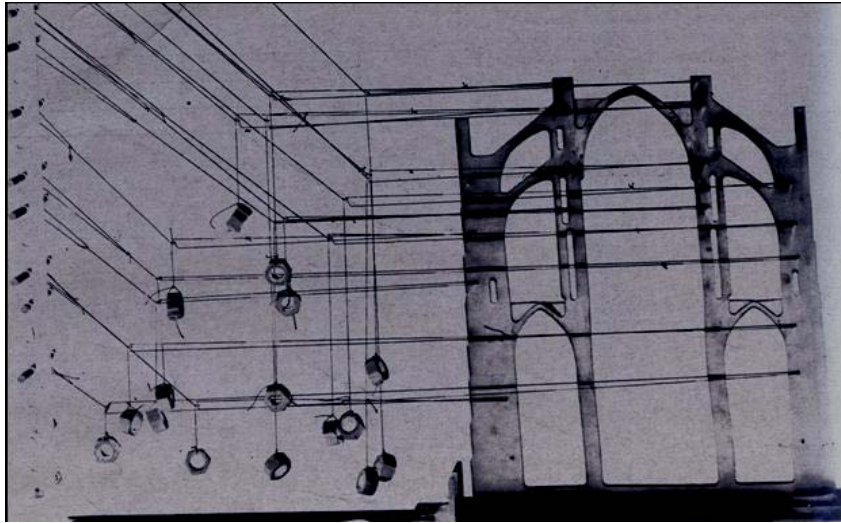
Figure 2-1: Mark's photoelastic studies on two-dimensional scaled models, reprinted from Mark (1984), with permission.

The earliest efforts discussed in Section 2.2 date back to the 1980s and range from qualitative visual comparisons based on field observations to quantitative comparisons of static tests. In Section 2.3, studies that extend model correlation to a calibration stage are discussed. Because the available literature addressing this topic is observed to implement *in situ* dynamic testing, it is necessary to highlight the characteristic behavior of masonry structures and review some of the previous work on dynamic testing of such structures. The second half of Section 2.3 provides a discussion of FE model calibration as applied to masonry structures in the context of linear dynamics. These studies are categorized by the sophistication of computational calibration methodology. The first to be discussed are studies comprised of manual parameter value adjustment. Automated procedures, based on optimization techniques and Bayesian inference, are discussed next. Many studies discussed in Section 2.3 follow a deterministic approach in that model parameters are assumed to be known with certainty and repeated experiments yield identical results. In Section 2.4, attention is given to stochastic calibration procedures that incorporate uncertainty in the calibration process by treating the input parameters of an FE model, as well as its output response, probabilistically.

2.2 Model Correlation

Several studies have been conducted with the purpose of comparing FE analysis predictions with visual, on-site observation or static experimental measurements. These studies provide a valuable resource, as they allow observation of static procedure advantages and disadvantages for the purposes of FE model correlation and calibration.

2.2.1 Visual Methods for Model Correlation

The earliest model correlation effort applied to masonry monuments was the visual comparison of crack locations to analytical estimates of the tensile zones. Mark and Hutchinson (1986) compared the available information on the existing cracks of the Roman Pantheon against the tension region predictions of several alternative FE models. Based on this comparison, the suitability of various modeling strategies was investigated (i.e., modeling of the hemispherical dome with and without the walls). Mark and Hutchinson eventually used the model to understand the cathedral's structural behavior under earthquake excitation. A similar work was completed for the simplified structural model of a historic cathedral (Ricart-Nouel 1991). These methods incorporated the visual inspections of existing cracks that are concentrated at a few locations in a historic masonry building. This visual approach is of limited effectiveness and is susceptible to significant error, especially when differential support settlements or long-term creep are present in the structure.

2.2.2 Static Methods of Correlation

For some structure types, the problems associated with visual methods have been remedied by destructive and nondestructive tests focusing on stress, strain, or deflection under controlled loading. For instance, Fanning and Boothby (2001) experimentally investigated the behavior of three masonry arch bridges under truck loading. The simplified analytical bridge models yielded reasonable agreement with the field test data. Based on this correlated analytical model, the authors provided guidance in the FE model development for such bridges—particularly in the selection of material properties and definition of abutment stiffness. In another stone arch bridge study (Fanning et al. 2005), service and high load level tests were used to establish the suitability of the authors' nonlinear FE modeling procedure for the given loading conditions. These methods, based on *in situ* strain or deflection measurements, were successful when applied to masonry bridges, however, the methods are impractical for larger masonry structures such as masonry cathedrals, due to the difficulty in sufficiently loading the structure to achieve a detectable response. Also, destructive tests on a historic cathedral will never be permitted for research purposes.

Due to the technical infeasibility of obtaining a detectable response from monumental structures such as churches, cathedrals, and state and municipal buildings, several researchers have attempted to examine the static behavior of such systems through scaled laboratory models. These studies typically compare measured strain, deformation, and ultimate strength of the test scaled model to those of FE model predictions. Creazza et al. (2001) investigated the three-dimensional behavior of a masonry barrel vault laboratory scaled model reinforced with fiber-reinforced polymers (FRP), both in the intrados and extrados. In the FE model, the authors treated the masonry as a homogenized material and simulated the FRP strips through an elastic

constitutive law. A barrel vault scaled model was tested to failure under a vertical quasi-static load located around the quarter span. The load was increased until the vault formed an unstable mechanism. The measured displacement and the failure load were compared with the FE model predictions to confirm the applicability of the developed damage model.

A very similar study with the same purpose was repeated a year later on a masonry, ribbed cross-vault scaled model and a masonry, barrel-vault scaled model by Creazza et al. (2002). This study focused on the locations and magnitudes of maximum strain and deformations as well as on the characteristics of the collapse mechanism under slowly increasing static load. A parallel approach was adapted by Theodossopoulos et al. (2003) to investigate the behavior of the cross-vaults through static tests conducted on wood scaled models representing an aisle vault of the partially collapsed Abbey Church of Holyrood in Edinburgh (Figure 2-2). The strains and displacements under gravity loading were recorded, and the failure mechanism due to progressive abutment movement was identified. The FE solutions of the deformations and of the collapse mechanism agreed with the experimental observations. In another study, Boothby et al. (2005) investigated the spandrel wall collapse of masonry arch bridges through a half-scale model. The experimental results compared favorably with those of the FE model. Accordingly, inferences have been made about the masonry arch FE modeling. The scaled model tests, when combined with FE predictions, have the potential to illustrate the behavior of the structures for load regimes that usually cannot be tested in real life—for instance, for collapse mechanisms. However, the scaled test models represent only a portion of the model, and thus have the drawback of excluding the actual elastic restraint exerted by adjacent elements, or boundary conditions. Accordingly, the alternative load paths within the structure are also absent from the analysis.
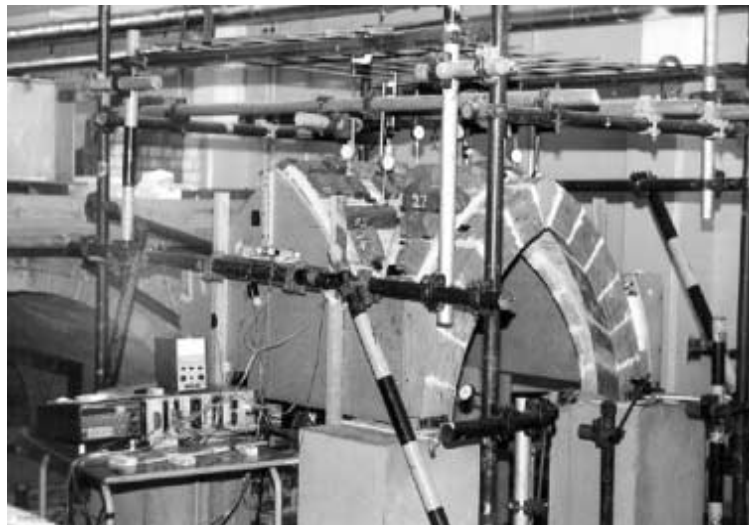
Figure 2-2: The dead load experiments conducted on the wood-mortar assembly, reprinted from Theodossopoulos et al. (2003), with permission.

2.3 Deterministic Model Calibration

This section highlights efforts in model calibration for FE models of masonry structures. The studies that will be discussed in this section invariably implement non-destructive dynamic testing as physical evidence. Because of the widespread application of dynamic testing, it is necessary to emphasize unique characteristics of masonry structures under dynamic loading. For this, an overview of solely experimental studies is first provided. Next, successful applications of deterministic calibration are presented.

2.3.1 Dynamic Tests

As a result of an extensive experimental program conducted on a series of Gothic cathedrals, Atamturktur et al. (2009a) discussed the practical issues related to the testing of monumental masonry structures. The authors emphasized that the connectivity of two masonry walls involves factors depending on the contact pressure, surface friction, and existing cracks, as well as the mechanical behavior of each stone unit and mortar joint. The interaction of these factors typically yields a rather flexible connection between structural components and allows local modes to be more pronounced relative to global modes. As a result, the structural component connectivity and load distribution are affected by the amplitude and location of the excitation. This aspect has also been noted by Sortis et al. (2005). Additionally, high dissipative forces in a masonry assembly make identification of low-amplitude dynamic features difficult.

Moreover, masonry is nonlinear and inelastic in the sense of its stress-strain law, and the assembly of mortar and masonry units is inhomogeneous due to the mortar joints. Thus, masonry tests the limits of the basic assumptions established for standard modal testing. Despite these challenges, it is possible to obtain highly coherent, reliable measurements from masonry structures. This section will highlight several successful experimental programs. Environmental conditions, such as temperature and moisture, also have an effect on the dynamic properties of masonry structures. Ramos (2007) presented the results from long-term monitoring of an ancient monastery and reported an average 6% variation in frequencies due to annual temperature fluctuations. Also, the absorbed moisture increased the mass of the stone units and reduced the stiffness of the mortar joints. During his studies on a masonry clock tower, Ramos reported a 4% reduction in the natural frequencies of a clock tower with the beginning of the rainy season.

Generally, experiments in controlled laboratory settings are largely immune from additional complications caused by support settlements, environmental loads, material deterioration, prior damage, or operational conditions. This is why laboratory experiments yield higher-quality measurements and clearer results than experiments conducted on existing masonry structures. However, only by extending the laboratory tests to existing structures can practical difficulties be incorporated and a realistic view be

gained. In this section, the laboratory studies will be discussed first, while studies investigating the behavior of existing structures will follow.

2.3.1.1 Scaled Laboratory Models

The literature concerned with damage detection and structural health monitoring has also provided a rich experimental background which is beneficial to model calibration studies. For instance, to investigate the spandrel wall separation, Armstrong et al. (1995a) tested two brick masonry arch bridge scaled models by impact hammer excitation. The authors were able to relate the deviations between natural frequencies and the mode shapes to the structural condition of the arch bridges. Armstrong et al. (1995b) also compared the dynamic stiffness of the structurally sound and defective scaled models to detect spandrel wall separation. Both of these studies concluded that dynamic experiments can be used for integrity assessment of existing masonry arch bridges, specifically for spandrel wall separation. However, the authors stressed the necessity to investigate the effects of a wider range of structural defects on the arch bridge dynamic characteristics. Bensalem et al. (1995 and 1997) investigated the dynamic response of brick arch scaled models using both hammer and shaker excitation. Through these dynamic tests, Bensalem et al. (1999) focused on detecting void presence and size in the arch bridge backfill. By observing the difference in the peak amplitudes of the frequency response functions, the authors were able to identify the presence of backfill voids.

Scaled masonry building laboratory models have also been a popular research subject. In 1996, Vestroni et al. completed experiments on a one-fifth-scale masonry building with a mechanical vibration exciter. First, the scaled model dynamic characteristics were investigated by inducing small amplitude vibrations. When the baseline modal parameters were obtained, forces with successively increased amplitudes were applied to the scaled model to induce structural damage. A reduction in the dynamic stiffness due to structural damage was observed through dynamic measurements. In 2000, Zembaty and Kowalski completed a shaker table experiment on a half-scale, two-story brick masonry building by using harmonic excitation and time-varying seismic excitation. The authors were able to identify eight clear modes by the harmonic excitation technique and only the first three modes through the seismic excitation technique. The variations in the modal parameters obtained by two different excitation sources are explained by the presence of large numbers of closely spaced modes, in other words, the characteristically high modal density of typical masonry structures.

Ramos et al. (2005) had success in establishing the relationship between damage and natural frequencies during his study on a full-scale masonry building scaled model built of rubble stone. Increasing numbers of cracks were induced by shaking tests (Figure 2-3). Modal identification, through operational modal analysis, was performed at each damage state and it revealed consistently decreasing natural frequencies as the damage level increased. However, a direct relationship between the crack patterns and dynamic response was not evident.
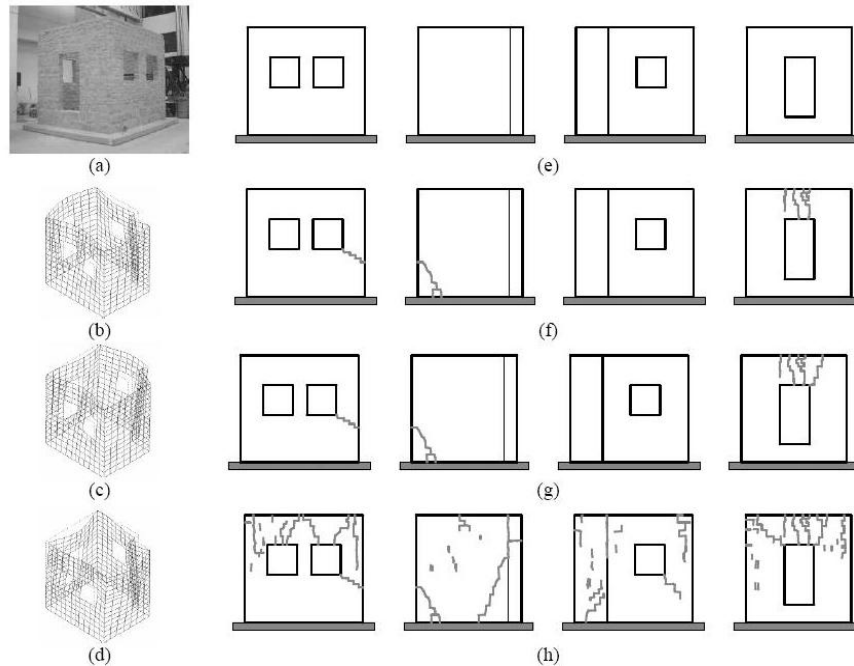
Figure 2-3: Masonry building evaluated at increasing damage levels: (a) general view; (b), (c), and (d) the first three mode shapes; (e) reference and damage scenario A; (f) damage scenario B; (g) damage scenario C; and (h) damage scenario D, reprinted from Ramos (2007), with permission.

In 2007, Ramos conducted a similar study on a replicate ancient masonry arch and wall. The scaled model was built with clay bricks of low compressive strength and mortar with poor mechanical properties to represent the typical material present in historic construction. Cracks were progressively induced in the scaled models through controlled static tests. In between these tests, operational modal analysis was performed to identify the modal parameters. Consecutive static tests indicated a clear loss of stiffness after the first crack. Natural frequencies and mode shapes provided evidence in agreement with the damage in the system. Ramos noted that the natural frequencies were significantly reduced while damping coefficients were significantly increased after damage. He also noted that the mode shapes generally remain unchanged before and after the damage.

2.3.1.2 Existing Structures

Slastan and Foissnerr (1995) measured the dynamic characteristics of several masonry residential buildings under ambient vibration and compared the dynamic characteristics of low- and high-rise masonry structures. The dynamic behavior of an old masonry building was investigated by Genovese and Vestroni (1998). Small-amplitude,

forced oscillations were used to excite the structure and the acceleration response of the building was recorded. The frequency response functions (FRFs) obtained at increasing excitation levels were compared to investigate the nonlinear characteristics of the masonry structure. Similar to their earlier study in the laboratory (Vestroni et al. 1996), the authors observed a reduction in the stiffness of the structure under increased force levels. Sigmund and Herman (1998) completed a similar study on historic masonry buildings, investigating the effects of different levels of excitation sources on the vibration response. The authors concluded that monitoring the dynamic characteristics has the potential to indicate the structural integrity.

Ellis (1998) completed a vibration-based damage detection study on 534 stone pinnacles of the Palace of Westminster in London. The author adapted both traditional modal analysis techniques using an impact exciter and operational modal analysis techniques exploiting the wind forces as an exciter. The fundamental natural frequencies of the pinnacles were measured and compared to each other. The pinnacles with an outlier fundamental frequency were identified as damaged pinnacles (Figure 2-4).
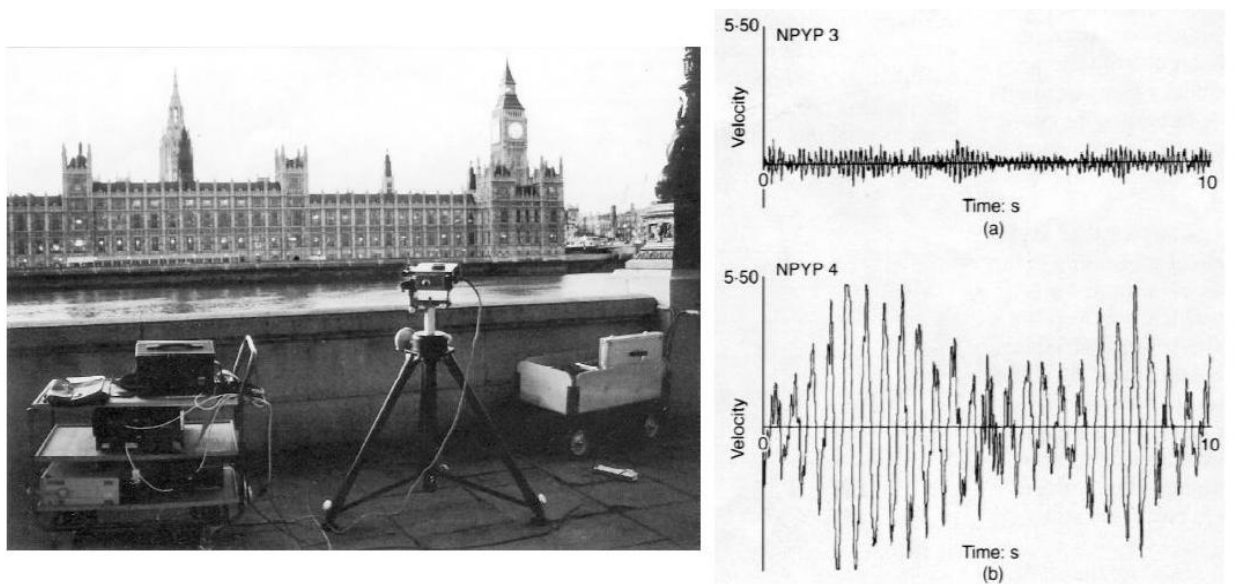
Figure 2-4: Laser-monitoring and velocity record of (a) undamaged, (b) damaged pinnacle, reprinted from Ellis (1998), with permission.

Zonta (2000) conducted an experimental program on a Roman amphitheatre which had been experiencing structural problems due to aging and material deterioration. The elliptical amphitheatre consists of a modular system divided by radial walls (Figure 2-5). Modal testing on the structure was carried out by using both operational and traditional modal analysis techniques. Both impact hammer and shaker exciter were used for the traditional modal analysis. The measurement locations were limited to four points on the wing wall; however, the author managed to identify the first eight modes of

vibration. The authors observed the frequency response of the wing wall to be independent of the vibration amplitudes, which is an indication of linear behavior.
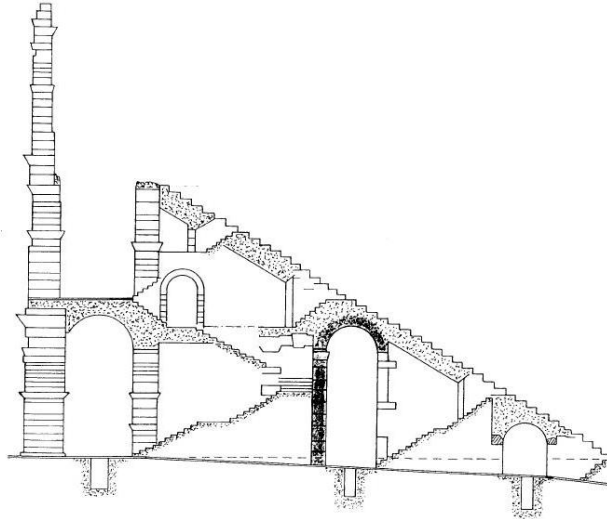
Figure 2-5: The section of the Roman amphitheatre, reprinted from Zonta (2000), with permission.

Vibration-based studies, just as they were used to detect damage, were also used to detect the improvements in the structural behavior after retrofit or strengthening campaigns. Turek et al. (2002) conducted ambient vibration analysis on a recently repaired, historical church. The identified modal parameters of the church before and after retrofit were compared and an increase in the dynamic stiffness was observed. Although the authors compared the measured modal parameters against the predictions of the FE model of the church, they noted that measurements recorded at a larger number of points with a denser grid were necessary to extract clear mode shapes in support of FE model calibration.

Increased dynamic stiffness was also observed in a similar study on a historic basilica by Antonacci (2001) and by Ramos (2007) on a historic masonry tower before and after retrofit. Both of these studies extended their experimental campaigns to the calibration stage. These studies are discussed in Section 2.3.2.2.

Brencich and Sabia (2008) conducted dynamic tests on an 18-span masonry bridge. The natural frequencies obtained through dynamic tests were compared to those estimated by the elastic three-dimensional models. The authors also mentioned the dynamic interaction between adjacent spans and the necessity to monitor the entire bridge to gather a complete understanding of the mode shapes.

Atamturktur et al. (2009b) investigated the feasibility of using vibration-based damage detection techniques for damage types that manifest themselves as coupled effects of Sabouret cracks (Heyman 1995) and geometric distortion of vaults, commonly caused by the settlement of foundations of buttresses. Two of the 10 nominally identical

masonry vaults of Beverley Minster, UK, at different structural damage states, were subjected to vibration testing with hammer excitation. The measurements were then configured in frequency, modal, and time domains. In the frequency domain, the amplitudes of FRFs acquired from the damaged vault were noticeably higher than that of the undamaged vault. However, the modal parameters derived from these FRF remained unchanged up to 10 Hz for both of the vaults. Because of the characteristic high modal density the authors could not identify the higher-order modal parameters adequately. Time domain regression methods proved sensitive to the damage present in the system.

2.3.2 Calibration Studies

Solely experimental methods are, by default, limited in their spatial resolution. Experiments integrated with an FE calculation, however, allow a more complete set of results, because a calibrated numerical model can deliver a variety of important structural properties. The extent of research efforts on model calibration applied to masonry structures is emphasized herein. Two different types of calibration approaches will be discussed. The first one is manual calibration, which is a trial-and-error-based approach performed manually by tuning selected parameter values. The second approach, automated calibration, is performed by constructing a series of loops around the FE code based on optimization procedures or Bayesian inference.

2.3.2.1 Manual Model Calibration

Manual calibration is substantiated by engineering judgment and is an appealing and convenient approach in calibrating the modeling parameters. However, by its nature, this method fails to incorporate the uncertainties of material properties and boundary conditions, especially when there are sources of uncertainty challenging understanding of the structural behavior. In the complex interaction between a masonry tower wall and an adjacent church wall, the calibration may be compensating for errors from other sources by tuning the originally correct model parameters. A manual calibration of parameters can be justified on the grounds that the initial model is a close representation of reality and any deficiencies have arisen from imprecise model parameters that are independent and uncorrelated. If the parameters have hidden dependencies or correlations, however, it is likely that they will not be observed during a manual calibration. Again, this will raise the problem that tuning one parameter may be compensating for an imprecision in another parameter. Keeping these problems in mind, various applications of manual calibration will be overviewed in the following paragraphs.

Antonacci (2001) obtained the natural frequencies and the global mode shapes of a basilica that had gone through moderate scale repair and strengthening. Transient dynamics tests were repeated before and after the repair using hammer excitation. The

authors observed a trend of increasing natural frequencies after the repair. Measured natural frequencies were used to tune the numerical model material properties. The calibrated FE model was then used to investigate the static behavior of the structures before and after the repair and strengthening. Arêdê et al. (2001) completed similar work on an ancient monastery church. In this study, Young's modulus of the surcharge infill was tuned based upon the experimentally obtained modal parameters. The calibrated model was then used to assess the seismic vulnerability of the structure.

Multitiered masonry temples in Nepal were the subject of a similar study (Jaishi et al. 2003). Three temples were tested with operational modal analysis techniques. The first three bending modes in both orthogonal directions of the temple were identified from the measurements and paired with the calculated modes based on visual inspection. The natural frequencies were observed to be as low as 1.6 Hz for the first bending mode. The identified frequencies were used to manually tune the uncertain material properties of the mud-brick walls of the temple. The Young's modulus magnitudes were significantly reduced to achieve a better correlation between the measured and calculated frequencies. Such an approach was applied to the vaults of Gothic cathedrals by Erdogmus (2004). Erdogmus identified the first axis-symmetric mode of the choir vaults of a twentieth-century cathedral built similar to medieval construction techniques. This mode was used as a reference to manually adjust the FE model boundary condition and material properties. The calibrated FE model was then used as a baseline for the development of FE models of two other complex vaulted historic churches. Atamturktur (2006) and Atamturktur and Boothby (2007) completed a complementary study on two masonry tile domes. Both studies obtained coherent and high-quality test data and identified 10 clear mode shapes. In these two studies, the authors used nondestructive and destructive techniques to identify the material properties of the tile and mortar, therefore, calibration parameters were confined to boundary conditions. Upon the completion of manual calibration, FE model predictions compared favorably with the measured results. The FE models were then used to assess the structural principles of Guastavino domes.

Júlio et al. (2008) applied a similar procedure to a clock tower adjacent to a faculty building at the University of Coimbra in Portugal. The tower was built of rubble stone with coarse stone masonry at the corners, and it exhibited degradation of joints, cracking of stone blocks, and biological growth. The tests were conducted using operational modal analysis techniques. The restraints imposed on the tower by the adjacent building walls and slabs and the soil structure interaction were uncertain, therefore, the authors were forced to make several assumptions regarding these connections. During test-analysis correlation to remedy the observed discrepancy, the authors altered the initially established boundary conditions by trial and error until an acceptable agreement was reached for the first five mode shapes. The authors acknowledged that without a survey of geometry and material of the surrounding structural components, it was not possible to validate the final boundary conditions in the sense that validation is defined in this dissertation. The material properties of the tower walls were further tuned to achieve better agreement between the measured and numerical frequencies. The calibrated model was then used to construct inferences about the structural integrity of the tower. Júlio et al.'s approach uncouples the calibration of boundary conditions and material properties, where the boundary conditions are

calibrated based on mode shapes and the material properties are calibrated based on natural frequencies. The same approach has been applied to a half-scale Guastavino dome specimen by Erdogmus (2008). The uncoupling of the boundary condition and material property calibration must be applied with caution when there are multiple material types in the FE model, as mode shapes are known to be sensitive to the relative ratios of the material property values.

2.3.2.2 Automated Model Calibration

Aoki et al. (2005) presented the results of a dynamic identification and model calibration campaign applied to a brick chimney. Both microtremor and acceleration measurements were collected due to the ground motion induced by a derrick car. The first three modes in two orthogonal directions of the tower were identified by Autoregressive Moving Average and Eigensystem Realization Algorithm techniques. The FE model of the chimney was built with 20-node isotropic solid elements assuming a fixed support at the base. By the use of Inverse Eigensensitivity Method (IEM), the elemental matrices of the FE model, such as mass and stiffness matrix of each FE, are calibrated. To alleviate the problems caused by the inevitable incompleteness of the measurements, a weighting function was applied to eliminate the calibration parameters that do not have significant influence on the outputs. As a result of calibration, for each FE a stiffness correction factor was obtained. The stiffness of the elements at the base of the chimney was observed to be reduced, while at the corners the stiffness was observed to be increased. The author explained the former by chimney-soil interaction and the latter by the iron angles at the corners.

The study completed by Júlio et al. (2008) on the masonry tower resembles an earlier study by Gentile and Saisi (2007). Both of the towers investigated in these studies presented severe difficulties in the identification of the interaction between the tower and the walls of an adjacent structure. The tower dealt with by Gentile and Saisi also showed signs of partial damage due to extensive vertical cracks. Gentile and Saisi represented the connection between the walls of the tower and adjacent cathedral using linear springs with a constant to be calibrated. Quantifying the material properties of defective structural components is challenging, if not impossible. Thus, Gentile and Saisi also selected the poorly known Young's modulus values of the defective walls as calibration parameters. Based on the extent of damage, the exterior walls were defined in six distinct regions with independent material properties. According to the modal parameters obtained through ambient vibration testing, the calibration was achieved by minimizing the difference between theoretical and experimental natural frequencies. The calibration was completed by both the IEM and Douglas-Reid (DR) method. The IEM represented the functional relationship between frequencies and the calibration parameters by Taylor series. Following that, Gentile and Saisi developed an iteration routine where the calibration parameters were evaluated. In the DR method, the relationship between the calibration parameters and the frequencies were approximated around the expected values defined previously. Also, a definition of a range within which the calibration parameters

could vary was also necessary for the method. The findings consistently yield lower Young's modulus values in the damaged regions when compared to the undamaged regions, supporting the potential of the vibration-based model calibration methods to deliver useful information about the damaged state of a masonry structure.

Ramos (2007) conducted tests on a masonry clock tower that, due to lack of maintenance, had undergone severe damage. Cracks, material degradation, biological growth, and loss of material were noted in the tower. Similar to Turek et al. (2002) and Antonacci (2001), Ramos obtained an opportunity to investigate the dynamic behavior of the tower before and after a strengthening campaign was undertaken. The tower was observed to vibrate at higher natural frequencies after the retrofit while the damping coefficients were observed to be lower. It must be emphasized that the correlation of the first five theoretical and experimental mode pairs is remarkable. This is perhaps due to the fact that the test structure was a standalone tower without uncertain connections to adjacent structures. The first five natural frequencies and mode shape vectors were used to calibrate the FE model by the nonlinear least squares method. Ramos obtained significantly lower Young's modulus results for the walls where damage was dominant.

In the next section, studies that address more complex structures with large numbers of uncertainty sources, such as churches and buildings, will be discussed. These studies will manage these sources of uncertainty by relying on probabilistic methods.

2.4 Stochastic Model Calibration

Advancing calibration beyond a deterministic approach requires considerations of uncertainty, both in experimentation and modeling. While deterministic model calibration is intended to reach a direct match between the analytically and experimentally derived comparative features, the objective of stochastic calibration is to reach a statistical correlation between the two. This can be achieved by formulating the input parameters probabilistically.

Deterministic methods can be considered as examining a single point in a cloud. In such a case, stochastic methods are concerned with clouds of points—where experimental point clouds are obtained from repeated experiments and analytical point clouds are obtained from repeated numerical experiments. By nature, a manual model calibration effort is deterministic, and for stochastic model calibration, an automated process is required. Studies of civil engineering systems that utilize the method of model calibration based on statistical principals merit discussion as it relates to the present study.

Antonacci et al. (2000), and in a later refined version, Sortis et al. (2005), presented a study on a two-story stone masonry structure. Both studies collected vibration measurements from the structure due to low-amplitude vibratory forces induced by shakers placed at four different locations. The modal parameters extracted from these measurements were used to calibrate the individual Young's modulus values of exterior wall segments of the corresponding FE model, based on a nonlinear output error approach. Both the input parameters and the output error were treated as random

variables with normal distribution. The optimal parameter values, which yield maximum posterior probability distributions for the input parameters and minimum for the nonlinear objective function, were sought. The calibration parameters, selected based on their significance according to the Fisher information matrix, were Young's modulus of four exterior wall sections. The discrepancies between the experimental and analytical modal parameters, after the calibration, were noted to be within the measured frequency variations obtained by exciting four different locations. Both studies also noted that optimization-based calibration is highly ill-conditioned due to the incompleteness of the measurements and it is important to aid the error-minimization tools with engineering judgment.

De Stefano (2007) conducted dynamic experiments on a masonry dome of a baroque chapel using four different excitation sources: ambient, hammer, dropped object, and wind turbulence caused by a helicopter. As a result, the first six modes were identified. The structure was divided into a number of substructures, within which the material of each substructure was assumed to be homogenous. To represent the interaction of the chapel with the neighboring buildings, elastic springs were added to the model. The most influential modeling parameters were selected based on a sensitivity analysis. The probability distribution of the parameter values for the selected calibration parameters were initially defined as uniform. A cost function, that is, the test-analysis deviations for the first five natural frequencies, was minimized through an algorithm known as Probabilistic Global Search Lausanne. The algorithm explores the domain defined by the calibration parameters, generating multiple alternative models to be run. Among these models, the algorithm selects those that show reasonable agreement with the measurements. Next, the calibration parameters of the models that passed the first elimination were perturbed one at a time and at each iteration, the probability distribution of these calibration parameters was then updated. The last step of this multimodel approach was clustering the final set of models that fit the minimum error requirements. With this approach, the author clustered five alternative models, which only differ from each other for the values of the calibration parameters.

The two studies discussed in this section both incorporate uncertainty in the calibration parameters by treating them probabilistically. However, in neither of these studies is the experimental variability accounted for, which is accomplished in a later study on a masonry cathedral. Atamturktur (2009) integrated large amounts of experimental and computational information collected from testing the choir vaults of the National Cathedral in Washington, DC. Measurement uncertainty was assessed from the replicated experiments. A design of computer experiments, which is used to explore variability of the model parameter domain, was run by perturbing model parameters. Both from the measurements and numerical analysis, comparative features were extracted probabilistically as mean and variance statistics. Using a Phenomenon Identification and Ranking Table, the uncertain parameters that were candidates for calibration were ranked based on the sensitivity of test-analysis comparative features. Bayesian inference was used to compound the prior knowledge about the calibration parameters together with experimental observations collected from vibration testing. Prior probability distribution incorporates expert judgment while the variance of measured features account for the experimental uncertainty. Bayesian inference resulted in updated knowledge of the

calibration parameters in the form of a posterior probability distribution. The details of the implementation of Bayesian inference in this study are given in Chapter 3.

2.5 Discussions and Conclusions

This literature review reveals the common need of analysts to find supporting evidence for FE solutions. Mark's photoelastic studies of plastic scaled models, Fanning's scaled masonry bridges, and recent applications of *in situ* dynamic tests convey one common message: until the model is validated with physical evidence, numerical predictions must be treated with due caution. These studies also illustrate that testing of existing buildings yields very useful information about its response characteristics. However, only by integrating these experimental measurements with numerical FE tools is it possible to gain a thorough understanding of the structural behavior of the building. Although experimental measurements are always incomplete in the sense of their spatial resolution, they play an instrumental role in model calibration that ultimately yields mathematical representation of the global structural behavior. However, there are several issues in the practical application of model calibration that remain to be addressed.

In the calibration of masonry system FE models, inaccuracies are observed to originate from many different sources. Therefore, calibration must be stochastic and account for uncertainties, both in the experimental measurements and the model definition. The tasks required for stochastic model calibration require extensive resources and expertise and are, therefore, currently not routinely practiced. However, the stochastic approach is a first necessary step to bring calibration of analytical models into the analysis mainstream.

It is important to distinguish between a calibrated model and a validated model. To gain validity and to quantify the accuracy of an FE model, an independent set of experimentally derived information, other than that used in the calibration, is necessary. Until this step is completed, there can be no justification of the FE solutions (Trucano et al. 2006). This requirement increases the already high demands on resources.

Manual calibration studies—or tuning of uncertain parameters to improve the agreement between calculations and measurements by trial and error—have a benefit, as they conveniently incorporate engineering judgment and expert opinion into the calibration process, which keeps the calibration from converging to an unrealistic model. However, in the manual approach, parameters are treated as deterministic values, and therefore, this approach has limitations in incorporating the uncertainties. The manual calibration approach becomes more successful in the absence of a structural configuration difficult to interpret by engineering judgment; for example, a complex interaction between two masonry components. In cases where several such sources of uncertainty are present, it is likely that the errors introduced by an inappropriate boundary condition are compensated by manual tuning of the material properties, or vice versa.

Obviously, the credibility of a calibrated model is increased as the amounts of experimental information accurately reproduced by the calibrated model increases. The

pertinent literature does not discuss how the decision about the completion of calibration is reached. There is a need to develop a measure of sufficiency for experimental information and an indicator of completion for the calibration exercise.

Automated calibration studies, commonly based on optimization techniques, can be stochastic and can incorporate uncertainties; however, they are not typically conceived to incorporate expert opinion, which is more successfully achieved by manual calibration approaches. An alternative is the use of Bayesian inference methods for the characterization of calibration parameters that can take both uncertainty and expert opinion into account.

The extent of research efforts in model calibration is presented herein with a specific emphasis on historic structures. Although the immediate benefits of model calibration are not as obvious in civil engineering as they are in fields where prototyping and mass production are common, the determination of modeling strategies learned through model calibration can ultimately serve the civil structural engineering community with an improved accuracy in numerical modeling. Calibrated FE models will enable a better understanding of historic monument behavior and ultimately enable successful repair and retrofit schemes. As a result of this review, it is concluded that the ever-increasing popularity of FE model calibration will result in the application of model calibration to a diverse group of structures.

Chapter 3

METHODOLOGY

The difficulty [in science-based prediction] is shifting from being able to perform complex simulations to validating the models and assessing the degree of credibility of predictions.

François Hemez

3.1 Introduction

Section 1.4 defined the concept of model calibration in a larger context and emphasized its role in relation to model verification and validation. To reiterate, when the disagreement between model predictions and measurements is believed to be due to imprecisely known parameters in the model, poorly known input parameters can be calibrated to improve the fidelity of the finite element (FE) model predictions to physical evidence. This task invariably requires the comparison of calculations with measurements. In the present study, this comparison is completed based on linear dynamics.

Linearity herein means that the principle of superposition is applicable, meaning that the structural response to simultaneous application of a number of forces can be obtained by summing the structural response to each individually applied force. This assumption is valid for most engineering applications. Also, for structures that exhibit nonlinear behavior, developing a reliable linear model must be considered as the first necessary step.

This chapter aims to provide a framework for model calibration in linear dynamics by discussing the fundamental steps of model calibration, as illustrated in Figure 3-1. In Section 3.2, an introduction to the implementation of linear dynamics in FE analysis is provided. This section presents the mathematical background for the computation of structural system natural frequencies and mode shapes, while the experimental approach to estimating the natural frequencies and mode shapes is discussed in Section 3.3. The FE analysis results are compared against experimental measurements through the comparative features. Comparative features can be one of the many outputs of the FE analysis. Section 3.4 discusses the appropriate selection of comparative features based on the characteristics of the structure dynamic behavior. This section also provides a discussion on the importance of the selected feature

dimensionality. The success of calibration depends not only on selecting suitable comparative features, but also on the calibration of the appropriate parameters.

Appropriate selection of the calibration parameters is guided by uncertainty propagation and effect screening analysis. Both of these procedures are introduced in Section 3.5. Test-analysis correlation is the step when the calculated and measured comparative features are compared against each other. In Section 3.6, different schemes of test-analysis correlation are discussed. Details of the stochastic calibration procedure are presented in Section 3.7. This section summarizes the adaptation of a Bayesian calibration approach as well as the implementation of Gaussian process models as fast running surrogate in place of the computationally expensive FE model.
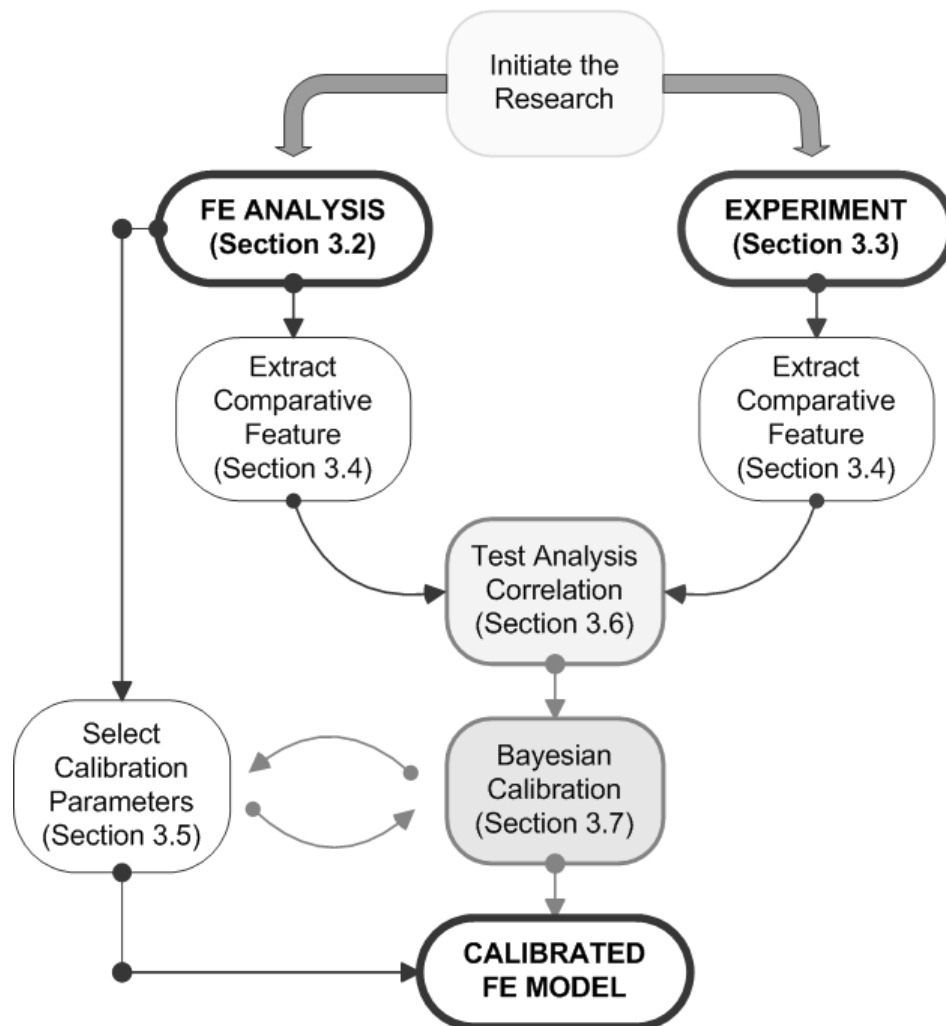
Figure 3-1: The model calibration process.

3.2 Finite Element Analysis

In structural dynamics, a mathematical model that can reliably predict the prototype's dynamic characteristics enables the design engineer to control certain important characteristics, such as maximum displacement or acceleration under a certain load. On the other hand, the demand to study structural dynamics of an existing structure stems from the need to assess performance of the structure under different conditions than those considered in the initial design. Increased operational loads due to a change in function, or reduced structural capacity due to damage or aging, are typical conditions that can vary greatly from the initial design.

Fundamentally, structure dynamic behavior depends on the dynamic equilibrium between external loads and the inertial, dissipative, and internal forces of the system at each instance of time. Therefore, in linear structural dynamics, the stiffness matrix constructed for static analysis is accompanied by mass and damping matrices (Equation 3-1). A simple single-degree-of-freedom system is shown in Figure 3-2.

$$M\ddot{d}(t) + C\dot{d}(t) + Kd(t) = F(t) \tag{3-1}$$

where, d(t) is the displacement, F(t) is the force, and M, C, and K are the mass, damping, and stiffness, respectively. The velocity and acceleration are derived from the displacement as the first and second derivative, respectively.
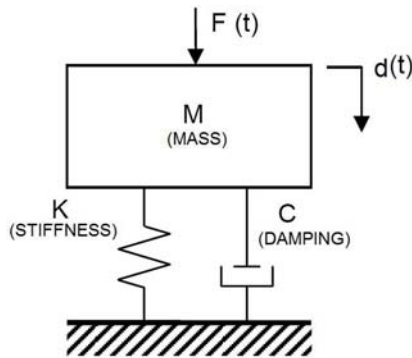
Figure 3-2: Schematic of single-degree-of-freedom system.

For a multiple-degree-of-freedom system, the terms of equation of motion, given in Equation 3-1, expand into vectors and matrices.

$$[M]\{\ddot{d}(t)\} + [C]\{\dot{d}(t)\} + [K]\{d(t)\} = \{F\{t\}\} \tag{3-2}$$

The solution of Equation 3-2 requires mass, damping, and stiffness matrices to be constructed. The FE method constructs these matrices through mesh discretization. However, the solution methods of structural dynamics do not specify the means from which these elemental matrices are derived. Therefore, to construct elemental matrices,

other approaches can be used in place of the FE method. In fact, many solution methods in structural dynamics predate the development of the FE method (Cook et al. 2002).

The second-order linear differential equation of motion given in Equation 3-2 yields the eigenvalue problem if the dissipative forces are omitted or if the system is assumed to exhibit proportional damping. The proportional damping assumption defines the damping matrix as a linear combination of mass and stiffness matrices. By solving the eigenvalue problem, one obtains the modal parameters of the structure: natural frequencies and corresponding mode shapes.

$$[[K] - \lambda[M]]\{\Phi\} = \{0\} \qquad (3-3)$$

where λ yields the eigenvalues, which are the squares of the circular natural frequencies.

$$\lambda = \omega^2 \qquad (3-4)$$

Φ is the eigenvector, the dimensionless mode shape vector corresponding to each of the system's natural frequencies (Equation 3-4).

Omitting the damping component, or assuming proportional damping, results in real normal mode shape vectors without phase components. In a real, normal mode, the maximum deformations are reached simultaneously at all nodes. In complex modes, the nodes exhibit time-dependent phase delays while reaching their maximum deformations. The topic of complex modes will be revisited in the next section, when modal analysis is discussed from an experimental point of view.

Direct solution of the characteristic eigenvalue problem is straightforward for systems with few degrees of freedom (Equation 3-3). Typically, eigenvalue problems are solved iteratively or based on repetitive similarity transformation (Friswell and Mottershead 1995). However, as the model size increases, the solution to the eigenvalue problem becomes increasingly expensive. The symmetric, banded nature of elemental matrices makes subspace iteration (Bathe and Wilson 1972) or the Block Lanczos method (Lanczos 1950) suitable for large FE eigenvalue problems. Today, structural dynamics calculation methods are tailored to reduce the computational requirements of the FE analysis, for example see Guyan Reduction (Guyan 1965).

The key component of modal analysis is the coordinate transformation of equation of motion back and forth between the modal domain and time domain. First a modal matrix *[Φ]* is defined by placing eigenvectors *{Φ}* in columns. Modal matrix is then normalized with respect to the mass matrix. The three elemental matrices of Equation 3-2 are converted into a modal model consisting of the defined modal mass, modal stiffness, and modal damping values:

$$[M_\Phi] = [\Phi^T][M][\Phi] = [I] \qquad \text{modal mass matrix}$$

$$[C_\Phi] = [\Phi^T][C][\Phi] \qquad \text{modal damping matrix} \qquad (3-5)$$

$$[K_\Phi] = [\Phi^T][K][\Phi] = [\omega^2] \qquad \text{modal stiffness matrix}$$

Next, the displacement vector *{d}* is expressed as linear combination of eigenvectors. Displacement, velocity, and acceleration vectors in physical coordinates are transformed into vectors in modal coordinates.

$$\{d\} = [\Phi]\{Z\} \qquad \text{where } \{Z\} \text{ is modal displacement matrix}$$

$$\{\dot{d}\} = [\Phi]\{\dot{Z}\} \qquad \text{where } \{\dot{Z}\} \text{ is modal velocity matrix} \qquad (3\text{-}6)$$

$$\{\ddot{d}\} = [\Phi]\{\ddot{Z}\} \qquad \text{where } \{\ddot{Z}\} \text{ is modal acceleration matrix}$$

Modal matrices, *{Z}* and derivatives, are functions of time, and can be considered as a fraction of eigenvector contribution to the overall system response *{d}* and to its derivatives. Because the system response is defined as combination of modal matrices, this method is also referred to as the Mode Superposition Method. Incorporating Equation 3-4 into Equation 3-6 and premultiplying by *[Φ^T]* yields Equation 3-7:

$$[\Phi^T][M][\Phi]\{\ddot{Z}\} + [\Phi^T][C][\Phi]\{\dot{Z}\} + [\Phi^T][K][\Phi]\{Z\} = [\Phi^T]\{F(t)\} \qquad (3\text{-}7)$$

Defining *[F$_\Phi$]=[Φ^T]{F(t)}*, the coupled equations are transformed into uncoupled equations in modal coordinates.

$$\{\ddot{Z}\} + [C_\Phi]\{\dot{Z}\} + \omega^2\{Z\} = [F_\Phi] \qquad (3\text{-}8)$$

The assumption of proportional damping yields a simple solution consisting of diagonal matrices. After the solution of the uncoupled equations in modal coordinates, the system response is transformed back into physical coordinates by using the same eigenvector matrices, or the results are used to obtain the response of the system in frequency domain.

Implementation of modal analysis in FE method has computational benefits. For many engineering applications only the lowest portion of the spectrum is needed, and calculation of the response vectors from generalized modal coordinates provides the required accuracy.

The FE analysis in structural dynamics is mature and discussed at length in several textbooks (see for instance, Cook et al. 2002, Zienkiewicz 1977, and Bathe 1982). Therefore, the numerical algorithms behind FE analysis will not be reported herein, even though the present study routinely implements these tools. However, guidance will be provided for successful FE analysis of masonry structures in Section 3.8.1.

3.3 Experimental Modal Analysis

As stated earlier, the purpose of the experiments is to obtain features that can be compared against the FE model. Among all the experimental methods that were attempted in the field of model calibration, the techniques of experimental modal analysis (EMA) have emerged as the most widely used and well established (Ewins 2000). EMA

provides a convenient and inexpensive means to extract features, as long as the system exhibits predominantly linear behavior.

EMA consists of two phases: the testing phase, during which the vibratory data are measured, and the postprocessing phase, during which the modal parameters are extracted from the measured vibratory data. These two phases of EMA are considered to be a combination of art and science by McConnel (2008). The scientific aspects of EMA, as McConnel defines them, are discussed in this section. The art component of EMA develops with accumulated experience on the tested structure. This will be discussed specifically for masonry vaulted monuments in Section 3.8.2.

In EMA, the most commonly used comparative features are the modal parameters: natural frequencies and mode shapes. The way FE-based modal analysis calculates modal parameters is discussed in the previous section. However, experimentalists take a different route to reach these modal parameters. A fundamental component of EMA is the construction of the frequency response function (FRF), and it is best explained with a single-degree-of-freedom system as illustrated in Figure 3-2. Replacing the excitation force, $F(t)$, with a force phasor, $F(t)=F_0 \, e^{j\omega t}$, and the response, $d(t)$, with a response phasor, $d(t)=d_0 \, e^{j\omega t}$, the equation of motion given in Equation 3-1 becomes

$$(-M\omega^2 + Ci\omega + K)d_0 e^{i\omega t} = F_0 e^{i\omega t}$$

(3-9)

where d_0 is the response vector and F_0 is the force vector. For a given force magnitude F_0, depending on the characteristics of the loading, the dynamic response d_0 may be less than or greater than the static response of the structure. FRF is computed as a ratio of the structural response $d(\omega)$ to the excitation force $F(\omega)$ in the frequency domain. FRF provides a physically meaningful interpretation of the dynamic input-output relationship, as expressed in Equation 3-10:

$$H(\omega) = \frac{d(\omega)}{F(\omega)} = \frac{1}{(-M\omega^2 + Ci\omega + K)}$$

(3-10)

As evidenced by Equation 3-10, FRF is a complex valued function with magnitude and phase components that form the bode plot (or real and imaginary components that form the Nyquist plot). The d_0 in Equation 3-10 gives the receptance FRF that operates on displacement response. If the measured response is velocity, it is called mobility FRF, and if the measured response is acceleration, then it is called accelerance FRF. The relationship between these three forms of FRF is given in Table 3-1.

Table 3-1: The Relationship between These Three Forms of FRF

Response Type		FRF Equation	FRF Type
Displacement	$\dfrac{d(\omega)}{F(\omega)}$	$\dfrac{1}{(-M\omega^2 + Ci\omega + K)}$	Receptance
Velocity	$\dfrac{\dot{d}(\omega)}{F(\omega)}$	$\dfrac{i\omega}{(-M\omega^2 + Ci\omega + K)}$	Mobility
Acceleration	$\dfrac{\ddot{d}(\omega)}{F(\omega)}$	$\dfrac{-\omega^2}{(-M\omega^2 + Ci\omega + K)}$	Accelerance

In vibration testing, acceleration is the most common type of measurement as it is applicable for a wide band of frequencies (currently between 0 and 20,000 Hz). The usable frequency range is 1–1000 Hz for velocity transducers and 1–100 Hz for displacement transducers (Bruel and Kjaer 1982 and Parker 2009). The performances of velocity and displacement transducers are compared to accelerometers in Figure 3-3. Because of wider frequency band of accelerometers, acceleration measurements will be the basis for the following discussion.
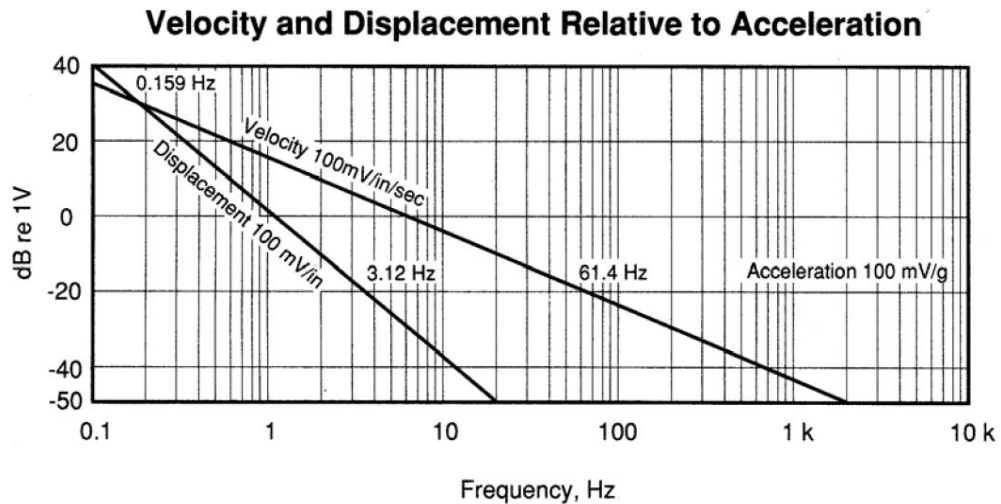
Figure 3-3: The frequency spectrum of displacement, velocity, and acceleration transducers (Parker 2009, with permission).

The graphical representation of acceleration FRF, presented in Figure 3-4, provides a convenient means for visual interpretation of structure dynamic characteristics. Consider a simple system of a single-degree-of-freedom mass and spring-

loaded by a time-dependent sinusoidal force with a constant magnitude. If the rate of force oscillation is swept through a frequency range, the FRF graph displays an asymptotic behavior at both low and high frequencies, as seen in Figure 3-4. When the forcing frequency is much lower than the natural frequency, the system stiffness dominates the response. When excitation frequency draws near the natural frequency, the response of the structure displays a sharp maximum, the height and width in frequency space of which is determined by the damping in the system. At much higher excitation frequencies, the FRF is determined by the mass of the system.
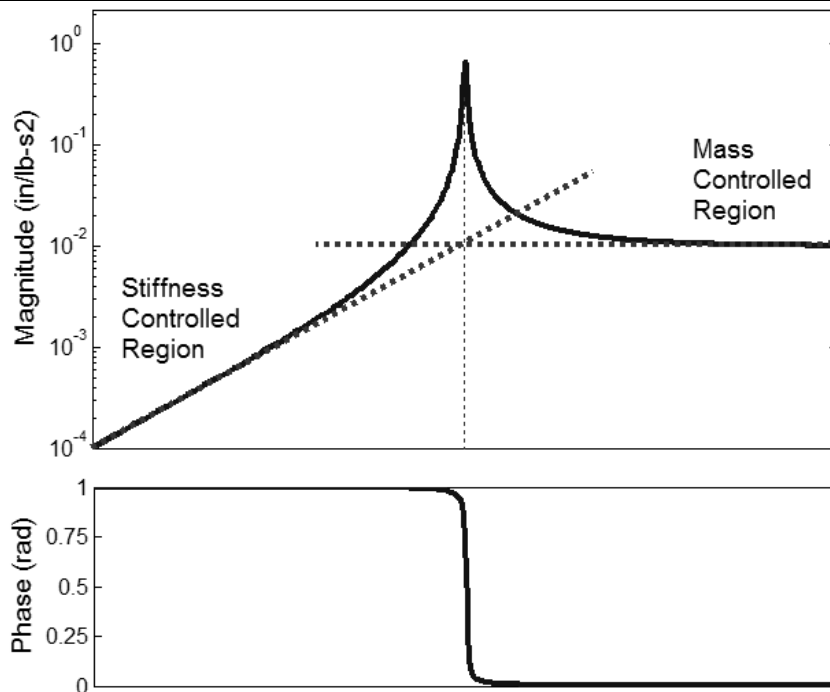
Figure 3-4:   Acceleration-based FRF in logarithmic scale: (top) magnitude, (bottom) phase.

The acceleration FRF can be conveniently constructed from the time-response measurements by taking the ratio of the Fast Fourier Transform (FFT) of the measured acceleration response and forcing functions. A series of steps occurs for the calculation of FRF (Figure 3-5): (1) acquiring the analog signal, (2) filtering higher frequencies with antialiasing filter, (3) digitizing the filtered signal with analog-to-digital converters, (4) applying a window function to prevent leakage, (5) performing FFT on windowed signal, (6) averaging to reduce the effects of noise, and (7) constructing the FRF. There are many important aspects to digital signal processing, and the topic has received significant attention in numerous textbooks (see Ewins 2000, Hatch 2000, Maia and Silva 1997, McConnel 2008, and Silva 2009).

ANALOG SIGNALS

INPUT

OUTPUT

ANTIALIASING FILTERS

AUTORANGE ANALYZER
ADC DIGITIZES SIGNALS

INPUT

OUTPUT

APPLY WINDOWS

INPUT

OUTPUT

COMPUTE FFT
LINEAR SPECTRA

LINEAR
INPUT
SPECTRUM

LINEAR
OUTPUT
SPECTRUM

AVERAGING OF SAMPLES

COMPUTATION OF AVERAGED
INPUT/OUTPUT/CROSS POWER SPECTRA

INPUT
POWER
SPECTRUM

CROSS
POWER
SPECTRUM

OUTPUT
POWER
SPECTRUM

COMPUTATION OF FRF AND COHERENCE

FREQUENCY RESPONSE FUNCTION

COHERENCE FUNCTION

Figure 3-5: The schematics of FRF computation from experimental measurements (Avitabile 2001, with permission).

In multiple-degree-of-freedom systems, the magnitude component of FRF displays sharp peaks at all resonant frequencies, while the phase angle is 90 degrees. Accordingly, at resonant frequencies, the real component of FRF converges to zero and the imaginary component reaches a maximum. The imaginary component of the FRF yields the relative deformations of measurement locations.

By identifying the frequency at which the sharp peaks of the FRF are centered, the natural frequencies of the system can be obtained. This simple approach of finding the natural frequencies is known as peak-picking (Bishop and Gladwell 1963). At these frequencies, plotting the imaginary component of the FRF for each measurement point conveniently yields the mode shapes (Figure 3-6).
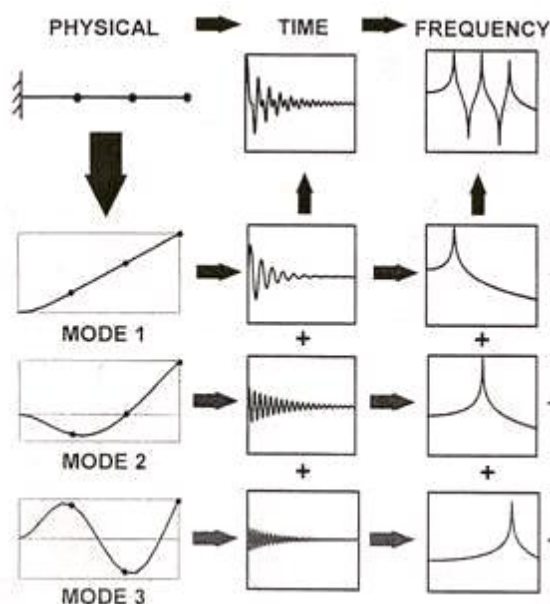
Figure 3-6: The derivation of mode shapes from imaginary FRF plots (Avitabile 2001, with permission).

This simple approach of constructing the mode shapes is known as quadrature response analysis (Pendered 1965). It is a single-degree-of-freedom system identification method that estimates modal parameters one mode at a time. It is most successful when applied to a clean, high-quality FRF with well separated modes of a lightly damped system. This simple method assumes the multiple-degree-of-freedom FRF to be a superposition of multiple single-degree-of-freedom FRFs. It is a fast and convenient way to find mode shapes and natural frequencies. Other popular single-degree-of-freedom frequency domain system identification methods are the circle fitting method (Kennedy and Pancu 1947) and rational fraction polynomial method (Li et al. 1994).

More sophisticated multiple-degree-of-freedom time domain methods are developed for successful system identification from complex FRFs where modes are closely spaced, the ambient noise is present, or FRF peaks are smeared due to high

damping. These methods determine the modal parameters indirectly by imposing a linear multiple-degree-of-freedom model on the measurement. Popular multiple-degree-of-freedom time domain system identification methods are Ibrahim time domain (Ibrahim 1977), least squares complex exponential method (LSCE) algorithm (Brown et al. 1979), eigensystem realization algorithm (ERA) (Juang and Pappa 1985 and 1986), and auto-regressive moving average model and its derivatives (e.g., ARMAX, ARMAVX) (Ljung 1999). Some of these multiple-degree-of-freedom time domain methods are also implemented in the frequency domain. For example, least squares frequency-domain, (frequency domain version of LSCE) (Mergeay 1983) and ERA-frequency domain, (frequency domain version of ERA) (Juang and Suzuki 1988).

The most suitable system identification method varies depending on system dynamic characteristics (e.g., lightly/highly damped, low/high modal density) and measurement characteristics (e.g., low/high signal-to-noise ratio, single/multiple run setup). An overview of various system identification methods emphasizing their merits and drawbacks can be found in Verboven (2002).

3.4 Selection of Comparative Features

Among all possible FE model outputs, those selected for comparison with physical evidence are called comparative features. In some cases, regulatory agencies or industry standards can impose a specific comparative feature. An example is the head injury criterion of the Federal Motor Vehicle Safety Standard Occupant and Crash Protection (FMVSS-208). In other cases, the selection of a response feature is dictated by the application. For instance, damping ratio is commonly used for the aeroelastic flutter of airplane structures. When such impositions do not apply, the burden of selecting the comparative feature falls to the analysts and experimentalists.

Because of an *a priori* decision to use modal parameters as comparative features in the present study, the groundwork has been laid in this chapter specifically for numerical computation and experimental identification of modal parameters. However, other alternative comparative features to modal parameters must be discussed.

3.4.1 Comparative Features in Linear Dynamics

When the measurements are collected, feature extraction is reduced to fitting a model to the measured data. This fitted model can be physics-based or data-based, linear or nonlinear, stationary or nonstationary. These characteristics determine the type of information the comparative feature can entail. Table 3-2 lists common and some uncommon features suitable for specific types of structural dynamics problems. This includes features that have clear, unambiguous physical meaning, such as modal parameters, as well as data-based features, such as temporal moments, that have less clear

physical interpretation. In practice, both physics-based and data-based features can be used successfully. However, working with features with physical significance helps the communication between experimentalists and analysts and should be preferred when possible (Hemez 2007).

Table 3-2: Examples of Comparative Features (Hemez 2007)

Linear, stationary, Gaussian vibrations
• Direct and inverse Fourier transforms; • Power spectral density; • Input-output transfer functions; • Frequency responses; • Modal parameters (frequencies and mode shapes).
Transient dynamics and mechanical shock response
• Peak values; • Energy content; • Decrement and exponential damping; • Shock response spectrum; • Temporal moments.
General-purpose time series analysis
• Autoregressive and moving average models; • Time-frequency transforms; • Wavelet transform; • Principal component decomposition.
Unstable, chaotic, multiple-scale dynamics
• State-space maps; • Poincaré maps; • Time-frequency and higher-order transforms; • Symmetric dot pattern; • Fractal analysis.

Because comparative features should be sensitive to the selected calibration parameters, the selection of comparative features is fundamentally tied to the selected calibration parameters. That is, modal parameters are only effective as comparative features when calibrating the input parameters that have significant influence on them.

3.4.2 Comparative Feature Dimensionality

Implicit in the definition of a comparative feature is the reduction of the dimensionality of raw measurement data. "Dimensionality" refers to the number of features analyzed. For example, the dimensionality of a vector of five modal frequencies is $N = 5$, while the dimensionality of a response signal sampled at 2^{10} points is $N = 1,024$.

The convergence of multivariate statistical tests that involve N features is typically proportional to N^2, not N. This means that N^2 samples (physical tests or computer runs) are required for the analysis. When the dimensionality is too high, trends cannot be identified unambiguously, and also direct comparison between the measurement and calculation is hindered. Data reduction can greatly simplify the management and statistical analysis of the oversized raw data. At the other extreme, one must be careful not to reduce information to the point where information regarding the calibration parameters is lost or too few dimensions make it impossible for patterns in the data to be recognized. For the last decade, this trade-off in data reduction has been a concern for the fields of structural health monitoring and damage detection (Farrar et al. 2007).

Researchers continuously seek the smallest feature dimension that maintains the information about the structure but is still manageable enough in size to make statistical inferences. In the absence of a quantitative means of determining how much relevant information a specific comparative feature contains for a given calibration problem, comparative feature selection is often conjectural, made based on past experience, and specific to each case. Inspired by the several successful calibration studies applied to masonry structures by using modal parameters, as discussed in Chapter 2, this study uses modal parameters as the comparative features. The dimensionality of the modal parameters, in other words, the number of modes that will be used during calibration, will be determined based on the number of the modes extracted reliably from the experimental measurements.

3.5 Selection of Calibration Parameters

The success of FE model calibration depends not only on selecting suitable comparative features but also on calibrating suitable input parameters. Fundamentally, selection of calibration parameters must be guided by the combined effects of parameter uncertainty and sensitivity. These two important factors are combined together in the Phenomenon Identification and Ranking Table (PIRT) (Pilch et al. 2001). PIRT originated in high-consequence modeling in nuclear reactor safety studies (Wilson and Boyack 1998). When the PIRT is successfully constructed, parameters of the FE model that are relatively certain to the analyst or parameters that are not influential on the desired solutions are removed from the calibration parameter list. A sample PIRT is illustrated in Table 3-3.

Table 3-3: Example Phenomenon Identification and Ranking Table

Parameter	Uncertainty	Sensitivity	Decision
Young's modulus of Material A (E1)	High	high	calibrate
Young's modulus of Material B (E2)	High	low	-
Thickness of Component 1 (t1)	Low	low	-
Thickness of Component 2 (t2)	Low	low	-
Stiffness Constants of Component 1 (K1)	High	high	calibrate
Stiffness Constants of Component 2 (K2)	High	high	calibrate

3.5.1 Parameter Uncertainty

Parameters that are used to represent the physical reality in a mathematical model are typically random variables due to their natural variations; therefore, at a minimum they should be represented with mean and standard deviation. In the context of model calibration, parameter uncertainty arises from the lack of knowledge of the analyst about the statistical properties of these random calibration parameters.

In the presence of repeated physical experiments on poorly known FE model parameters, lack of knowledge about the parameter values would be reduced to the natural variability of the parameter, provided that a large enough family of experiments are conducted to be statistically representative. The experimentally obtained statistical properties of the parameters can then be quantitatively incorporated in the PIRT (Hills 2006). Coleman and Steele (1999) extensively discuss parameter uncertainty.

In the absence of repeated physical experiments on calibration parameters, for instance, material tests on extracted coupons, quantification of parameter uncertainty becomes a difficult task to achieve, if not impossible (Mace et al. 2005). Because of this, in PIRT, parameter uncertainty can be considered qualitatively through expert judgment based on prior knowledge about the structure (Table 3-3). For instance, Young's modulus of steel is well known and virtually uniform within a member, therefore, it can be considered more certain compared to the Young's modulus of the material in an old vernacular mud-house. Before proceeding to the next section, it is assumed that the analysis at least has *a priori* estimates for the minimum, nominal, and maximum values of the FE model parameters.

3.5.2 Parameter Sensitivity

In numerical modeling, sensitivity analysis may mean different concepts in different fields. Its first role in model calibration is to support the parsimony approach (Trucano et al. 2006). The parsimony approach aims at the reduction of the number of calibration parameters, and the parameter sensitivity is instrumental during the calibration parameter selection/elimination process.

The second main role of sensitivity analysis is appraisal of hidden interactions among parameters. Often parameters have combined effects on the outcome that cannot be represented by the sum of their individual effects (Saltelli et al. 2004). If this interaction is strong, it may cause a problem in that calibrating one parameter may be compensating for an imprecision in another parameter. It is advisable to fix one of these calibration parameters at their nominal values or to perform coordinate transformation of the correlated parameters to obtain new relatively uncorrelated parameters. An alternative solution to this problem can be achieved by uncoupling the correlated or dependent parameters such that each parameter is calibrated against an independent comparative feature (Williams 2008a).

The sensitivity of an FE model solution, whether local or global, to any parameter in the FE model can be determined by sensitivity analysis. Fundamentally, sensitivity analysis measures the changes in the model output due to a unit change in each of the input parameters. If the monitored model outcome is local, then it is called local sensitivity analysis—also known as gradient. If the monitored model output is global, then it is called global sensitivity analysis, or effect screening. In either case, sensitivity analysis ranks the parameters of the FE model on which the desired model solutions are the most dependent.

Local sensitivity analysis is gradient-based and it is expressed around a local point, X^o, and in a given direction (see, for instance, Rabits 1989) (Figure 3-7).
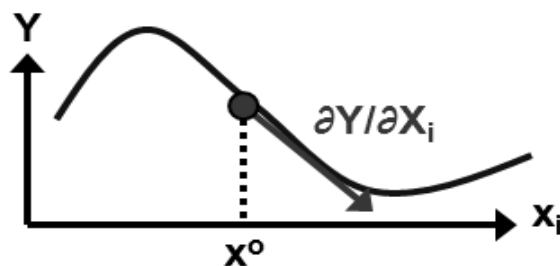
Figure 3-7:   The schematic of gradient-based sensitivity analysis, local sensitivity analysis (reprinted from Hemez 2007, with permission).

For instance, consider an output Y to be a function of parameters X_i, for i = 1,2…n.

$$Y = f(X_1, X_2, X_3 ... X_n)$$

(3-11)

Then, sensitivity of the variation in Y to a single parameter X_i can be found by

$$S_i = \frac{\partial Y}{\partial X_i}$$

(3-11)

where the parameter X_i is perturbed around its nominal value, X_i^0 (see Figure 3-7). The variation in Y can be explored under different conditions, when X_i is varied by a fixed fraction of its nominal value or by a fraction of its standard deviation.

Because local sensitivity analysis provides information only about the variability of a parameter around a local point X^o, it does not provide the effect of a parameter on the global variability of the outcome. This question is answered by a more involved process instead, global sensitivity analysis.

Global sensitivity analysis is typically performed based on sampling techniques, in which the model is executed repeatedly at parameter values sampled from the distribution of the input parameters (Cukier et al. 1978, Helton et al. 1991). The sampling of the domain defined by the parameters is most effectively designed by the tools that are known as design of experiments (see Montgomery 2000 and Myers and Montgomery 2002). Design of experiments aims to gain maximum information about the random parameters by minimum sampling points. There are numerous sampling design types, among which Full Factorial, Central Composite, Monte Carlo, and Latin Hypercube are the most common. Each of these design types is suitable for a specific problem. The different sampling procedures used in the Monte Carlo and Latin Hypercube designs are illustrated in Figure 3-8**.**

After the parameters are sampled, based on the selected design type, the parameter samples are fed to the numerical model. Depending on the number of samples collected, the FE model is run multiple times and a model output is obtained corresponding to each parameter sample. This multirun method is known as forward propagation of uncertainty, and it detects the variability of the FE model output due to the variability of the input (Figure 3-9)**.** Forward propagation of uncertainty is an important component of fast-running surrogate model development and will be used during the calibration process implemented in the present study (see Section 3.7.1).

Strictly speaking, the output response variability due to the variability of FE model input parameters should first be studied for the selected comparative features as the output, for instance, the modal parameters. This is because comparative features will later be correlated with the experimental comparative features. Literature presents examples of sensitivity analysis applied to other model output (e.g., FRFs, static displacements, and mode shape derivatives) (FEMtools User Manual 2007).
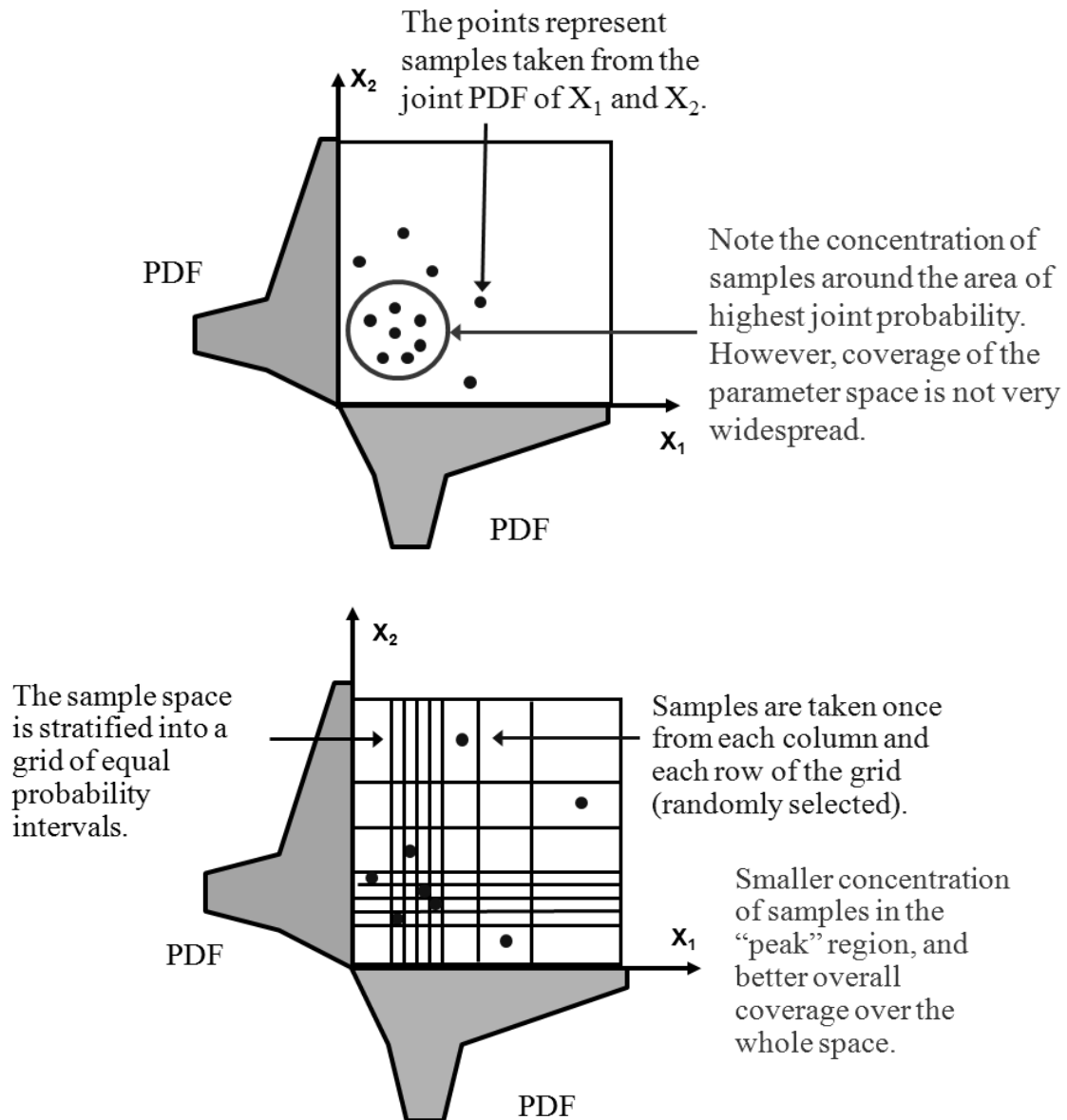
Figure 3-8: The Monte Carlo sampling and Latin Hypercube design of experiments (reprinted from Hemez 2007, with permission).

Distribution of Parameter	FINITE ELEMENT MODEL	Distribution of Solution
PDF (α)		PDF (ω)

Sample the PDF of the Parameter   **Run the Finite Element Model at each Sample**   **Construct the PDF of the Solution**
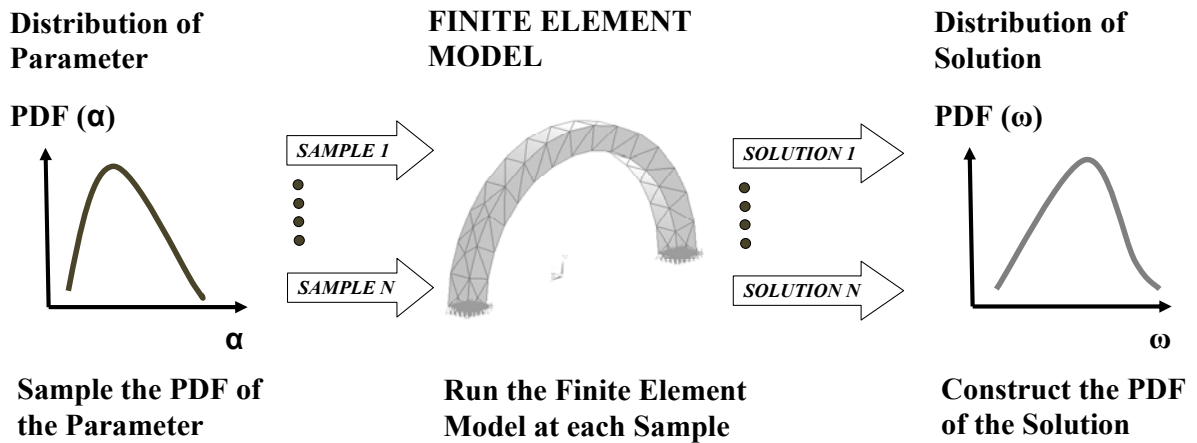
Figure 3-9: The operative procedure of parameter sampling.

After the parameter uncertainty is propagated to find the model output variability, the primary causes of this model output variability must be identified. Typically this is achieved through effect screening. Effect screening is the process of identifying which parameters, e.g., X_1, X_2, or parameter combinations, e.g., X_1, X_1X_2, $X_1X_3^2$, best explain the output variability. Common approaches to affect screening are expectation decomposition schemes (Saltelli et al. 2004) and analysis of variance (ANOVA). ANOVA aims at separating the statistical variance caused by a particular parameter from that caused by other parameters. R^2 statistic of ANOVA estimates the ratio of variability of the model output, when X_i is kept constant to the total variability of the model output when X_i is also varied.

$$R^2 = 1 - \frac{\sigma^2(\hat{Y})}{\sigma^2(Y)} \tag{3-12}$$

which is equal to Equation 3-13.

$$R^2 = 1 - \frac{\sigma^2(E[(Y \mid Xi)])}{\sigma^2(Y)} \tag{3-13}$$

A large R^2 value for a parameter, compared to those of other parameters, indicates that X_i has a significant effect on the output. Typical effect screening results are represented for a seven-parameter model in Figure 3-10. In Figure 3-10, the parameters 1, 4, and 7 are shown to be the most influential on the response of interest.

Effect Screening
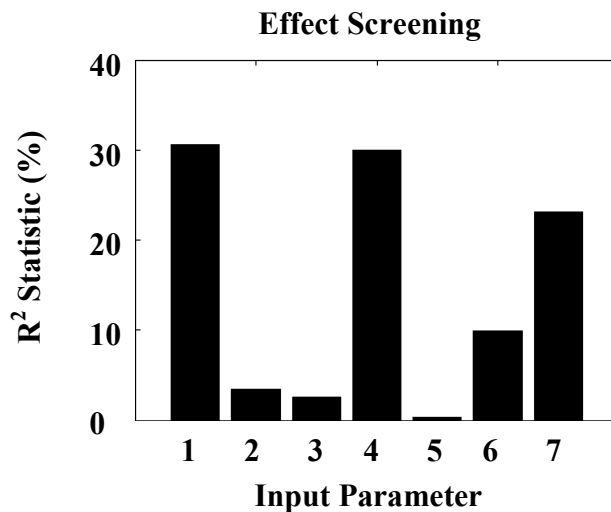
Figure 3-10: A visual interpretation of R^2 statistics of ANOVA.

3.6 Test-Analysis Correlation

The operational philosophy of model calibration is the comparison of the FE solutions against physical evidence. Model calibration is a knowledge-based process, and regardless of the sophistication of its tools, the success of model calibration relies on the suitability of a series of decisions made while building the initial FE model. This initial FE model must be a close enough representation of reality to initiate the automated calibration. Therefore, an automated calibration must be preceded by a test-analysis correlation.

The FE model of a bridge, for instance, may be developed by modeling the girders with beam elements or with three-dimensional solid elements. Similarly, one can consider including the barriers in the FE model, or excluding them. The bridge abutments can be represented as fixed or hinge conditions available in the FE model, or by using linear or nonlinear springs. The importance of investigating alternative model schemes to obtain a model sufficiently close to reality has been stressed by many researchers (Brownjohn and Xia 2000, Pavic et al. 2002, Bagchi 2005, Pavic et al. 2007).

A correlation metric is required to compare the success of these alternative FE models in matching the experiments. The specifications of these metrics are the most important component of the correlation processes. Correlation metrics are mainly dictated by the selected comparative features. They may be as simple as taking the difference of two features or as complex as statistical correlation analysis (Hemez 2007).

During test-analysis correlation, major problems arise due to the mismatch of number of degrees of freedom in the FE model and experimental set-up and due to the

inaccuracies of the initial FE model. FE models typically have significantly larger numbers of degrees of freedom compared to the test campaigns. There are three main approaches to the degrees of freedom mismatch between the FE model and test campaign: (1) reducing the FE model solution, (2) expanding the test data, (3) truncation of the FE model solution without reduction (Friswell and Mottershead 1995, FEMtools 2007). For the first approach, reduction techniques allow the full system matrices of the FE model to be reduced down to a few degrees of freedom. The most popular and perhaps the simplest reduction method is the Guyan reduction, through which the elemental matrices are partitioned into master and slave coordinates (Guyan 1965). Alternatively, the partitioning procedure can be applied to the computed eigenvectors, a method known as SEREP (O'Callahan et al. 1989, Avitabile et al. 1989, Avitabile et al. 1992). However, from the point of view of model calibration, calibration of a reduced FE model has limited physical meaning (Dascotte 2004). For the second approach, expansion of measurement data is invariably done according to the initial FE model, whether using elemental matrices of the FE model or by using its modal predictions. The test data expansion according to the information obtained from a known-to-be inaccurate FE model may yield erroneous results, and the subsequent calibration may be adversely affected. Therefore, examples of such procedures will not be discussed herein. The last option is the mere truncation of the large degrees of freedom of an FE model to only a few of those that were selected as measurement data points. Although this option limits the test analysis correlation to a select few locations on the structure, it is immune from potential complication and errors of the reduction and expansion processes.

After the test and analysis comparative features are matched in size through reduction, expansion, or truncation, the correlation metrics can be calculated. The two main types of correlation metrics are the fidelity-to-data metric and the regression metric. The fidelity-to-data metric measures disagreement between measurements and numerical model output. Taking the difference between calculated and measured natural frequencies is a fidelity-to-data metric. The regression metric measures the correlation between measurements and numerical model output. The statistical correlation of the mode shapes can be identified as the cosine of the angle between the two vectors representing the mode shapes. If the calculated and measured mode shape vectors align perfectly, the angle between the two vectors would be zero, and the correlation would be equal to unity. Conversely, if these two modes are completely unrelated, their vectors would be perpendicular to each other, and the correlation would be equal to zero. The relation of finding the angle between two vectors is given in Equation 3-14 and is widely known as the Modal Assurance Criterion (MAC) metric (Allemang and Brown 1982).

$$MAC(\{\phi_M\},\{\phi_T\}) = \frac{\left|\{\phi_M\}^T\{\phi_T\}\right|^2}{(\{\phi_M\}^T\{\phi_M\})(\{\phi_T\}^T\{\phi_T\})} \qquad (3\text{-}14)$$

where $\{\Phi_M\}$ is the mode shape vector of the model, and $\{\Phi_T\}$ is the mode shape vector of the test.

Over the last three decades, several correlation metrics were developed in the context of linear dynamics. Examples include eigenvalue orthogonality criterion, which checks whether the measured mode shape vectors transform the mass and stiffness

matrices in diagonal forms (recall Equation 3-5); coordinate MAC, which applies the MAC principle on spatial degrees of freedom; coordinate orthogonality check, which investigates how much spatial degrees of freedom contribute to the orthogonality check; displacement assurance criterion, which applies the MAC principle to displacement vectors; and signature assurance criterion, which applies the MAC principle to FRF vectors (FEMtools User Manual 2007).

Test-analysis correlation can also be classified by the amount of available information, and it can be as simple as a visual comparison in viewgraph form (Figure 3-11a). The most common approach for deterministic models is the feature-to-feature comparison (Figure 3-11b); however, this type of correlation has the risk of deriving erroneous conclusions (Figure 3-12). The deterministic test-analysis correlation may compare the sampling points that are not representative. To guarantee that the expected values of the two random distributions, the mean values must be calculated. This requires the probability distribution of the variable to be constructed.

Distribution-to-feature correlation is seldom meaningful and not commonly adapted (Figure 3-11c). Figure 3-11d represents the first-level distribution-to-distribution correlation where only the numerical error bounds are incorporated as a result of a verification study. Figures 3-11e and f show the increasing sophistication levels of distribution-to-distribution correlation considering the uncertainty due to lack of knowledge as well. This type of correlation necessitates statistical analysis and is the only way to incorporate the uncertainties into the calibration process.
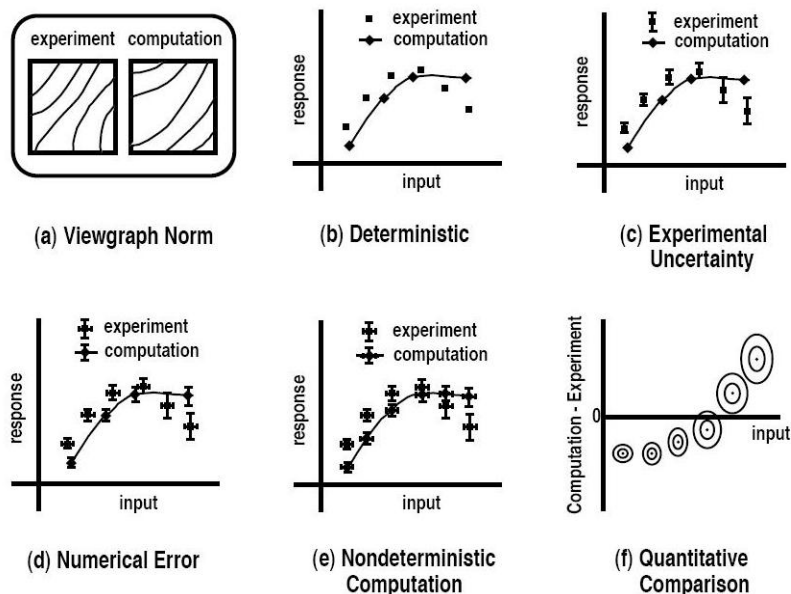
Figure 3-11:   The increasing levels of sophistication for test-analysis correlation (Oberkampf et al. 2002, with permission).

The ease of comparing EMA comparative features with FE solutions is the rationale for the popularity of EMA in model calibration. However, when modal

parameters are used in test-analysis correlation, pairing of mode shapes becomes a crucial and often a problematic task. Difficulties arise because the initial FE model, as stated earlier, is imprecise: thus (1) it may predict the modes in the wrong sequence; (2) it may fail to predict some of the modes; or in the worst case (3) it may predict the modes as linear combinations. All of these potential problems require careful, perhaps automated, mode tracking through the test-analysis correlation. This topic will be discussed in greater detail in Chapter 4.
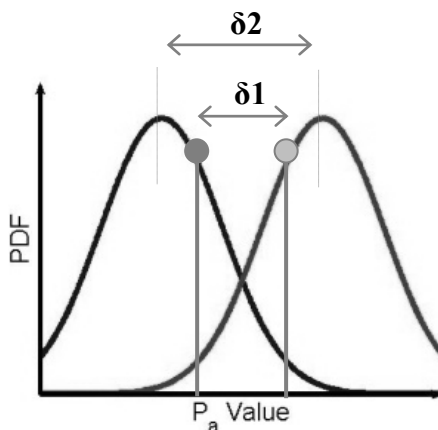
Figure 3-12: The feature-to-feature comparison (δ1) versus distribution-to-distribution comparison (δ2).

3.7 Bayesian Model Calibration Under Uncertainty

In model calibration, one attempts to improve the predictive abilities of an initially inaccurate computer simulation through comparisons of one (univariate) or more (multivariate) of its solutions with incomplete and imprecise physical observations (Friswell and Mottershead 1995). The procedure implemented in this study for the characterization of modeling parameters has two fundamental components: mathematical formulation of calibration algorithm and propagation of uncertainty, which are discussed in the next sections.

3.7.1 Mathematical Formulation of Calibration Algorithm

An FE model can be judged to be valid based on (1) the accuracy of the model parameters and (2) the adequacy of the model. The former can be remedied by the parameter-calibration approach while the latter can be remedied by the bias-correction

approach. In this study, the imprecise parameters of the FE model will first be calibrated against experimental measurements to improve the fidelity of the FE model to physical evidence. However, because an FE model is only a mathematical approximation of reality, and thus inadequate to a certain extent, even when the best parameter values are used, a bias error will remain between the model predictions and experimental measurements.

The approach implemented in this study will be introduced in the following paragraphs. Detailed theoretical background of the adapted methodology can be found in Higdon et al. (2008) and Kennedy and O'Hagan (2000).

The method is developed from the following relation for experimental measurements $Y(x_i)$:

$$Y(x_i) = \zeta(x_i) + \varepsilon(x_i), \qquad i = 1,......,n \tag{3-15}$$

where $\zeta(x_i)$ denotes the true response of the actual physical system, $\varepsilon(x_i)$ represents the experimental error, and n represents the number of control variables (x_i). Accordingly, the experiments are conducted at n different settings.

The controlled variables define the validation domain, that is, the domain of configurations, settings, or operational conditions under which the model is developed to make predictions. The most important distinction between controlled variables and calibration parameters is the lack of control over the latter during physical testing. Calibration parameters are either introduced by a specific choice of model, by a specific assumption, or by virtue of being parameters that cannot be measured or controlled experimentally.

The true response of the actual physical system where $\zeta(x_i)$ is then broken down into a simulator and a discrepancy term that denotes the discrepancy between the simulator and reality.

$$Y(x_i) = \eta(x_i, \theta) + \delta(x_i) + \varepsilon(x_i), \qquad i = 1,......,n \tag{3-16}$$

where $Y(x_i)$ and $\eta(x_i, \theta)$ are experimental and numerical predictions, $\delta(x_i)$ corresponds to the discrepancy term representing the bias, and $\varepsilon(x_i)$ represents the random experimental error. θ here denotes the best but unknown values for the calibration parameters. However, because θ is unknown, during forward propagation of uncertainty, the model is executed at a family of settings, t:

$$\eta(x_j, t_j), \qquad j = 1,......,m \tag{3-17}$$

where m denotes the number of computer runs. The model output is only known at m different settings, while the experimental output is only known at n different settings.

Because an understanding of the formulation of each of these components of Equation 3-17 is fundamental, each item is discussed separately in the following sections.

3.7.1.1 Surrogate Model – $\eta(x, t)$

As mentioned previously, for cases where the simulation is demanding of computational resources, an FE model can be run only at a limited number of settings (at limited values of *(x, t)*, where *x* is the control variable and *t* is the calibration variable). Thus, to forecast the model predictions at settings other than those sampled, a surrogate model will be fit to the available data. There is a clear distinction between an FE model, which depends on the physical relationships of elements and their characteristic properties, and a surrogate model, which is a purely mathematical function that defines the relationship between input and output while entirely disregarding the involved physics.

Common surrogate models take the form of polynomial fits. In this study, however, the numerical model is replaced by a Gaussian process model (GPM). A GPM can be fully described by its constant mean, $\mu(x)$, and covariance structure (Equation 3-18). Details of its formulation can be found in Santner et al. (2003) and Higdon et al. (2008):

$$COV\left((x,t),(x't')\right) = \frac{1}{\lambda_\eta} \prod_{k=1}^{p_x} \rho_{\eta,k}^{4(x_k - x'_k)^2} \times \prod_{k=1}^{p_t} \rho_{\eta,p_x+k}^{4(t_k - t'_k)^2} \tag{3-18}$$

λ_η and ρ_η are called hyper-parameters. λ_η is to control the marginal precision of the surrogate model and ρ_η is to control the dependence strength for each control and calibration parameter. p_x denotes the number of control variables and p_t denotes the number of calibration parameters. The parameter $\rho_{\eta,k}$ represents the correlation between model outputs evaluated at input parameters by varying the parameters in k^{th} dimension.

Among various surrogate models, a GPM is preferred to define a prior form of an unknown function for two reasons. First, it is nonparametric and thus no prior assumption is necessary about the parametric family of the function. Second, a GPM is very flexible and smooth, which enables it to represent nonchaotic continuous systems remarkably well. However, the construction of an intricate input-output map requires a number of computer experiments to be performed beforehand at sampled input values.

After the GPM is constructed based on the *m* computer runs defined by the design of experiments, the subsequent steps in calibration operate only on the GPM, which means that if the GPM is not constructed accurately, the calibration will converge to irrelevant solutions. The common practice is to consider that accurate GPM surrogates are obtained when the number of computer experiments is 10 times or more the number of calibration parameters (Williams 2008b).

3.7.1.2 Discrepancy Model – $\delta(x)$

The role of the discrepancy term in this formulation is analogous to the bias term as implemented in the bias correction approach. The discrepancy term is an error model

intended to develop an independent estimate of the inadequacies in the model predictions at all controlled parameter settings. The discrepancy is defined as the Euclidian distance between the mean of the physical measurements and the mean of the numerical model output at the true but unknown calibration parameter values. Higdon et al. (2008) replaces Kennedy and O'Hagan's discrepancy term with a GPM. The GPM for discrepancy model has a zero mean. Its covariance function takes the following form:

$$COV(x,,x^{'}) = \frac{1}{\lambda_\delta} \prod_{k=1}^{p_x} \rho_{\delta,k}^{\;4(x_k - x^{'}_k)^2} \tag{3-19}$$

where λ_δ and ρ_δ are called hyper-parameters. λ_δ is to control the marginal precision of the discrepancy model and ρ_η is to control the dependence strength for each control and calibration parameter.

One cannot calculate the discrepancy until the true input parameters are found. However, one cannot estimate the true input parameter without knowledge of the discrepancy. The solution of Kennedy and O'Hagan (2000) for this seemingly paradoxical problem is explained in the discussion of propagation of uncertainty.

The addition of an independent error estimator, the discrepancy term, is the far-reaching accomplishment of these earlier studies. However, because this study is conducted without the controlled variables, the discrepancy term will be a scalar, and thus will be less meaningful than earlier studies by Higdon et al. (2008), which operate on varying settings of controlled variables.

3.7.1.3 Experimental Errors – $\varepsilon(x)$

Although physical observations are subject to random and bias errors, they constitute our best representation of physical reality. Thus, the calibration process is obligated to tolerate experimental errors. Experimental uncertainty is typically categorized in two groups: (1) measurement uncertainty, for instance due to instrumentation and data processing, and (2) natural variability of the structure, for instance in heterogeneous materials.

The variability of physical experiments can only be studied by repeated experiments. However, the experiments are typically costly and time-consuming relative to the FE models. It is a common application to repeat only a portion of the experiment. For instance, in a test setup with k measurement points, repeating the experiments at a select few measurement points ($<<k$) can reduce the required resources yet can still yield reasonable information about the inherent variability in the experiment.

In engineering and science, experimental errors are commonly incorporated in the analysis with the help of probability theory. Typically, the error term is defined as a zero-mean Gaussian random variable. Such an approach is best justified by the central limit theorem. If we assume that the experiments are conducted with rigor and are immune from systematic errors due to such factors as bias in the equipment, the experimental error can be considered to be a summation of a large number of independent processes.

According to the central limit theorem, these sources would collectively converge to a normal distribution (Hogg and Craig 1978).

3.7.2 Propagation of Uncertainty

When both the FE model input and FE model output are treated in a probabilistic manner, two types of uncertainty propagation are required. Determining how much uncertainty in the selected calibration parameters causes variability in the output is referred to as forward uncertainty propagation. The inverse uncertainty propagation, in contrast, investigates the sources of uncertainty in the output by focusing on the variability of calibration parameters (Figure 3-13).

The forward propagation of uncertainty consists of a family of computer runs repeated at the sampled input parameters to observe the variability in the FE model outcomes, as discussed in Section 3.5.2. As long as a large enough number of samples are generated, this sampling approach converges to the actual distribution of the output parameter. The number of necessary samples depends strictly on the order of complexity of the sampled behavior and on the type of sampling design.

Inverse propagation of uncertainty is computationally more involved as it conceptually requires the FE model to be inverted. However, for real engineering solutions, the requirement of inverting an FE model is practically prohibitive because of the discretization-based approximate approach inherent in the FE analysis.
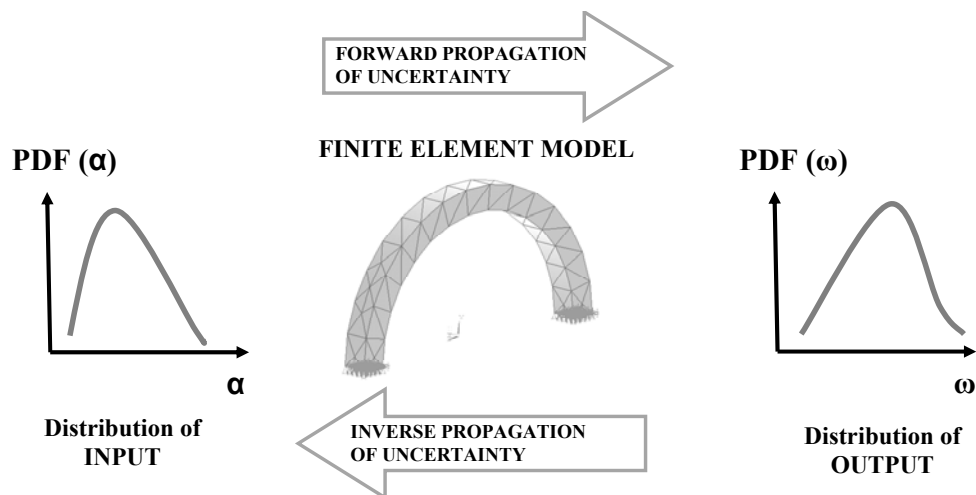

Figure 3-13: The operative philosophy of model calibration.

In stochastic model calibration, the inverse propagation of uncertainty forms the basis of the statistical inference problem. In theory, if the uncertainty in input can be

reduced, the uncertainty in the output will also be reduced. Thus, the inverse propagation of uncertainty is usually called upon in model calibration activities to seek the sources of the output uncertainty.

In the formulation adapted in this study, the inverse propagation of uncertainty is replaced by a large cohort of forward propagation of uncertainty via Markov Chain Monte Carlo (MCMC) sampling. MCMC performs a random walk in the domain defined by the calibration parameters defined by α_1 and α_2 in Figure 3-14 according to the probability distribution of the calibration parameters: $P(\alpha_1)$ and $P(\alpha_2)$. In the absence of better knowledge, the probability distribution of calibration parameters can be assigned equal probability for all possible values between an upper and lower limit. During each random walk, the model calculates the selected output response according to the sampled parameter values. Comparative feature is defined by ω in Figure 3-14. The acceptance criterion for the sampled parameters is guided by the likelihood estimation $P(\omega \mid \alpha_1, \alpha_2)$. The current sample point (in the domain of the calibration parameters α_1 and α_2) is rejected if it reduces the likelihood that the set of calibration parameters is correct. If the current sample point is rejected, the random walk returns the last accepted point and the probability distributions of the calibration parameter remain unchanged. However, if the sample point is accepted, the posterior distributions of calibration parameters are obtained. These posterior distributions of the calibration parameters become the prior distributions in the next random walk. According to the current priors, MCMC performs another random walk from the last accepted point to the next point (Figure 3-14). The repeated feedback in Bayesian inference progressively characterizes not only the posterior distributions of the calibration parameters, defined by α_1 and α_2 in Figure 3-14, but also the hyperparameters of the GPMs, λ_η, λ_δ, ρ_η, and ρ_δ. That is to say, if there are n MCMC iterations, there will be n different sets of estimates for hyperparameters and calibration parameters that are accepted by the likelihood function. By using the hyperparameters of the GPM of the discrepancy term, one can now construct the error model, and by using the calibration parameter values along with the hyperparameters of the simulation emulator, one can construct the surrogate model. Thus, the method defines all possible values of $\eta(x; t)$ and $\delta(x)$ that, when added together, reproduce the experiments as described in Equation 3-17.

The mean estimates of the posterior distribution provide the most likely values for the calibration parameters. These values, when obtained through stochastic calibration, can later be used in a deterministic study. The standard deviation of the posterior distributions captures the remaining uncertainty in the parameter values. Theoretically, as the amount of physical evidence increases, the remaining uncertainty converges to the natural variability of the materials. Further discussion on this statement can be found in Atamturktur et al. (2009a).
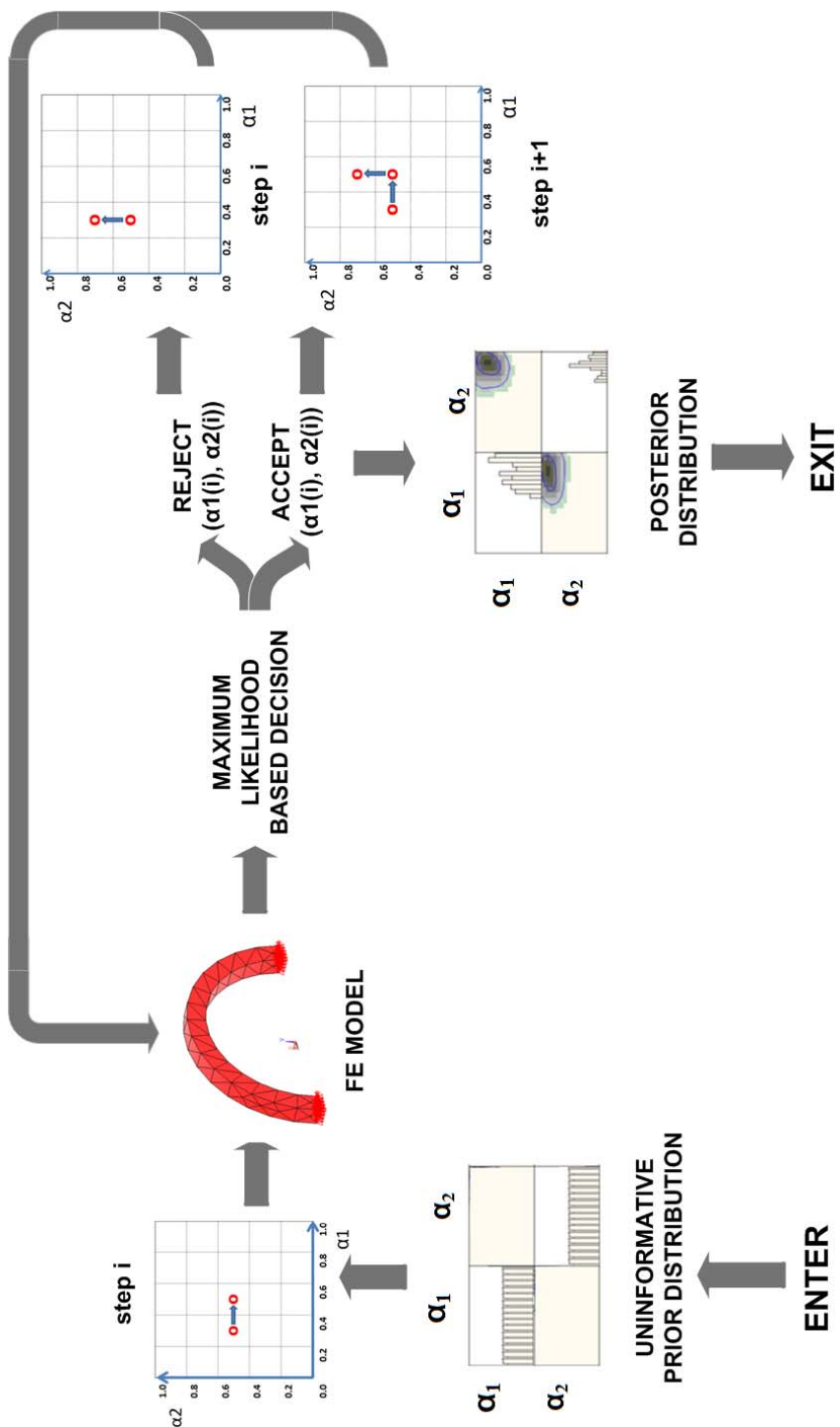
Figure 3-14: Combining MCMC with the context of Bayesian inference.

3.8 Special Considerations for Masonry Structures

Boothby and Atamturktur (2007) discussed some of the principles of unreinforced masonry and provided basic instructions in preparing an FE model of complex vaulted masonry structures using widely available, modern tools of structural analysis. In Section 3.8.1, the most important aspects of this paper are summarized.

As emphasized in Section 3.3, modal testing is an art as much as it is a science (McConnel 2008). The success of modal testing depends heavily on the experience about the test structure. Atamturktur et al. (2009a) highlighted the particular challenges of low-amplitude vibration testing on historic masonry structures. In Section 3.8.2, relevant aspects of this paper are summarized.

3.8.1 FE Model Development for Masonry Monuments

Two main FE modeling approaches are available for masonry structures: micromodeling and macromodeling. The former focuses on the heterogeneous states of stress and strain using the properties of individual masonry units and mortar joints. For micromodeling, the amount of computational effort necessary for analysis of an existing building is impractical. Macromodeling, in contrast, assumes homogenous constitutive behavior for the masonry and mortar assembly and, therefore, is commonly applied to model large-scale structures. The suitability of the homogenized material property assumption has been confirmed in numerous studies (Creazza et al. 2002). Therefore, the discussion in this section will focus on macromodeling.

There are four main aspects related to the structure that need to be defined in FE model development: (1) geometry, (2) material properties, (3) boundary conditions, and (4) loads. The coupling and dependencies between these further complicate the problem—for instance, connectivity conditions depend on material properties, and material properties may change according to loading, whether due to time-dependent material behavior or due to material nonlinearity. Moreover, decisions must also be made regarding the (1) element types and (2) meshing according to the available options in the FE program. All of these factors will be discussed in the following sections. The illustration and examples will be provided with reference to computerized FE program ANSYS, version 11.

3.8.1.1 Geometry

FE model development starts with geometric model generation. Typically, building survey measurements or available construction drawings can be used to locate reference points that define the curved geometry of a three-dimensional vaulted structure.

The profile of load-bearing arches of the vaults, unless seriously distorted due to loading or settlement effects, can be adequately characterized by the coordinates of span, rise, and quarter-point rise. The vault ribs generally have a constant thickness, therefore, any means of determining the dimensions of a rib, whether by measurements or consulting drawings, is sufficient. The actual shape of the vault web between ribs can then be generated with few additional measurements taken from the curved web surface. Vaults are often provided with a filling from the supports up to the haunches and the height of this filling must be measured. The thickness of webbing may be difficult to determine unless there are holes in the vault. Impact-echo and other noninvasive tools for the determination of thickness are available for use (Sansalone 1997).

Complex molding profiles or multiple colonnettes on the ribs and piers are practically impossible to model accurately, and the effort spent on attempting to model these shapes often degrades the model's accuracy because of unavoidable poor aspect ratios in meshing. The physical geometry of the piers and ribs of vaults are typically simplified to rectangles that preserve the area and moments of inertia of the original cross section. Figure 3-15 depicts such simplification for the cross sections of ribs of Washington National Cathedral. It must be noted that the error introduced by this geometric simplification cannot be remedied via calibration of other FE model parameters. The suggested principle is to simplify the geometry unless the geometrical details impact the dynamic response that the model must capture. This can be decided by isolating a structural member, such as a rib, and analyzing it with the original and simplified cross-sectional geometry.

a) Highly ornamented rib.   b) Simplified rib geometry.
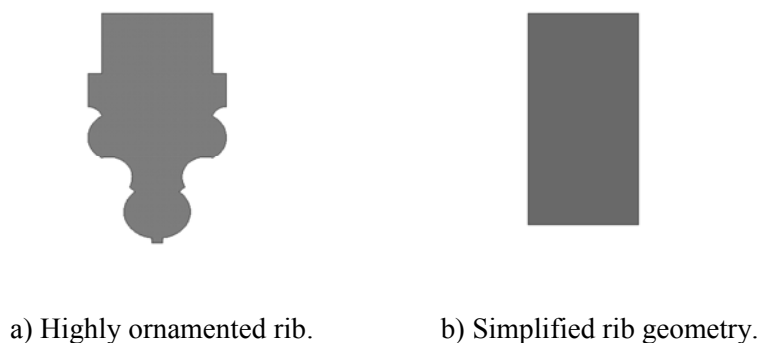
Figure 3-15: Property-preserving simplification of the rib geometry.

Although theoretically possible, implementing geometric properties as calibration parameters is problematic because of difficulties in meshing these complex geometric forms (see Section 3.8.1.3). Therefore, obtaining the most reliable geometric properties available is a high priority—errors caused by remaining inaccuracies must simply be accepted.

3.8.1.2 Element Type Selection

In most FE packages, modeling capabilities are available to represent a structural dynamics response using a variety of element types and selection mainly depends on the degrees of freedom they provide.

Shell elements are economical compared to solid elements. Vault webbing can be successfully modeled by shell elements as they incorporate interactions between membrane forces and bending moments that characterize the behavior of vault webbing. Shell elements can represent bending, membrane, and shear stiffness.

Shell elements can be used to model both singly curved or doubly curved surfaces of varying thickness. Both quadrilateral-form (four node) and triangular-form (three node) elements can be defined by shell elements. Typical shell elements have six degrees of freedom at each node: translations in the nodal x, y, and z directions and rotations about the nodal x, y, and z axes. Shell elements with mid-side nodes have improved ability to fit curved surfaces compared to other shell elements without the mid-side nodes.

In this study, shell element SHELL93 in ANSYS is used (Figure 3-16). For the triangular-form element, six nodes and the three thickness values for the corner nodes must be defined. For quadrilateral-form elements, the definitions of eight nodes and four corner thickness values are required. The displacement variable is interpolated in quadratic fashion within these elements (ANSYS 11.0 2009).

Solid elements, on the other hand, are suitable for vault ribs and walls. In solid elements along an edge without a mid-side node, the displacement variable varies linearly, while along an edge with a mid-side node element, the displacement variable varies parabolically. SOLID95 in ANSYS has mid-sides nodes along the edges and a total of 20 nodes with three degrees of freedom per node: translations in the nodal x, y, and z directions (Figure 3-17). Prism-shaped, tetrahedral-shaped, and pyramid-shaped elements may also be formed by SOLID95 elements as shown in Figure 3-17. Solid elements typically require at least a nine-element cross section for computational accuracy.
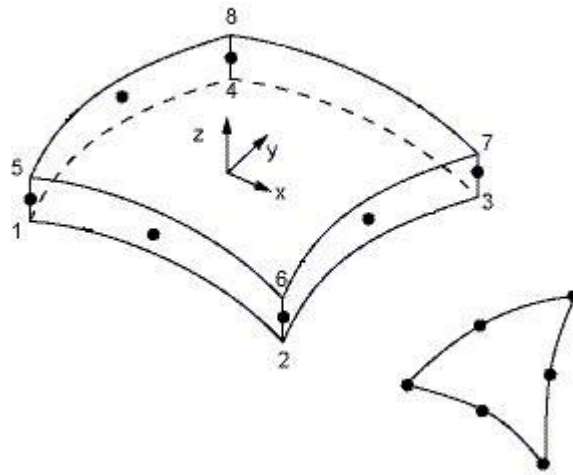
Figure 3-16: SHELL93 in ANSYS reprinted from ANSYS tutorial (2009), with permission.
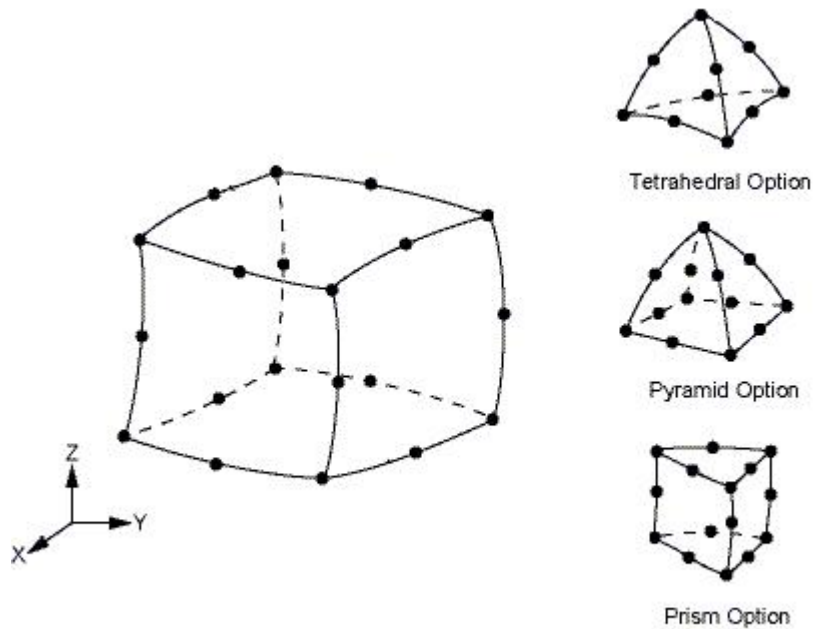
Figure 3-17:   SOLID93 in ANSYS reprinted from ANSYS tutorial (2009), with permission.

3.8.1.3 Meshing

Meshing is the systematic process of discretizing the geometric model into finite elements. While meshing, there is always a trade-off between reducing the computational time and increasing the resolution and the accuracy of the solution. Steenackers and Gullaume (2006) emphasized that FE models with coarse mesh girds tend to overestimate the stiffness of the structure and this artificial stiffness increases in turn results in the overestimation of natural frequencies. Also a mesh that is too coarse can result in severe numerical truncation errors, while a mesh that is too fine will result in excessive run times. The truncation errors can be determined by tools of solution verification (Hemez 2007). Solution verification is performed by comparing model solutions to a reference solution. The reference solution can be obtained by various methods, one of which is to perform multiple runs of the same problem with successively refined meshes, then, using an extrapolation technique, to estimate the solution that would be obtained if the calculation could be carried out with "infinite" resolution, that is, $\Delta x \rightarrow 0$. The two main tools that support solution verification activities are the development of solution error Ansatz models and the grid convergence index (GCI). Solution error Ansatz models describe the properties of asymptotic convergence of discrete solutions, while the GCI can be used to estimate bounds of numerical uncertainty (Roache 1998). These techniques apply only to FE model runs performed within the regime of asymptotic convergence.

The solution error Ansatz model is an equation that describes the rate at which the discrete solution $y(\Delta x)$, obtained by running the calculation at increasingly reduced mesh size Δx, converges to the reference solution $y^{Reference}$. The equation takes a functional form:

$$\left| y^{\mathrm{Re}\,ference} - y(\Delta x) \right| = \beta(\Delta x^{p})$$

(3-20)

where the symbol β is a pre-factor coefficient and "p" denotes the rate of convergence. The triplet $(y^{Reference}; \beta; p)$ represents the unknowns of the Ansatz equation and a mesh refinement study with a minimum of three runs provides enough equations to estimate these unknowns.

Alternatively, the rate of convergence of the numerical method can be estimated as

$$p = \frac{\log\left(\dfrac{y(\Delta x_{M}) - y(\Delta x_{C})}{y(\Delta x_{F}) - y(\Delta x_{CM})} \right)}{\log(R)}$$

(3-21)

where Δx_{C}, Δx_{M}, and Δx_{F} refer to the coarse-mesh, medium-mesh, and fine-mesh element sizes, respectively, provided that convergence is monotonic. Symbol R denotes a refinement ratio that is assumed, without loss of generality, to be constant, that is, $R = \Delta x_{C}/\Delta x_{M} = \Delta x_{M}/\Delta x_{F}$. When the mesh size is not uniform, the mesh size can be approximated as

$$\Delta X = \left(\frac{V}{N_e} \right)^{\frac{1}{D}} \tag{3-22}$$

where V denotes the area or volume of the computational domain, N_e is the total number of finite elements and D denotes the dimensionality of the problem ($D = 2$ for a two-dimensional geometry and $D = 3$ for a three-dimensional geometry) (Hemez 2007).

A mesh refinement study is carried out for a two-dimensional arch modeled with SHELL93 elements in ANSYS. Finite elements are halved in each dimension of the mesh, so the refinement ratio is $R = 2$ and the number of elements between any two successive runs is multiplied by a factor of four. Table 3-4 lists the resonant frequencies of modes 1 to 3 for the four meshes analyzed.
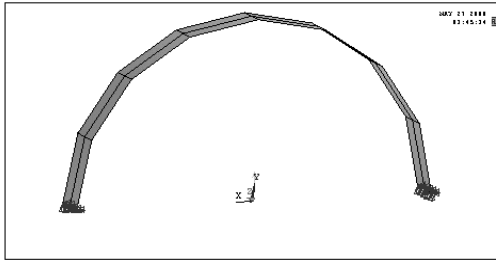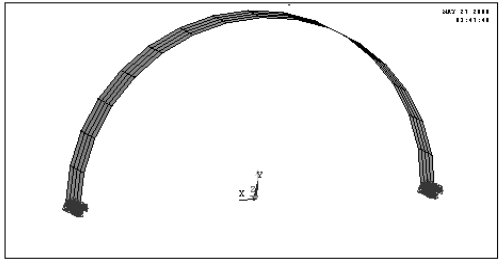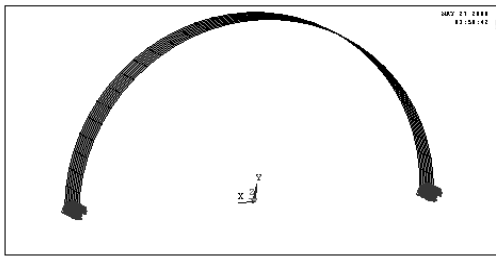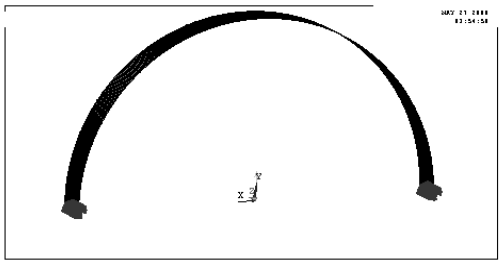
When the rate of convergence is estimated using either the first group of three (coarse, medium, fine) runs or the second group of three (medium, fine, extra-fine) runs, the value of $p = 2$ is consistently obtained. It means that convergence is second-order as $\Delta x \rightarrow 0$, which matches the formal order of accuracy of SHELL93 elements. (These elements define quadratic shape functions, hence, $p^{Theory} = 2$.)

The reference solution that these discrete solutions converge to, as $\Delta x \rightarrow 0$, can be estimated from

$$y^{Reference} = \frac{R^p y(\Delta x_F) - y(\Delta x_M)}{R^p - 1} \tag{3-23}$$

as 0.09317 Hz for the first resonant frequency. It means that, should the coarsest mesh size be used to run the calculation, one expects a 0.12% overestimation of the first natural frequency. Likewise, running the calculation at the coarsest mesh size overestimates the second natural frequency by 0.5% only. These levels of numerical error (due to mesh size) are small compared to the typical variability of measurements that results from vibration tests. It is concluded that, as long as a mesh size finer than $\Delta x \leq 30$ cm is used to discretize the FE model, numerical error will not pose a problem.

Table 3-4: Results of the Mesh Refinement of an Arch Discretized with SHELL93 Elements

Coarse Mesh (16 Elements)		Medium Mesh (64 Elements)	
Mode-1 Frequency	0.09328 Hz	Mode-1 Frequency	0.09317 Hz
Mode-2 Frequency	0.28596 Hz	Mode-2 Frequency	0.28458 Hz
Mode-3 Frequency	0.58312 Hz	Mode-3 Frequency	0.57486 Hz
Fine Mesh (256 Elements)		Extra-fine Mesh (1,024 Elements)	
Mode-1 Frequency	0.09317 Hz	Mode-1 Frequency	0.09317 Hz
Mode-2 Frequency	0.28449 Hz	Mode-2 Frequency	0.28448 Hz
Mode-3 Frequency	0.57429 Hz	Mode-3 Frequency	0.57426 Hz

3.8.1.4 Material Properties

The stress-strain law of masonry is largely nonlinear. Masonry units exhibit inelastic behavior both in tension and compression due to irreversible softening effects. In tension, after the crack develops normal to the stress, softening occurs because closing stiffness of the crack is much less than Young's modulus of the material. In compression, softening occurs due to the development of cracks parallel to stress and crushing of concrete.

In common applications, masonry assemblies are anisotropic and inhomogeneous due to the presence and orientation of mortar joints. When analyzing the global response of the structure, modeling the real behavior of a masonry assembly is practically impossible, and thus approximations and assumptions must be made to represent the materials in the FE model. Boothby and Atamturktur (2007) emphasized that although it is by far simplest to work with linearly elastic, homogeneous, isotropic material properties, significant progress in the assessment of a masonry structure can be made using this simple form of constitutive law.

Masonry material properties can be obtained by consulting reference documents, by conducting tests on extracted material coupons, by conducting tests on refabricated prisms of similar material, or by methods of nondestructive evaluation.

Consulting reference material often provides limited information, as the material property values for historic masonry assemblies are poorly known for several reasons. One main difficulty is that historic structures lack a standard formulation for mortar; moreover, there is almost never archival documentation available about the content of the mortar used in the construction. Additionally, changes occur to the properties of mortar due to the effects of hardening with aging. Conducting material tests poses unique challenges because of the difficulty in keeping a mortar joint intact during the extraction process. The extraction of masonry prisms follows the procedure of ASTM C1587. The determination of the properties of the extracted mortar can be made according to ASTM C1324 (Boothby and Atamturktur 2007).

Refabrication of masonry and mortar prisms in laboratory, using mortar of similar properties to the original mortar, allows an estimate of tensile and compressive properties of the homogenized assembly. Prisms are tested for compressive strength properties according to ASTM C1314, while stiffness properties may be determined by the application of ASTM E111. Flexural bond strength may be tested according to ASTM E518 (Boothby and Atamturktur 2007).

Semidestructive or nondestructive evaluation techniques are also commonly applied to determine the material properties of masonry systems. Semidestructive flat-jack testing can be used to determine the elastic stiffness properties or compressive stresses of solid masonry (ASTM C1196 and ASTM C1197). Nondestructive methods can also be used to determine material properties of masonry structures. These methods include acoustical, ultrasonic imaging, and impact-echo (Binda and Saisi 2002).

3.8.1.5 Boundary Conditions

When only a subcomponent of a structure is of interest for the analysis, the modeled portions of the structure are supported by the portions excluded from the model. Hence, assumptions are needed while quantifying the physical properties of these supports and representing them as idealized boundary conditions. Because many physical responses, such as stresses, strains, and modal parameters, are highly sensitive to the boundary conditions, the precise definitions of boundary conditions are crucial to accuracy. This can be illustrated on a simple two-dimensional arch (Figure 3-18). The arch is modeled with 64 SHELL93 elements in ANSYS. It has a 6-m radius, 1-m depth, and 0.1-m thickness.
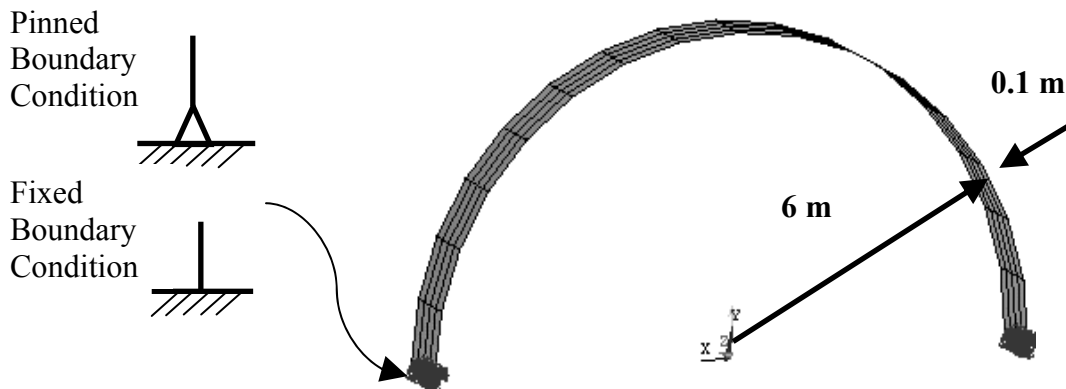
Figure 3-18: Two-dimensional arch example.

The maximum vertical displacement of the arch and support reactions under gravity loading are observed to differ significantly when the arch is modeled with fixed boundary conditions restraining all the translational and rotational degrees of freedom versus pinned boundary conditions restraining only the translational degrees of freedom. The observed changes in the predictions are almost identical to changes that would be introduced by overestimating the Young's modulus (or density) of the homogenized stone and mortar assembly by a factor of 100%. As seen, boundary conditions, if modeled inaccurately, can cause significant inaccuracies in the model.

The task of defining boundary conditions is challenged because neither fixed nor pinned boundary conditions occur in real structures. In some situations, a fixed or pinned boundary condition approximation may be a close enough representation of the reality. Shear and moment connections in steel structures are good examples of this. In other situations, the connection can only be approximated realistically by a semifix (or semiflexible) representation. Translational or rotational springs can be used to represent these types of boundary conditions. The springs can be linear or nonlinear in the restraint they provide. Linear springs are advantageous because the only variable is the spring constant to define the force-displacement diagram. Nonlinear springs may be used for

more sophisticated analysis; however, the necessary properties of force-displacement diagrams are often unknown.

3.8.1.6 Loads

After the boundary conditions are assigned, the initial model is ready for analysis. The loading condition for which the response is desired is defined by what is known about the structure and what is expected to be learned from the FE model. Loading conditions take, for example, the form of static loading, abutment movement, gravity loading, wind loading, or time-varying seismic loading. Typically, static analysis is used to examine the structural behavior under self-weight or service loading conditions. Therefore, static analysis requires gravitational acceleration and, if present, external loads due to nonstructural components to be defined. Modal analysis is independent from load input, as it delivers the characteristics of the mass and stiffness distribution of the structure. Transient and harmonic analysis options are available in FE analysis to simulate the seismic, wind, or blast events. These analysis options require time-dependent loading to be defined by the user.

3.8.2 Dynamic Experiments on Masonry Monuments

The use of experimentally obtained modal parameters (natural frequencies, modes of vibration, and modal damping ratios) and their derivatives for model calibration necessitates an accurate identification of these structural system parameters. Both traditional modal analysis and operational modal analysis may be used for this purpose.

Traditional modal analysis applies a known, controlled excitation to the structure, while operational modal analysis exploits unknown, natural excitation sources. Traditional modal analysis has the benefit of enabling the experimenter to control the excitation type, location and amplitude, and the preferential excitation of selected modes of vibration. Operational modal analysis has the benefit of eliminating the need for controlled excitation, therefore, it is generally more economic and less logistically challenging compared to traditional modal analysis.

Atamturktur et al. (2007) applied both traditional and operational modal analysis techniques on a Gothic cathedral. Traditional modal testing was conducted with an impact hammer excitation. The operational modal testing was conducted with various excitation sources: carillon bells, peal bells, orchestra, organ, and ambient vibration. The authors stated that certain natural frequencies found by traditional modal analysis were omitted from the sequence of frequencies determined by the operational modal analysis. Also, traditional modal testing with hammer excitation was emphasized to yield cleaner FRFs and clearer mode shapes compared to operational modal analysis.

The present study is, therefore, confined to traditional modal testing. Common excitation devices used for traditional modal analyses are impact hammers, shakers, and heel-drops. Among these controlled excitation devices, the impact hammers have proven themselves to be portable and more feasible compared to shakers or heel-drop tests; therefore, further discussion will be confined to hammer testing.

In hammer testing, both the acceleration response of the structure and the impulse of the hammer are recorded in time domain. These signals are then transferred into the frequency domain. The ratio of the system response to the hammer impulse yields the FRF. As discussed in Section 3.1, through these FRFs modal parameters are extracted.

From a practical point of view, modal analysis always remains incomplete due to the limitations in number of measurement points. The incompleteness of measurements, combined with the problems posed by spatial aliasing, force the test-analysis correlation to be completed with only a few lower-order modes (Denoyer and Peterson 1996 and Bagchi 2005). A realistic objective for the tests described herein would be to develop a test campaign to accurately identify the first 10–15 modes of typical masonry vaults.

3.8.2.1 Instrumentation

Providing an even and uniform excitation is difficult with an impact hammer due to the high crest factor. Also, the inherent damping in masonry structures tends to absorb the localized energy introduced by the impact force before it propagates to distant accelerometer locations. The energy level must be adjusted to excite all measurement locations sufficiently above the ambient noise level without inducing nonlinearity in the system. The more the structure has cracks and separations, the more it will be prone to problems due to nonlinearity. With the impact hammers, the softest tip, which offers the lowest frequency range, must be used to keep the undesirably high frequencies from filling the lower-frequency spectra.

The usual driving-point response to a typical impact blow is initially limited to 1.5–3.0% g and decays rapidly to 0.02–0.05% g, which is the typical level of ambient vibration. An accelerometer sensitivity of 1 V/g or greater is suitable (Hanagan et al. 2003). If the vibration response is measured perpendicular to the curved vault surface, significant uncertainties are introduced when mounting the transducers on rough masonry texture and in decomposition of the collected response into three coordinates. Given the double curvature of the vault surface, however, vertical or horizontal mounting of transducers requires some form of a mounting base.

The placement of the exciter must be decided according to the anticipated mode shapes. In general, the complex geometry of the vaults yields clustered modes that, near the point of excitation, are excited in phase and amplify the motion while they tend to neutralize each other at other points. By analyzing multiple datasets due to excitations at different locations, it may be possible to isolate these repeated or closely spaced modes. Moreover, some particular modes, hidden when the excitation point coincides with the nodal lines, may be acquired when the impact force is applied elsewhere. Experience gained through field tests conducted on masonry vaults reveals four optimum excitation

locations for acquiring comprehensive definition of the vaulted system, even when the number of available transducers is limited. The first point, the crown (Point 1 in Figure 3-19), primarily excites the modes that are made up of symmetric vertical motion. The rest are on the diagonal (Point 8 in Figure 3-19), transverse (Point 12 in Figure 3-19), and longitudinal ribs (Point 3 in Figure 3-19), which excite the bending modes. System identification from the FRFs obtained by exciting these locations would also be easier, as each impact location activates only a select few of the modes.
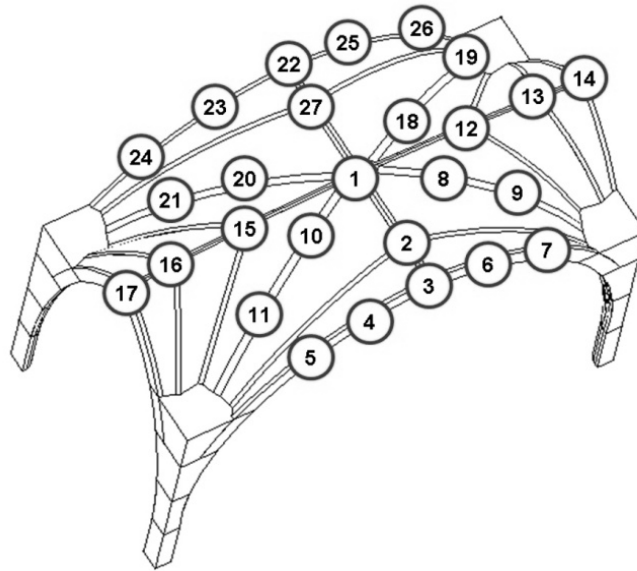
Figure 3-19: Test grid adapted during the tests on Washington National Cathedral, DC.

The primary modes of the typical vaulted systems, as illustrated in Figure 3-20, are rather easy to detect. However, the higher-order modes become much more complicated. Even insignificant deviations in the excitation location or angle may stimulate different modes and degrade the quality of the mode-shape definitions.
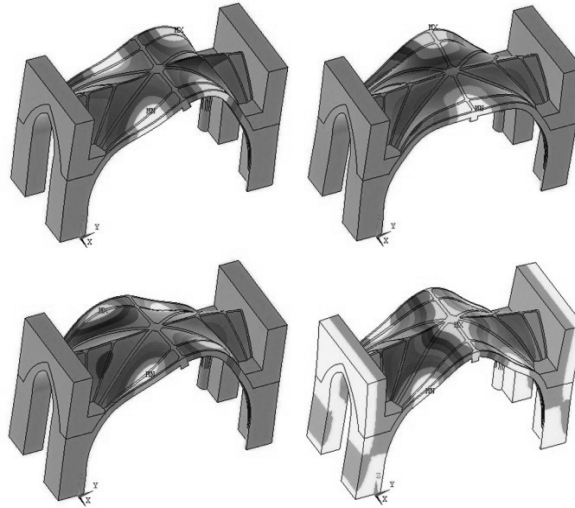
Figure 3-20: The primary modes of vertical vibration in complex vaulted systems.

3.8.2.2 Data Acquisition

The upper limit of the frequency bandwidth of interest is provided by the number of modes desired to be identified and their frequency range. Atamturktur et al. (2009a) reported the modal test results from five historic Gothic churches of varying architectural style, age, and geographic location. The results of these tests showed that, for exercises intending to extract up to the first 10–15 modes of vaulted sections of Gothic structures, a 50 Hz usable frequency bandwidth is sufficient.

Masonry systems tend to have high damping, caused by the friction forces between the stone units and opening and closing of the cracks. As the structural response dies out rather rapidly due to high damping, it may be tempting to acquire the measurements in a short time window. However, the clustered modes of the vaults necessitate a reasonably fine-frequency resolution (Δf <0.2 Hz), which in turn necessitates a relatively long data-capture time ($T > 5$ seconds). Because Fourier transform from time domain to frequency domain occurs at discrete frequencies inversely proportional to total data capture time (T), there is always a trade-off between the frequency resolution and data capture time.

$$\Delta f = \frac{1}{T} \tag{3-24}$$

Exponential window functions, commonly used to avoid leakage problems or to eliminate the environmental noise, have been found undesirable for modal testing of

masonry structures since they introduce artificial damping to the measurements and potentially cause low-amplitude modes to be dominated by high-amplitude modes (Avitabile 2001).

3.9 Concluding Remarks

In this chapter, the scope of model calibration is expanded from one that ignores the presence of uncertainty to one that relies on the definition and propagation of parameter uncertainty. Calibration in the Bayesian framework is not an optimization problem, which minimizes a cost function representing a form of disagreement between the test and analysis. Instead, the procedure discussed herein is a process of iterative characterization of probability distributions of the parameters. As the iterative calibration takes place, uncertainty in the calibration parameter distributions will be reduced, and in turn the uncertainty in the model output is also reduced. The need to tackle the problem of calibration probabilistically is driven by our inability to define the model parameters and conduct experiments in a deterministic way.

The tasks discussed in this chapter are neither inexpensive nor rapid enough to be immediately implemented in routine civil engineering. However, they may be developed into a procedure useful in management of complex structures.

Chapter 4

WASHINGTON NATIONAL CATHEDRAL

All models are wrong; some are still useful.

George Box

4.1 Introduction

The vaults of Gothic churches are among the most vulnerable elements of historic structures and certainly among the most challenging structural components to analyze. Gothic churches are built with empirical techniques balancing the gravitational forces exerted by rib vaults with the nave walls, buttresses, and piers in a way that is not yet fully understood. Traditional methods, based on the states of stress or strain, are not generally applicable to the three-dimensional force-balance problem of rib vault analysis. As a result, three-dimensional tools of finite element (FE) analysis have gained popularity in the analysis of these structures. This dissertation targets complex vaulted systems, particularly for their static, quasistatic, and dynamic analysis through the FE method.

In FE analysis, it is advantageous to model only a portion of the structure, typically the portions where the structural problems are present, instead of modeling the entire church. Subcomponent modeling not only reduces the computational time of the FE model, but also significantly reduces the necessary preliminary work; for instance, compare the geometric survey and inspection of an entire church versus a small portion of the church. Despite their major advantages, subcomponent models are very difficult to build, because they require accurate identification of force transfer from the subcomponent FE model to the adjacent but unmodeled structural components.

This chapter illustrates the application of stochastic model calibration, introduced in Chapter 3, to the subcomponent FE model of Washington National Cathedral choir vaults. The poorly known parameters of the FE model, such as the selected material properties of masonry assembly and spring constants that represent the support components of the subcomponent model, will be calibrated based on experimental measurements, so that the calibrated FE model reproduces the physical reality with increased fidelity.

4.2 Description of the Structural System

The Washington National Cathedral was designed as authentic Gothic Revival architecture in the early twentieth century and construction began in 1903. The construction technique of the Cathedral closely followed medieval techniques by using quarried stone without reinforcement. Similar to medieval examples, the construction was interrupted several times over a century and the Cathedral was eventually completed in 1990 (Washington National Cathedral 2004).

The Cathedral is vaulted with even-level crown, fan vaults elevated above the stone piers. This study focuses on one of the nominally identical fan vaults in the choir. The vaults are composed of stone ribs and webbing supported by stone piers, walls, and buttresses (Figure 4-1). The plan view of the Cathedral indicating the location of the test vault of interest is given in Figure 4-2, while the section view of the vaults is given in Figure 4-3. The geometric dimensions of the vaults are illustrated in Figure 4-4.

(a)   **(b)**
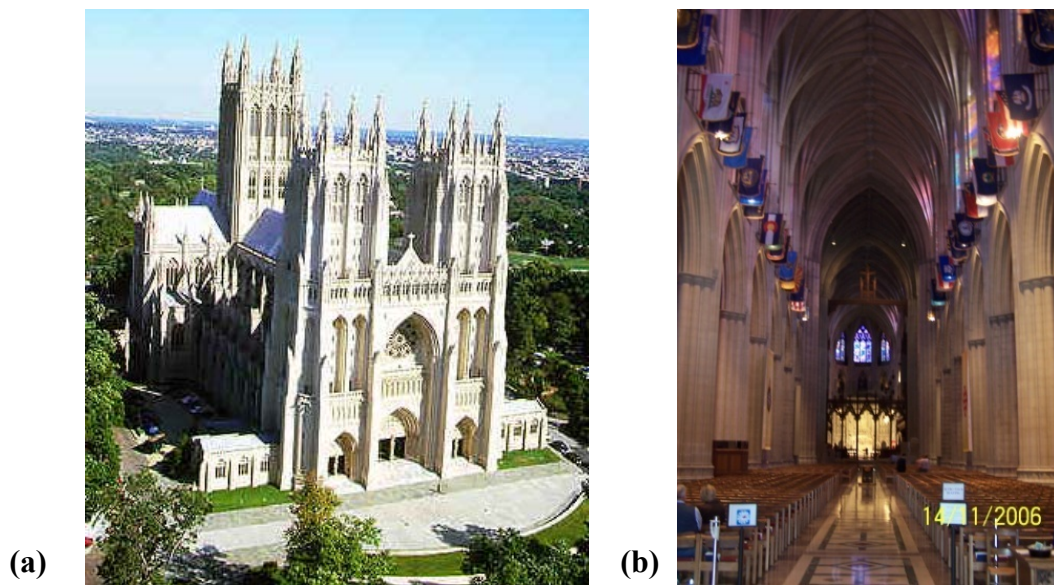
Figure 4-1: The nave of the National Cathedral: a) exterior view, b) interior view.

Because the focus of this dissertation is directed towards stochastic calibration methods, working on a complex and uncertain civil engineering system is only natural. The reasons why the Cathedral is selected for the present study are threefold. The first reason is that the author had easy and unlimited access to the structure for field investigations and dynamic testing. The second reason is that the Cathedral, being a relatively young structure, provided an example of medieval style construction without severe complication of accumulated damage and undocumented prior repairs. This aspect is certainly responsible for the good quality correlation obtained between test and analysis results. The third reason is the fact that full geometric drawings of the Cathedral

were available to the author. This aspect increased the fidelity of the FE model geometry to the existing structure.
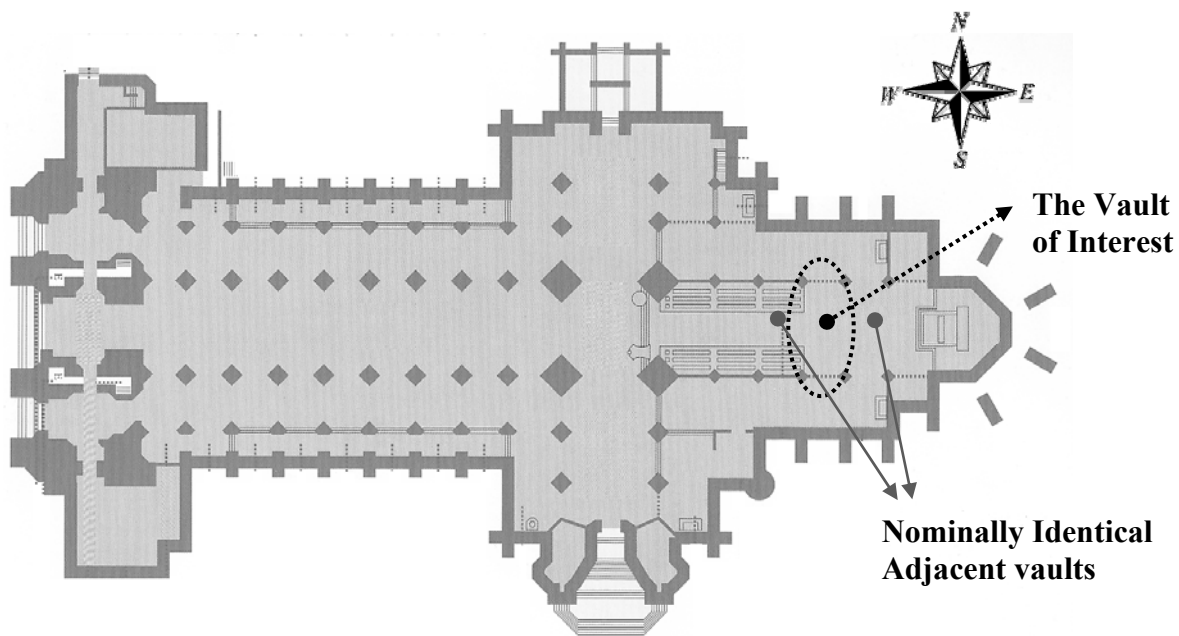
Figure 4-2: Plan view of Washington National Cathedral.
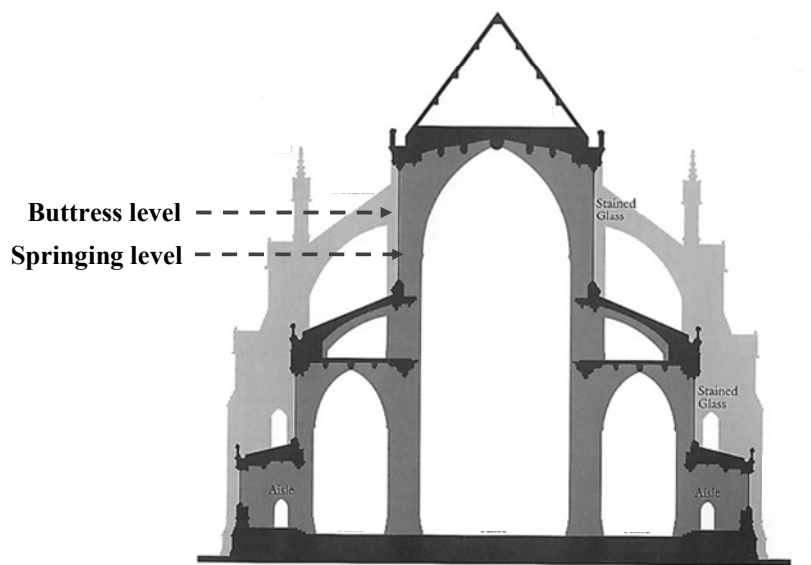
Figure 4-3: Section view of Washington National Cathedral.

4.3 Finite Element Model Development and Parameterization

The first objective is to create an FE model of the masonry vaults. A subcomponent FE model that includes only the structural components above the springing level is built. Because the Washington National Cathedral is a recent construction, a set of construction drawings is available, and the geometry of the vaults used in this chapter is primarily derived from these documents. The structural components, moldings, and decorations are replaced with simpler rectangular forms respecting the cross-sectional area and moment of inertia. Information about any potential factor that may induce nonsymmetric behavior, whether due to prior damage or construction variations, is difficult to obtain and to incorporate in the FE model. Therefore, the model geometry is idealized and the model is built based on a double symmetry assumption (see Figure 4-4). This aspect of the FE model will be further investigated during test-analysis correlation.

The FE model is built based on the *a priori* assumption of linearly elastic, isotropic constitutive behavior. By comparing the predictions of the FE model with measurements, the extent to which this assumption is acceptable will be investigated.

Table 4-1 presents the expected ranges for material properties of the vaults. These upper and lower limits for limestone are tabulated according to published tests. Erdogmus (2004) completed a test on a spare limestone specimen obtained from Washington National Cathedral and homogenized the Young's modulus of this specimen with expected values of type O mortar. The Young's modulus range for the limestone mortar assembly obtained in Erdogmus (2004) is rather large, because it not only represents the variability of the properties of both limestone and type O mortar but also the variability of the thickness of the mortar joints.

Table 4-1: Limestone, Brick, and Concrete Material Properties Expected Range

Component	Material Type	Modulus of Elasticity (E)		Density (d)
		Low	High	Nominal
Walls, Columns, Vault ribs, & webbing	Indiana Limestone and Type O Mortar	8×10^9 N/m^2 *	21×10^9 N/m^2 *	2100 kg/m^3
Fill	Concrete	21.5×10^9 N/m^2	24.8×10^9 N/m^2	2100 kg/m^3
Walls	Brick	7.5×10^9 N/m^2	11×10^9 N/m^2	2100 kg/m^3

*These values neglect the presence of voids and cracks. Therefore, lower values may be observed in existing structures.

(a)   Plan

18.0 m

1.8 m   **1.8 m**

6.6 m

R=8.6 m

R=6.2 m

9.6 m

4.6 m

5.0 m

**(c)   Elevation
Looking West**

9.6 m

4.6 m

5.0 m

**(b)   Elevation
Looking North**

6.6 m

1.9 m   **1.9 m**

Figure 4-4**:** Geometric dimensions of the vaults.
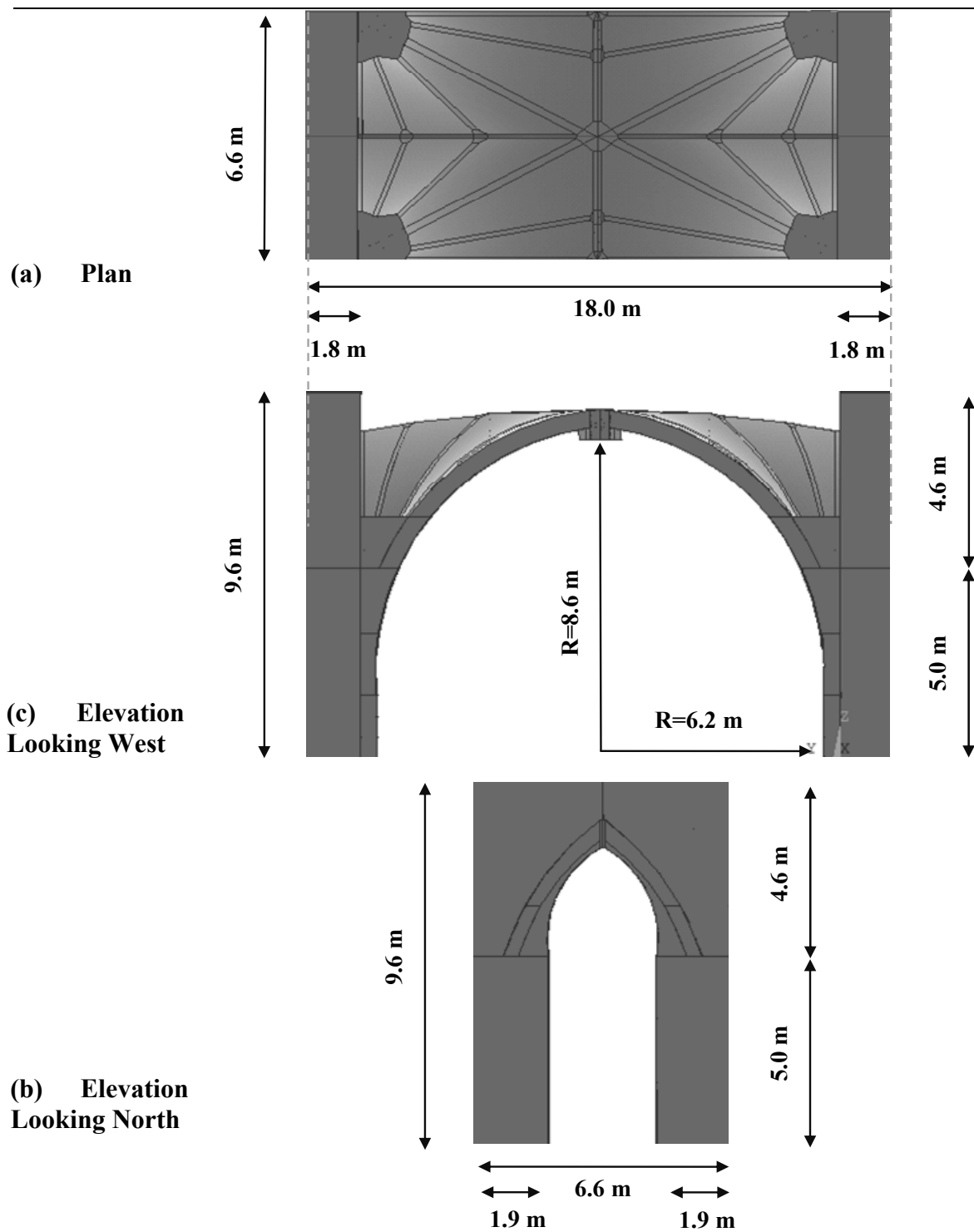
The upper and lower limits for the material properties of concrete had to be estimated for this study, since no prior study in literature addressed the issue and specimens for laboratory testing were unavailable. The Young's modulus of the fill is estimated based on a concrete compressive strength of 3000–4000 psi. The upper and lower limits for the material properties of brick are obtained from the extensive manual of the National Research Council (1982).

Figure 4-5 illustrates the construction of the Cathedral vaults, where the limestone ribs and vault webbing as well as the brick nave walls can be seen. Figure 4-6 presents the element and material types used in the development of the model. Although the ribs, piers, and webbing are all built of limestone, their material properties are evaluated independently, and parameterized as $\theta 1$, $\theta 4$, and $\theta 5$, respectively. This is done to address three issues: (1) the potential use of limestone from different quarries for different structural components, (2) the difference in mortar joint thickness, and (3) the differences in material behavior between highly and lightly loaded members due to load-dependent material behavior of stone units. The concrete fill and the brick upper nave walls are parameterized as $\theta 2$ and $\theta 3$, respectively (Figure 4-6).
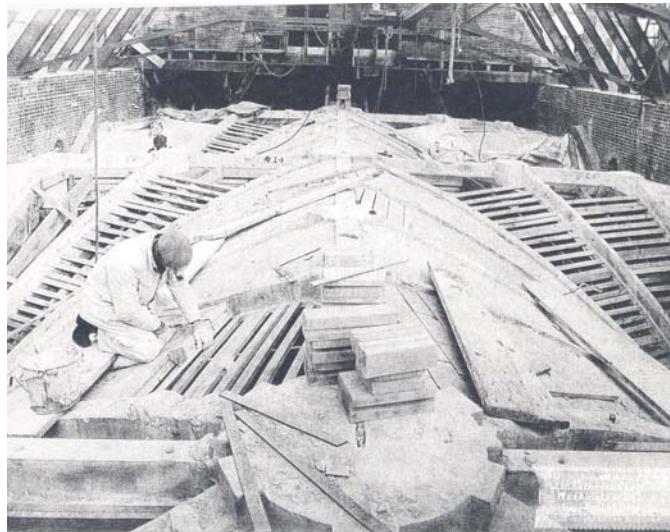
Figure 4-5: The construction of the Cathedral (Cathedral Archives, with permission).
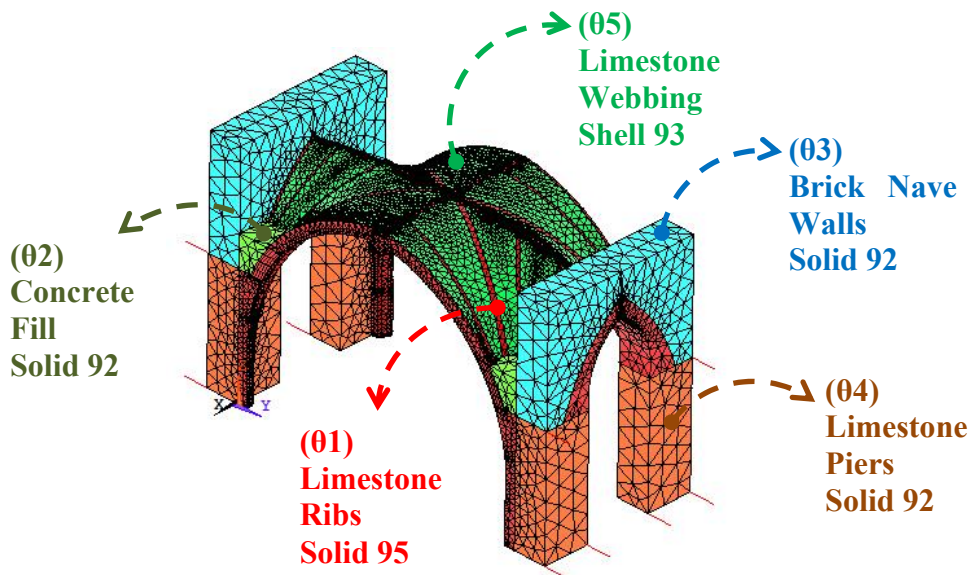
Figure 4-6: Full bay model of Washington National Cathedral: element and material types.

Compared to the rest of the structure, the components immediately adjacent to the vaults, such as upper portions of nave walls and piers, as well as the concrete fill, have a greater influence on the structural behavior of the vaults. To simplify the FE model, components, which are not in immediate contact with the vaults, are replaced by boundary restraints. The effects of the buttressing system and of lower nave piers are replaced with linear springs exerting restraints on horizontal translation (Figure 4-7). However, *a priori* knowledge on the stiffness characteristics of these two types of linear springs is highly uncertain, therefore, these characteristics are likely candidates for calibration. To reduce the size of the problem, the pier-to-pier variations between four piers or buttress-to-buttress variation between four buttresses are ignored, and the springs for all four quadrants of the vault are assumed to be perfectly symmetrical.

Figure 4-7 presents boundary conditions definition in the full bay model. The vertical movement of the pier bottoms is expected to be negligible compared to their horizontal movement. Therefore, at the springing level, the bottoms of the piers are fixed in vertical translation (z direction in Figure 4-7). Similarly, the deformation along the longitudinal direction of the cathedral is also expected to be minimal because the vault of interest is supported by two nominally identical vaults on two sides. Therefore, horizontal translation (x direction in Figure 4-7) at the pier bottoms is restrained. For the horizontal translation in the transverse direction (y direction in Figure 4-7), the bottoms of the piers are restrained by two linear springs, of which the constant is kept as a variable to be calibrated ($\theta 6$ in Figure 4-7). The horizontal restraining effect of a second-level buttress is represented by a single linear spring, with an independent spring constant. Aside from

Center Line

Center Line

Linear Spring
Type 1: Springing Level
Type 2: Buttress Level
(y direction)

x

y

(a)   Plan

Restrained in x direction

Center Line

(θ7)
Linear Spring Type 2
Buttress Level
(y direction)

(b)   Elevation
Looking West

z

y

(θ6)
Linear Spring Type 1
Springing Level
(y direction)

All Pier Bottoms
Restrained in
Vertical Direction
(z direction)

Center Line

Restrained
in x direction

(c)   Elevation
Looking North

z

x

All Pier Bottoms
Restrained in
Vertical Direction
(z direction)

Figure 4-7: Full bay model of Washington National Cathedral, boundary conditions.

the factors previously discussed for masonry connections such as material properties, workmanship, and existing cracks, the horizontal restraint of the buttresses is dependent on the geometric form of the buttresses and the soil condition at the support of the buttresses. As a result, this horizontal restraint is highly uncertain, and thus the stiffness constant of the buttress level springs are parameterized to be calibrated ($\theta7$). Both faces of the vaults, along the longitudinal direction of the Cathedral, are restrained in x direction to represent the restraint from the adjacent nominally identical vaults (Figure 4-7).

4.4 Dynamic Experiments

Physical evidence for the FE model calibration was obtained in the form of acceleration response of the vaults due to impact hammer excitation (Figure 4-8). The impact hammer type was selected according to the necessary impact force required to excite the vaults sufficiently above the ambient vibration level and to obtain a high signal-to-noise ratio. A 5.5 kg PCB model 086D20 instrumented sledge-hammer, capable of applying a peak force of 22 kN, was found to be suitable for these purposes. During the tests, the typical excitation amplitude applied to Washington National Cathedral choir vaults was about 2.5 kN.
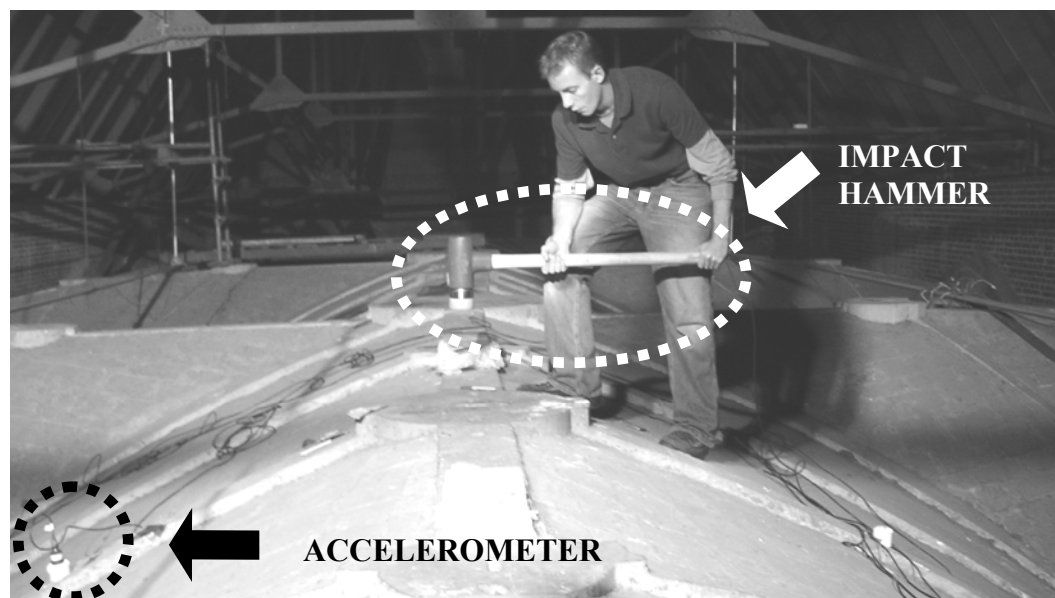
Figure 4-8: Vibration testing equipment in action.

Model 393A03 uniaxial seismic accelerometers, manufactured by PCB Piezotronics, Inc., with a frequency range of 0.5–2000 Hz and a sensitivity of 1 volt/g

were used. The accelerometer layout on the choir vault can be seen in Figure 4-9. Point 1 (crown), point 3 (longitudinal rib), point 8 (diagonal rib), and point 12 (transverse rib) were selected as the excitation locations. These locations were selected to excite the maximum number of fundamental modes of the vaults.
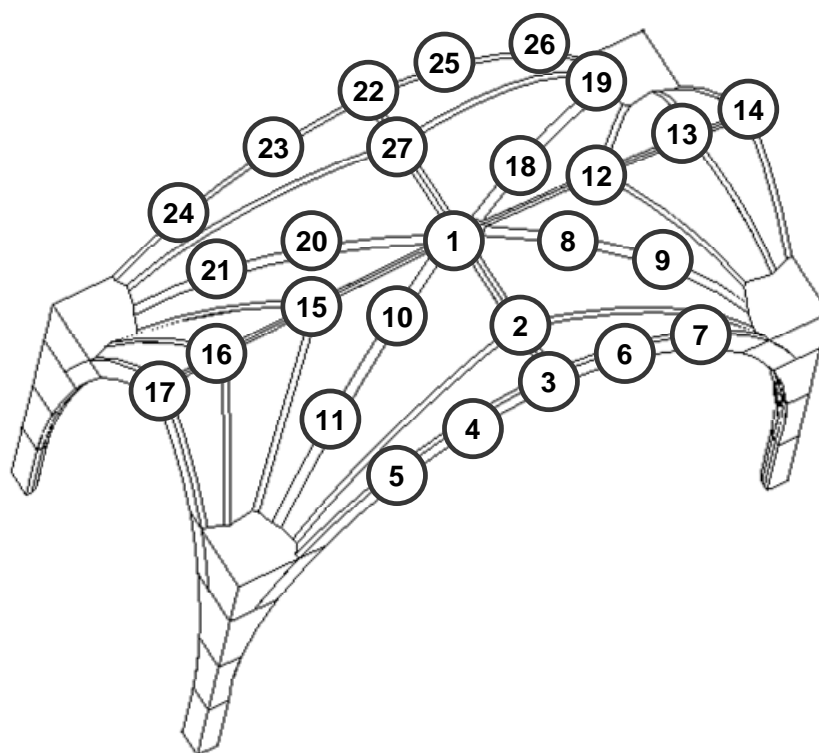
Figure 4-9: The 27 measurement points at the bosses where ribs intersect and at every third point of the diagonal and transverse ribs.

The data were processed and recorded by a Dactron data acquisition system, manufactured by LDS Test and Measurement, Ltd. The record length and sampling frequency were adjusted to 1024 and 187.5 Hz, respectively, so that the response of the vaults attenuated within the time frame of 5.4 seconds. The response of the vaults was fully captured in a single time frame and the leakage of higher-frequency energies over the lower frequencies was prevented. A typical time domain measurement of hammer impulse and acceleration response can be seen in Figure 4-10. The variables of signal-processing equipment are given in Table 4-2.

(a) Impact Hammer excitation.   (b) Response of the Vault.
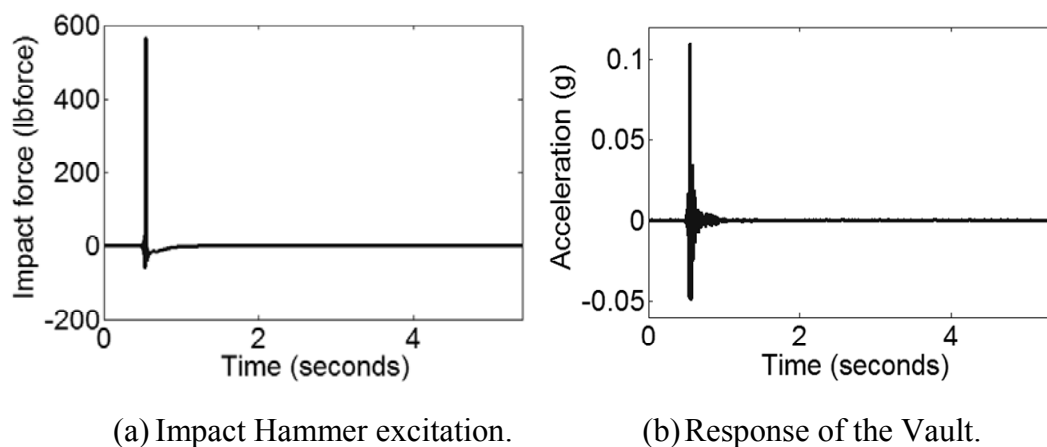
Figure 4-10: Typical response history measurements: a) hammer impact, b) vibration response.

Table 4-2: The Variables of the Digital Signal-Processing Equipment

Parameter description	Parameter value
Data acquisition time	5.46 s
Frequency resolution	0.18 Hz
Frequency bandwidth	93.75 Hz
Frequency range of interest	1–36 Hz
Sampling frequency resolution	187.5 Hz
Total number of samples	1024
Number of frequency lines	450
Number of averages	5
Window function	Boxcar (no window)

The frequency response functions (FRFs), previously defined in Section 3.1, of five repeated tests were averaged to reduce the degrading effects of ambient vibration and to quantify the quality of the measurements in the form of coherence functions.

The general assumption of modal analysis is that the system is linear, stationary, and time-invariant. The structure of interest here can safely be considered to exhibit a stationary response. The time-varying effects are primarily caused by environmental variations, such as temperature and moisture. These effects are minimal for the duration

of the experiment. However, the linearity assumption remains to be checked through reciprocity checks and linearity checks.

Because a linear system must obey the laws of reciprocity, the deviation from the reciprocal behavior can be used to assess the validity of the linearity assumption. Figure 4-11 demonstrates the comparison of response at Point 12 due to an excitation at Point 1, with the response at Point 1 due to an excitation at Point 12. The area of the disagreement between the two FRFs is calculated to be only 11.3% of the total area under the average of the two FRFs over the entire frequency range and 7% over the frequency range up to 40 Hz. Reciprocity checks, when repeated at other measurement locations, yielded similar results. It must be noted that these discrepancies are also due to test-to-test variability from hammer excitation, accelerometer placement, ambient vibration, and equipment noise. Therefore, it is evident that discrepancy due to reciprocity is even less than 7%.
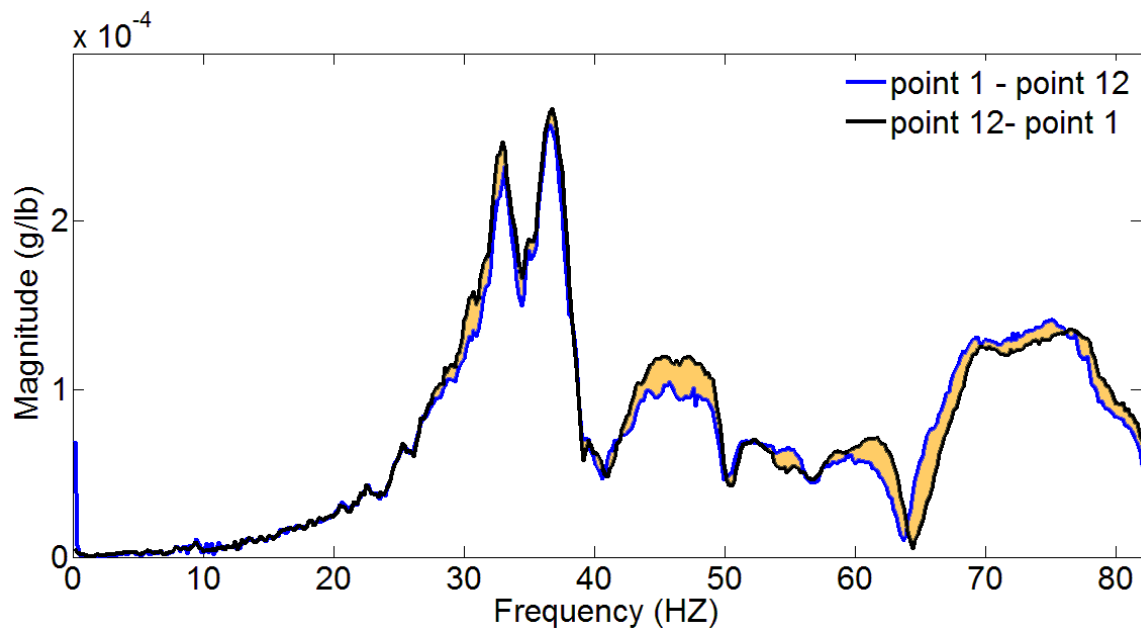
Figure 4-11: The reciprocity check between points 12 and 1.

Determining whether the deviations in the reciprocity check is acceptable is another aspect where judgment is necessary. Considering the inherent variations in the testing as well as in the tested structure, obtained correlation between FRF(1,12) and FRF(12,1) is deemed to be acceptable. Also, the peaks of these two FRFs remain nearly unchanged, therefore the modal parameters identification will only be very minimally affected by the presence of the deviations.

The main problem associated with hammer excitation is the inability to maintain a constant excitation across averaged datasets. This requires exciting at constant force and a constant angle with the vibration surface. In theory, a linear system has a unique FRF at varying excitation levels; therefore, in theory, variations in hammer excitation should not

pose deviations between FRFs provided that the structure exhibits linearity. Thus, deviation between the FRFs obtained at varying excitation levels can be used to confirm the linear response of the structure for the excitation levels of interest.

The typical excitation during the test varied between 500 lbs and 700 lbs. Figure 4-12 portrays the frequency domain response measurements as well as the coherence function for these two excitation levels. The area of the disagreement between the two FRFs is calculated to be only 5.5% of the total area under the average of the two FRFs over the entire frequency range and 4.5% over the frequency range up to 40 Hz.
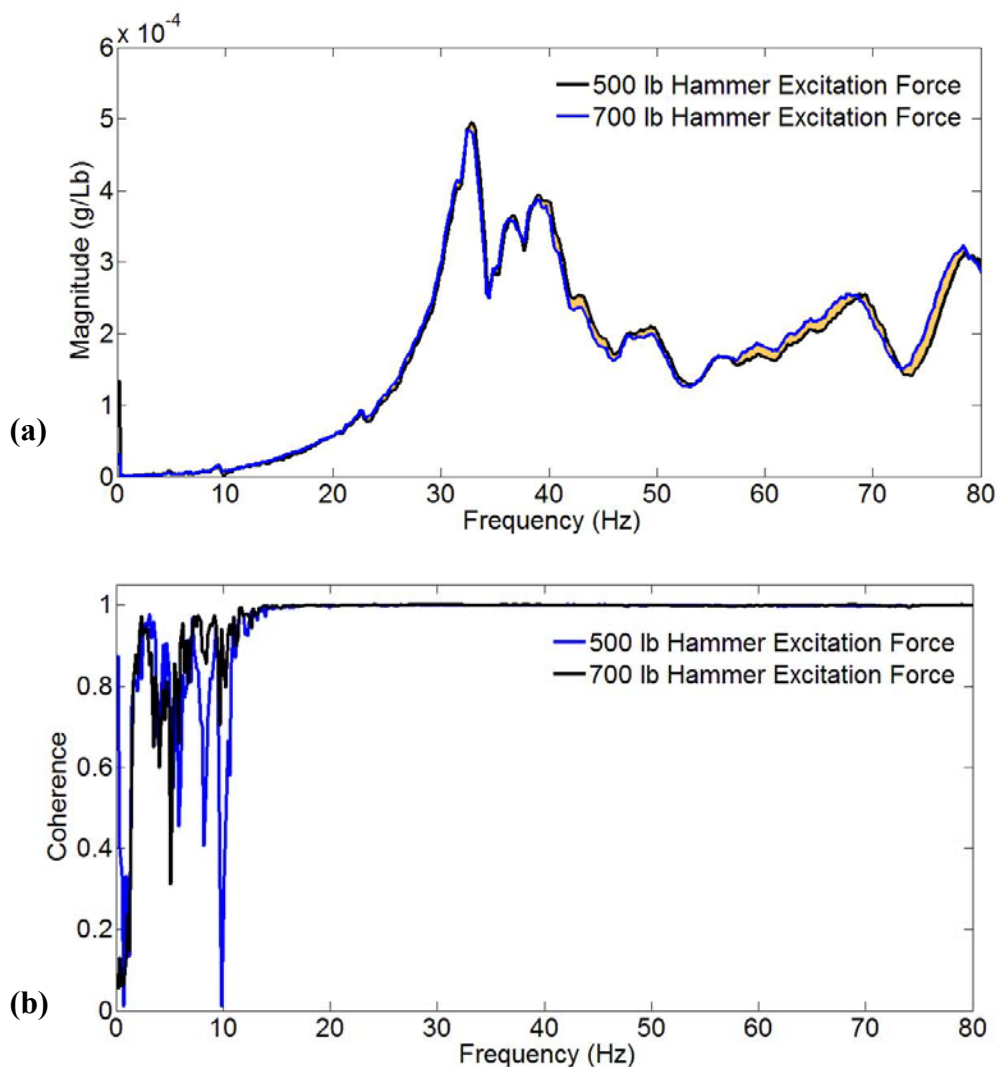
Figure 4-12: The linearity check with varying input levels: a) the driving point magnitude FRF for at the crown of the vault, b) the corresponding coherence function.

4.5 Selection of Comparative Features

Time-history measurements are highly sensitive to ambient vibration and instrumentation noise. As a result, comparing two time histories with each other is only meaningful when based on an averaging scheme over a long duration (see statistical moments for instance, Hemez 2007). Also, comparing the time-history response measured from the vaults against the simulated time-history response would not be meaningful unless the damping is included in the FE model.

Because of the complications of using raw time-history measurements, modal parameters, introduced in Chapter 3, are selected as comparative features. Modal parameters reduce raw acceleration time-history measurements into lower dimensional information about the structure and make probabilistic test-analysis correlation computationally manageable. Also, modal parameters are less sensitive to test-to-test variability and ambient vibrations compared to a time-history measurement or an FRF. Therefore, the use of modal parameters automatically reduces the degrading effects of extraneous vibrations. Modal parameters are especially suitable when used in studies on complex vaulted systems, because mode shape animations obtained from the test and analysis offer a convenient and fast visual comparison. Finally, modal parameters have been successfully applied to masonry structures, as discussed in Chapter 2. These earlier successful studies increase confidence in using modal parameters in the present study.

From the 18 sets of raw acceleration time-history measurements collected from the choir vaults of Washington National Cathedral by exciting four different excitation points, the mean and standard deviation of the first eight out of nine modal parameters were extracted by eigensystem realization algorithm (ERA) (Juang and Pappa 1985 and 1986). However, the first mode, which is a transverse bending mode, is consistently missed by ERA method. This mode, however, is obtained by both Quadrature Response Analysis methods and ME'Scope software; therefore, information about its standard deviation is derived from the coherence function (See Section 5.2 for the related discussion). The mean values and standard deviations of natural frequencies for the first nine modes are presented in Table 4-3, while the mode shape of the second and third modes are illustrated in Figure 4-13.

The mode shape vectors include the relative displacement of 27 measurement points and thus they have a higher dimensionality than natural frequencies. However, identification of mode shapes from experimental measurements, especially in this study, is less accurate compared to the identification of natural frequencies. High damping inherent in masonry systems makes the mode shapes complex-valued and the normalization of these complex modes always introduces some errors. Also, at the nodal lines of a mode, where the theoretical displacement of that node is predicted as zero by the FE model, measured displacement may be nonzero, whether due to ambient vibration, imperfect mounting of the accelerometer, or the transverse sensitivity of accelerometers. An attempt to force an FE model to reproduce these imprecise mode shapes would only degrade the success of the calibration. It is more reliable to limit the comparative features to the natural frequencies and exploit the general characteristics of mode shapes in test-analysis correlation.

Mode 2

Mode 3
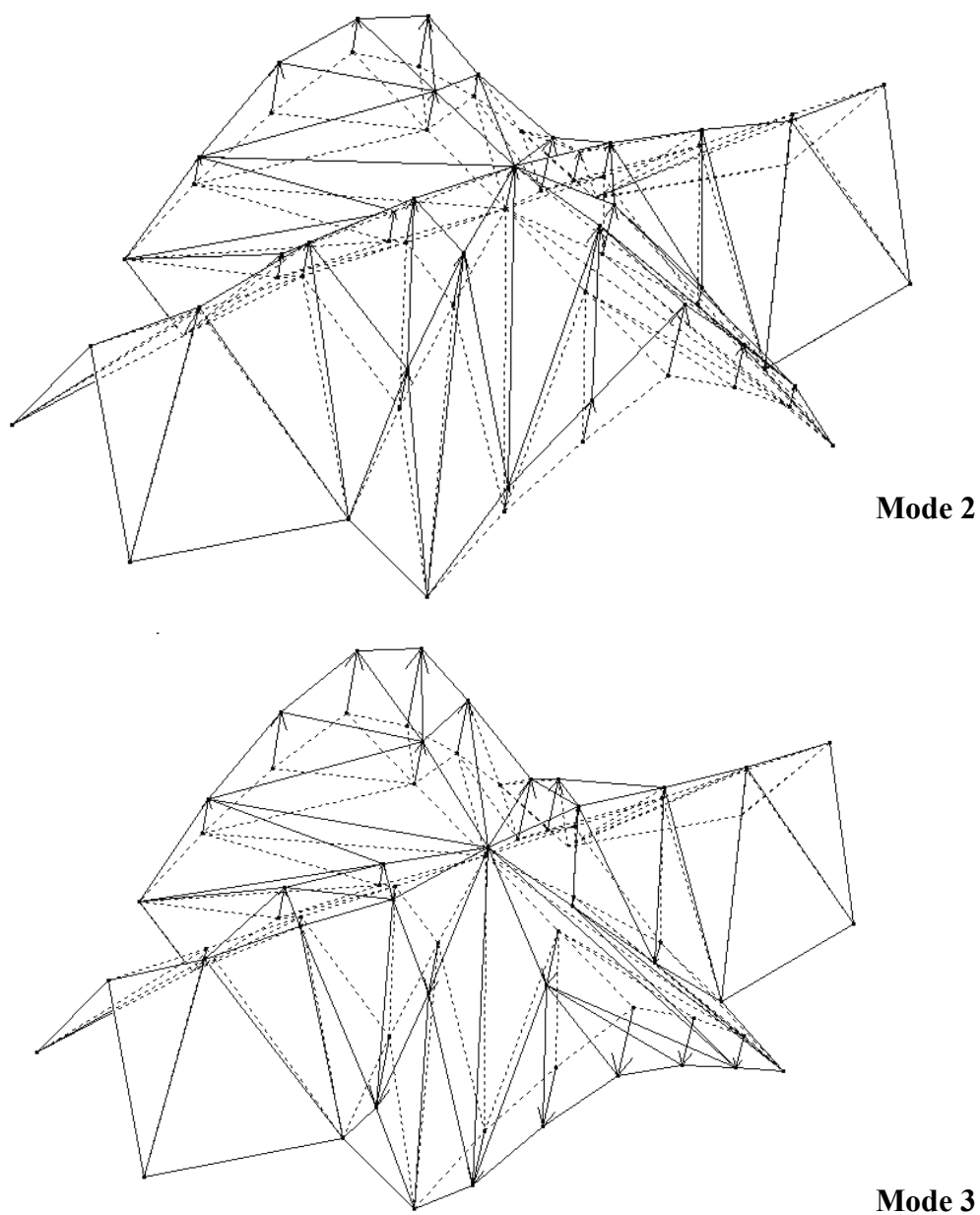
Figure 4-13: The mode shape vectors for modes 2 and 3 superimposed on the vault geometry.

Table 4-3: Mean and Variance of Natural Frequencies for Excitation at the Crown of the Vault

Mode	1	2	3	4	5	6	7	8	9
Mean (Hz)	4.94*	9.60	12.3	13.9	14.5	15.9	17.4	18.6	23.1
Std (Hz)	0.4	0.3	0.25	0.6	0.7	0.7	0.49	0.86	0.64
Coefficient of Variation	0.08	0.03	0.02	0.04	0.05	0.04	0.03	0.05	0.03

*The identification of this mode is completed with ME'Scope software.

4.6 Selection of Calibration Parameters

In the development of the FE model, a total of seven input parameters are evaluated (Table 4-4). It is important to mention that for the material properties of three structural components (ribs, webbing, and piers), the Young's modulus are defined as variables, while densities of these structural components are not included in the variable list. This is because of the known correlation between the stiffness and mass of a structure. As discussed in Chapter 3, for a single-degree-of-freedom system increasing the stiffness twice would have the same effect on the modal parameters as reducing the mass by half. Such correlations may cause the calibration routine to converge to a numerically viable but physically incorrect solution. Therefore, the density of the materials is kept at their nominal values as provided in Table 4-1. Poisson's ratio is known to have a minimal effect on the dynamic response of these structures (Atamturktur and Boothby 2007), and thus a constant value of 0.2 is assigned for all elements.

Among these seven input parameters, only those to which the modal parameters are sensitive can be calibrated when modal parameters are used as comparative features. Therefore, the influence of each of the seven input parameters on the natural frequencies of the modeled substructure is investigated through an effect screening analysis (Figure 4-14). Often, selection and elimination of parameters according to analysis of variance require judgment-based decisions.

Table 4-4: Input Parameters of the FE Model

Parameter	Description	Material
(θ1)	Young's modulus of ribs	Limestone and Mortar
(θ2)	Young's modulus of fill	Concrete
(θ3)	Young's modulus of walls	Brick
(θ4)	Young's modulus of piers	Limestone and Mortar
(θ5)	Young's modulus of webbing	Limestone and Mortar
(θ6)	Stiffness constants of spring Type 1	-
(θ7)	Stiffness constants of spring Type 2	-
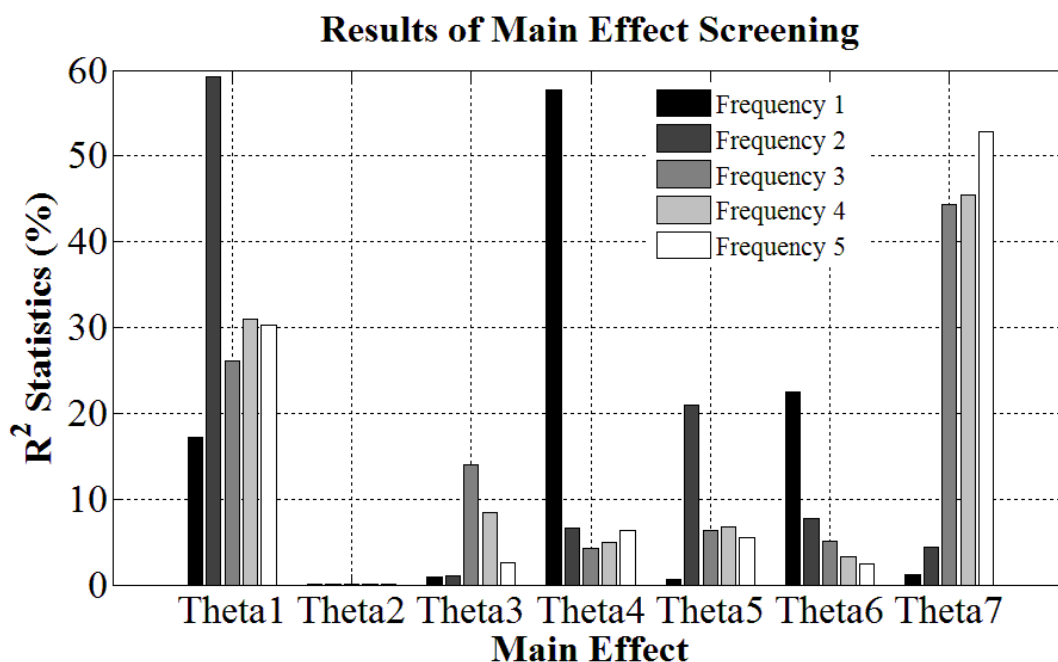
Figure 4-14: Sensitivity analysis applied to the seven parameters of the FE model.

In Figure 4-14, the main-effect screening with analysis of variance revealed θ1, Young's modulus of limestone at ribs, and θ7, stiffness constant of the springs replacing the buttresses, as the most influential parameters on the first five natural frequencies. This graph also indicates that the Young's modulus of concrete fill and the brick nave walls were less influential on the first five natural frequencies of the vaults. As a result, these two parameters may not be efficiently calibrated with respect to natural frequencies. If higher-order modal information was available, perhaps it would have been possible to calibrate these two parameters as well. Concrete fill and brick nave walls were taken off

the calibration parameter list and kept constant at their estimated mean values. This is an example of the limitations an analyst faces due to the scarcity of experimental information. Eliminating the relatively insensitive parameters from further investigation will later reduce the computational cost during iterations of calibration. Eliminating the relatively insensitive parameters also helps to avoid the ill-conditioning during calibration.

Another point that requires judgment is in determination of the calibration parameter upper and lower bounds within which the algorithm will perform random walks. The material parameter ranges provided in Table 4-1 are too large for calibration purposes, and narrower ranges must be defined by a manual but systematic process. However, first the ranges of boundary conditions must be determined.

Regarding the boundary conditions, the only study that has adapted linear springs to define an uncertain connectivity between two masonry members was by Gentile and Saisi (2007). In their study, linear springs are added at the masonry tower wall to account for the adjacent masonry building. Gentile and Saisi, without providing the details, mention using the broad comparison of FE solutions with the experimental results to determine the stiffness constants. In this dissertation, this approach is implemented in a systematic manner.

The spring constants depend on the stiffness of the subcomponent FE model as well as the number and the distribution of springs. However, determination of the upper and lower limits for spring constants is not difficult, as the behavior of the modeled structure is asymptotic at the very low and very high stiffness constant values. Figure 4-15 represents the first natural frequency of the Washington National Cathedral vaults when the constant of the springs at the buttress level are varied between free condition (k = 0 N/m) to almost fully rigid condition (k = 10^{10} N/m) while every other parameter was kept at their nominal value. As is evident in Figure 4-15, for varying values of θ6, the first natural frequency varies between 3.85 Hz and 4.85 Hz. There is a smaller range within which the structure response exhibits semiflexible connection. At stiffness values lower than approximately 10^6, the structure responds as if it has a free boundary condition at the buttresses, while at stiffness values higher than approximately 10^8, the structure responds as if it has fixed boundary conditions at the buttresses. It is between those limits the spring constant provides the desired semiflexible restraint.

As emphasized in Chapter 3, as the FE model parameters are perturbed, the sequence of predicted modes may change. In other words, the modes may swap order when the FE model is executed multiple times at sampled parameter values. This issue creates significant problems during effect screening and calibration, and therefore necessitates a rigorous mode-tracking procedure. However, this same issue becomes instrumental, when defining the lower and upper limits of the calibration parameters.
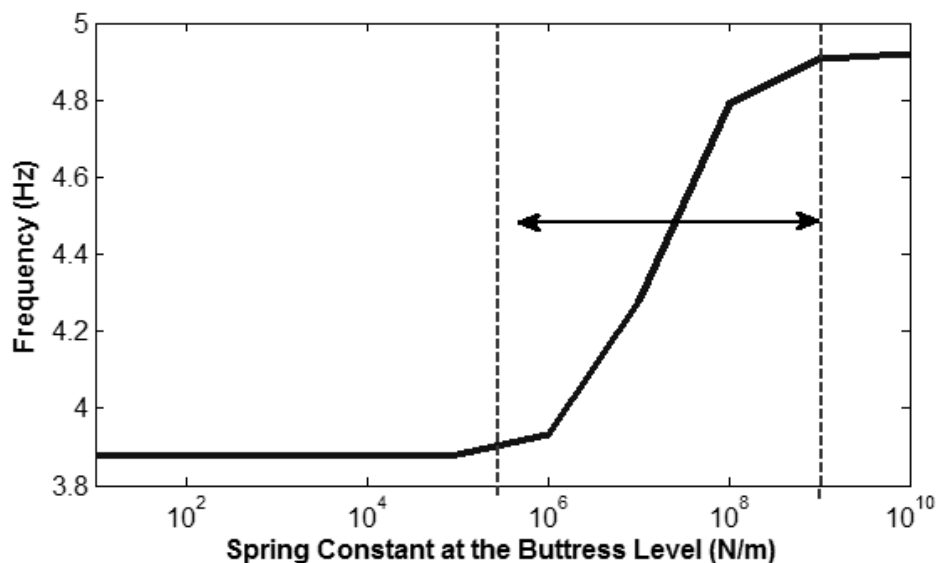
Figure 4-15: The first natural frequency versus buttress level spring constant.

For instance, when the constant of the springs at the buttress level of Washington National Cathedral is varied between a free condition ($k = 0$ N/m) and an almost fully rigid condition ($k = 10^{10}$ N/m) and every other parameter is kept at their nominal value, the predicted mode sequence is altered. Figure 4-16 presents this mode swap for the fourth and fifth modes. This particular parameter is observed to yield the correct mode shape sequence only when the parameter value is lower than $k = 5 \times 10^7$ N/m.

The parameter values at which the mode swap occurs can be conveniently used to narrow the parameter bounds before initiating the automated calibration process. After completing the similar systematic exercise for each calibration parameter, it is observed that the correct mode shape order for the first five modes is only obtained when the ratios between Young's modulus values of the limestone and the spring constants fall within a certain range. It is also observed that when the values of these parameters exceed the maximum and minimum ranges given in Table 4-5, one of the first five modes is missed or the modes are predicted out of sequence by the FE model. Therefore, for each parameter, two boundary values are assigned within which the true value is believed to be present based on the mode shape correlation.
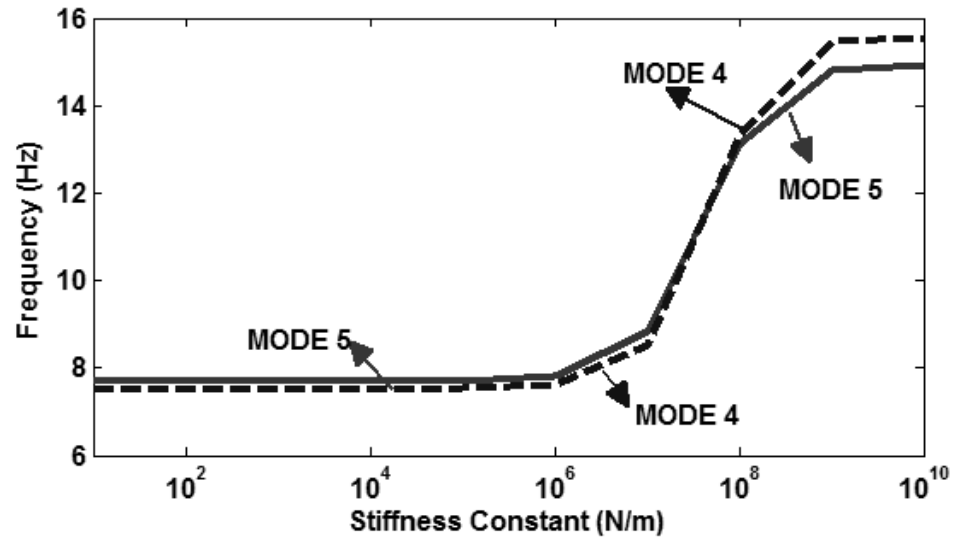
Figure 4-16: The mode swap as a single calibration parameter is perturbed.

Table 4-5: The Parameter Ranges for Calibration Parameters

Parameter	Description	Minimum Bound	Maximum Bound	Type of Distribution
(θ1)	Young's modulus of ribs	2×10^9 N/m²	8×10^9 N/m²	Uniform
(θ4)	Young's modulus of piers	6×10^9 N/m²	14×10^9 N/m²	Uniform
(θ5)	Young's modulus of webbing	1×10^9 N/m²	5×10^9 N/m²	Uniform
(θ6)	Stiffness constants of spring at the springing level	2×10^7 N/m	8×10^7 N/m	Uniform
(θ7)	Stiffness constants of spring at the buttress level	5×10^7 N/m	15×10^7 N/m	Uniform

4.7 Test-Analysis Correlation

As discussed in Section 4.3, the acceleration response of the vault was measured in the vertical direction. However, the hammer impact force also excited modes with predominant horizontal movement and less dominant vertical movement. As long as the

vertical acceleration of the vault is detectible by the accelerometers, the vertical components of these modes can still be identified and used in calibration.

Another common problem during mode-shape pairing is aliasing when higher-order mode shapes appear as lower-order mode shapes. Aliasing occurs as a result of the spatial incompleteness of the experimentation and makes the pairing of higher-order modes difficult. After the fifth mode, aliasing was observed to pose problems as higher-order modes started to replicate the first five modes. To have credible mode pairing, the maximum number of paired modes is limited to five.

The FE model has more than 200,000 degrees of freedom in all three coordinate directions, while the experiments have 27 degrees of freedom, all in the vertical direction. Because of this mismatch, the FE model degrees of freedom must be truncated down to those that are measured during the tests. The FE model mode shapes are constructed by capturing the relative deformation of the FE nodes located nearest to the coordinates of measurement points. However, it was practically impossible to perfectly line up the coordinates of the measured points with the FE model nodes; therefore, this mode truncation will partially degrade the mode shape correlation.

The easiest way of comparing the test and analysis mode shapes is overlaying the normalized mode shape vectors. In Figure 4-17, relative displacements of 27 measurement locations are plotted against the node numbers of these measurement locations. Although Figure 4-17 provides a convenient means of comparing the measured and calculated mode shapes, they do not provide spatial information about the particular mode shape. In Figure 4-17 the FE predictions of the first five modes are also given, in order to provide the typical deformation characteristics of the vaults.

In Figure 4-17, experimentally obtained mode shapes are indicated in a solid line. Mode shapes predicted by all 128 FE simulations are indicated in stars. These 128 simulations are obtained by a two-level full-factorial design. The spread of the stars thus indicates the variability in the FE solutions, as a result of the forward propagation of uncertainty. The mean value of the 128 simulation solutions at each node is indicated by the dotted line. According to this principle, the first five experimental mode shapes are paired with the calculated modes and are illustrated in Figure 4-17. The observable deviations between the measurements and FE solutions are attributed to the difficulties in vertical mounting of accelerometers on curved surfaces, in precise matching the coordinates of measurement and calculation nodes, in application of a purely vertical excitation force during tests combined with the transverse sensitivity of accelerometers, and in system identification of clustered modes.

Also, accumulated damage in the structure as it stands today may induce unsymmetrical mode shapes. However, even when irregularities in the structure are known through inspection, their incorporation in the FE model is quite challenging. Modeling strategies for irregularities in a masonry structure—e.g., internal voids in the walls and piers, missing stone units, existing cracks and hinges, and biological growth—are not available in literature. However, even to investigate the suitability of alternative modeling strategies, a reliable baseline FE model is the necessary first step. Illustration of the development of this baseline FE model is the goal of the present dissertation.

(a) Mode 1 correlation.

Mode 1 elevation.

Mode 1 plan view.

(b) Mode 2 correlation

Mode 2 elevation.

Mode 2 plan view.
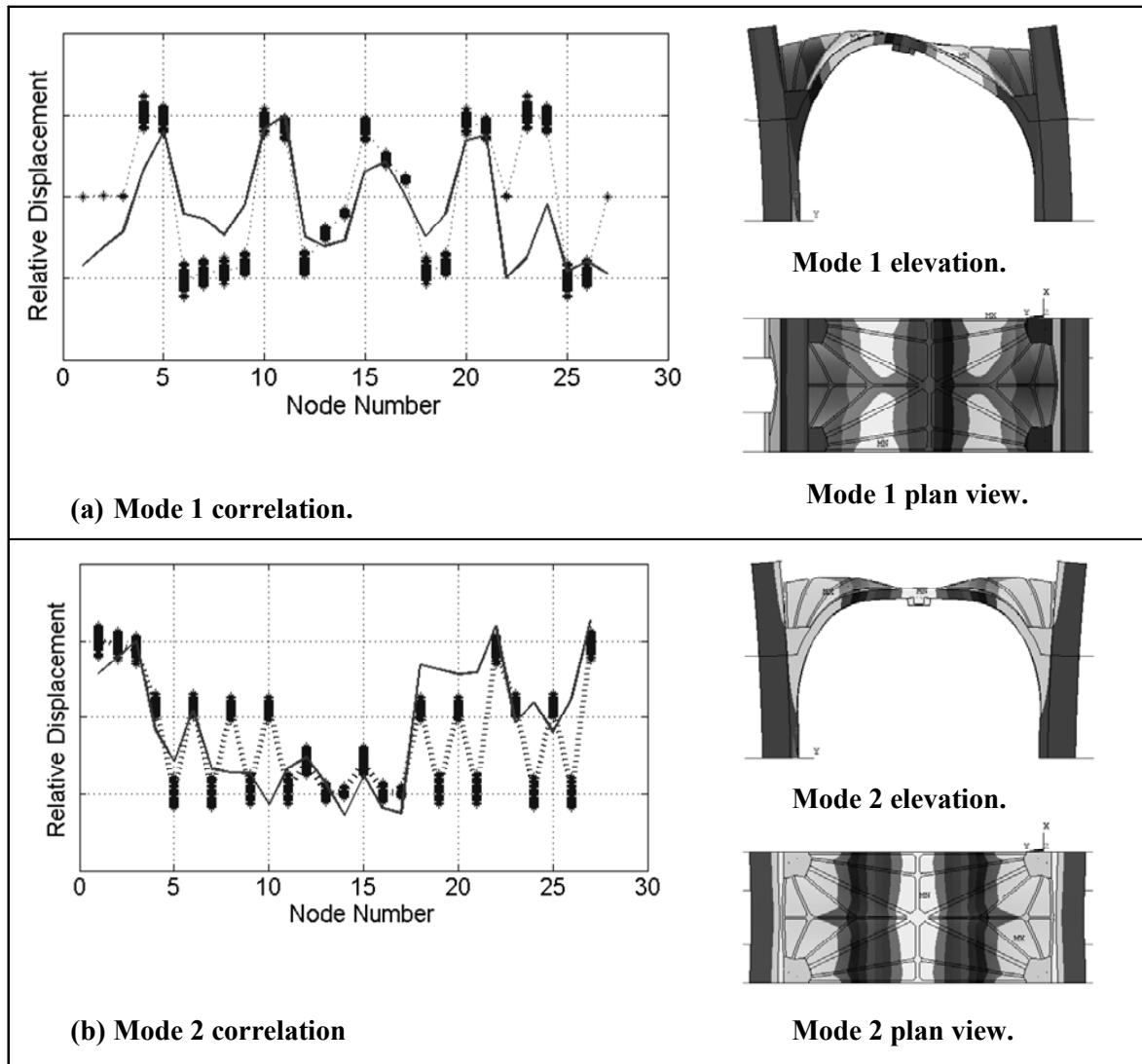
Figure 4-17: Initial mode-shape pairing of the first five modes.

Geometric variability of the vault due to construction imperfections may also result in experimental mode shapes being unsymmetrical. On the other hand, the FE model is built based on double symmetry assumption and would only yield symmetric mode shapes. To investigate how sensitive mode shape vectors are to a change in a geometry property, the model is executed with 10% reduced web thickness. The mode shapes and natural frequency variations are observed to be no more than 3% for the first five modes.
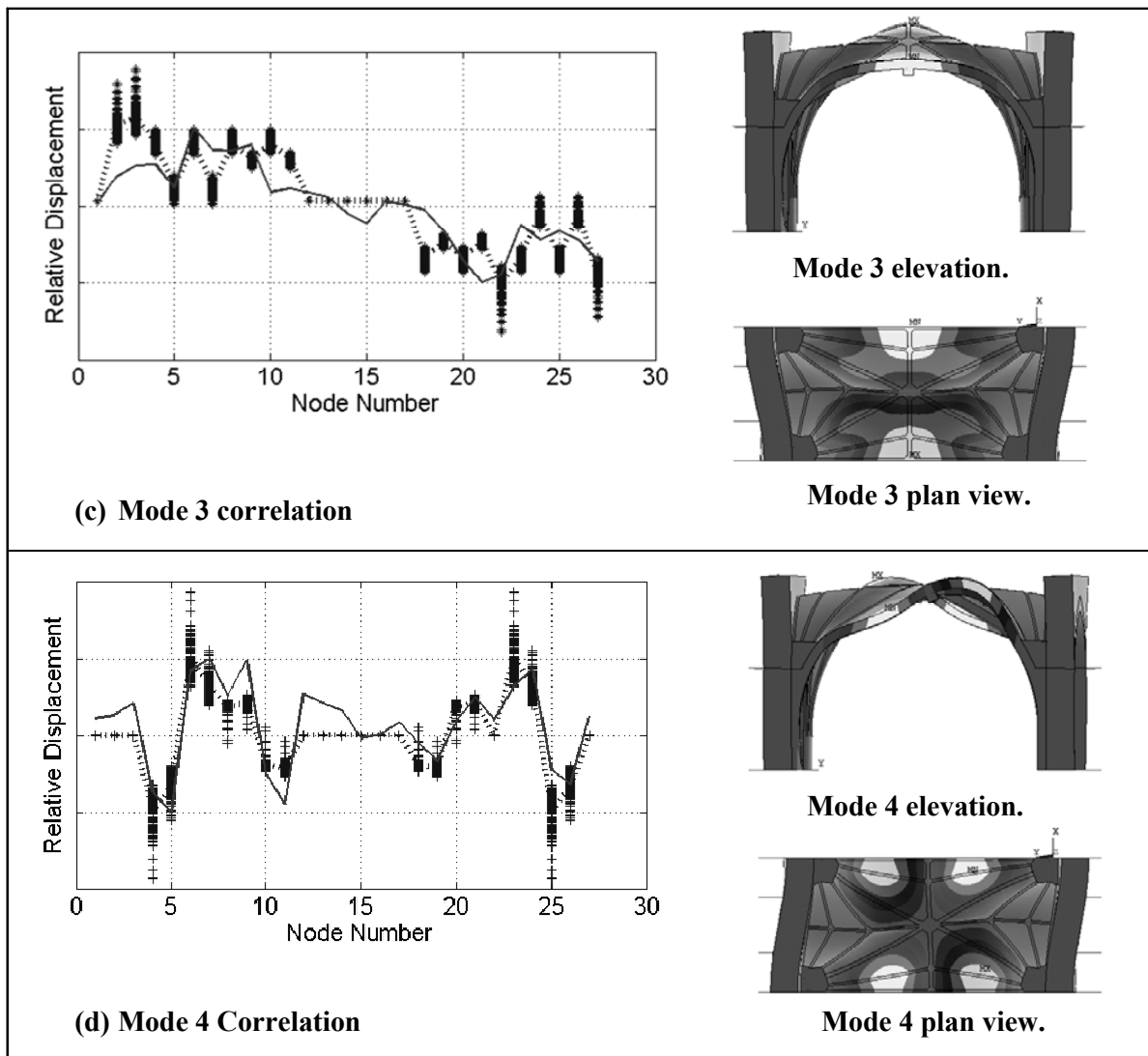
(c) Mode 3 correlation

Mode 3 elevation.

Mode 3 plan view.

(d) Mode 4 Correlation

Mode 4 elevation.

Mode 4 plan view.

Figure 4-17: Initial mode-shape pairing of the first five modes (continued).

(a) Mode 5 Correlation

Mode 5 elevation.

Mode 5 plan view.
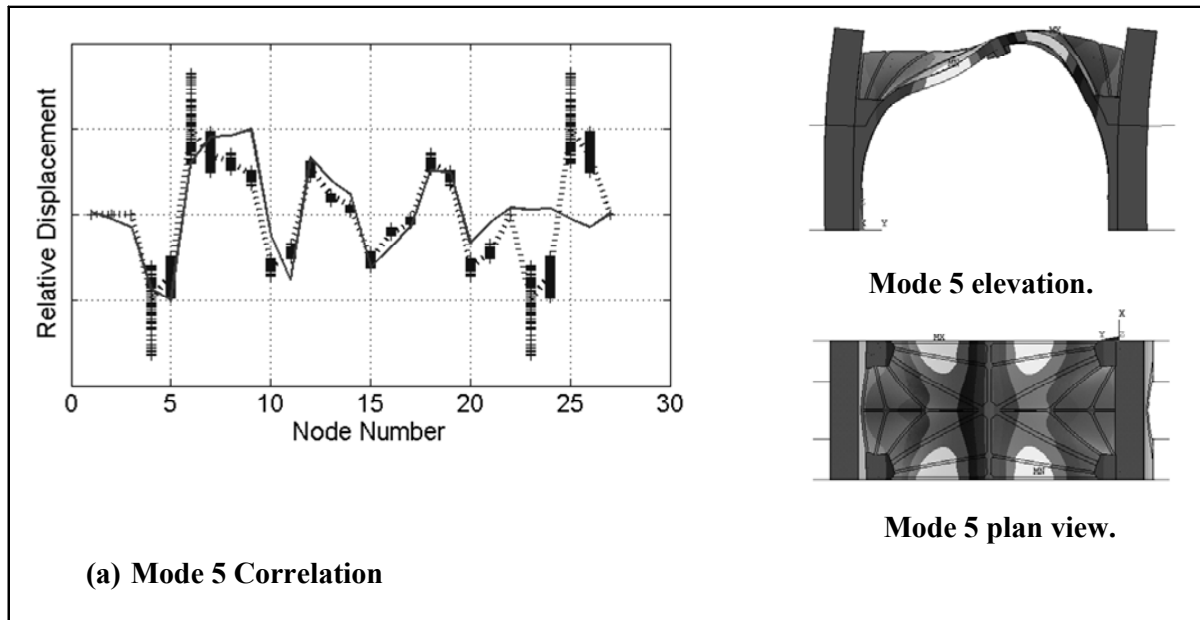
Figure 4-17: Initial mode-shape pairing of the first five modes (continued).

Considering the above-mentioned complications, test-analysis correlation in this study is expected to be of lesser quality compared to those typically obtained for laboratory specimens or simpler structural systems. This was exemplified when Ramos (2007), while obtaining close agreement between the test and analysis mode shapes for a laboratory arch specimen and for a standalone masonry tower, had significant difficulties in his test-analysis correlation of a historic vaulted structure. Ramos's attempts at mode correlation when applied to a historic basilica remained incomplete. Considering the relatively limited success of earlier studies on vaulted masonry structures, correlating the first five modes is considered satisfactory for our purposes. The mode shape pairing for the first five modes is given in Table 4-6.

Table 4-6: The Experimental Modes Matched with the Initial FE Modes

Experiment		Finite Element Analysis		
Mode	Frequency (mean ± 1 std)	Mode	Frequency (min and max values)	
1	4.94 Hz ± 0.40 Hz	1	3.7 Hz	5.2 Hz
2	9.61 Hz ± 0.30 Hz	2	6.3 Hz	8.9 Hz
3	12.3 Hz ± 0.25 Hz	3	9.7 Hz	13.8 Hz
4	13.9 Hz ± 0.60 Hz	4	10.1 Hz	14.3 Hz
5	14.5 Hz ± 0.70 Hz	5	10.3 Hz	14.5 Hz

From the start, it is evident that this FE model configuration will fail to identically match the second experimental natural frequency considering two standard deviations. However, the goal of Bayesian calibration is not to reach an FE model which can identically match the experiments. Instead, the goal is to obtain an FE model that can statistically correlate with the physical evidence.

4.8 Characterization of Modeling Parameters

Once the measured and calculated modes are paired, the imprecisely known FE model parameters, three material properties ($\theta 1$, $\theta 4$, and $\theta 5$) and two spring constants ($\theta 6$ and $\theta 7$), which are identified as influential on the dynamic characteristics of the vaults, can be calibrated. Experimental information from the first five modes is available in the form of natural frequencies and the corresponding mode shape vectors. Due to the challenges in obtaining precise mode shape vectors, mode shapes are only used for mode pairing while natural frequencies are used as comparative features during calibration.

Assuming that the calibration parameters are uncorrelated and independent, uniform probability is assigned to all five calibration parameters; that is, every point within the defined range of a parameter has an equal probability of being sampled. There are two reasons for this approach. The first one is that information about the *a priori* probability distributions of calibration parameters is not available, and in fact this lack of knowledge is the primary motivation of the calibration exercise. The second reason is that assigning equal probability, from a computational point of view, is safer than making an unwarranted assumption about the *a priori* distribution of these parameters. This is because assigning an erroneous prior distribution may force the Markov Chain Monte Carlo (MCMC) random walks to focus in a certain region in the parameter domain, leaving other regions insufficiently explored.

Within their predefined range, parameters are sampled with Latin-hypercube maxi-min design (Montgomery 1997). To train a surrogate model reliably, the rule of

thumb is generating 10 times more computer experiments than the number of calibration experiments (Williams 2008a). Therefore, a total of 50 samples are generated from uncorrelated, uniformly distributed calibration parameters and accordingly the FE model is run 50 times, at each of the sampled parameter sets. Next, the Gaussian process model is trained to represent the mathematical relationship between 50 sets of calibration parameters and 50 sets of output response.

Random walks of MCMC consume 100 iterations at seven step sizes to determine which step size is most suitable for the given problem. This means that the first 700 points visited (and accepted) are not included in the posterior distributions. This aspect of the algorithm also helps to avoid potential bias that may occur due to the starting point of the random walks.

Figure 4-18 illustrates the posterior distribution functions for the calibration parameters. In Figure 4-18, $\theta 1$ denotes the Young's modulus for limestone of the ribs; $\theta 4$ denotes the Young's modulus for limestone of the piers; $\theta 5$ denotes the Young's modulus for limestone of vault webbing; $\theta 6$ denotes the spring constant for the pier tops; $\theta 7$ denotes the spring constant for the flying buttresses.
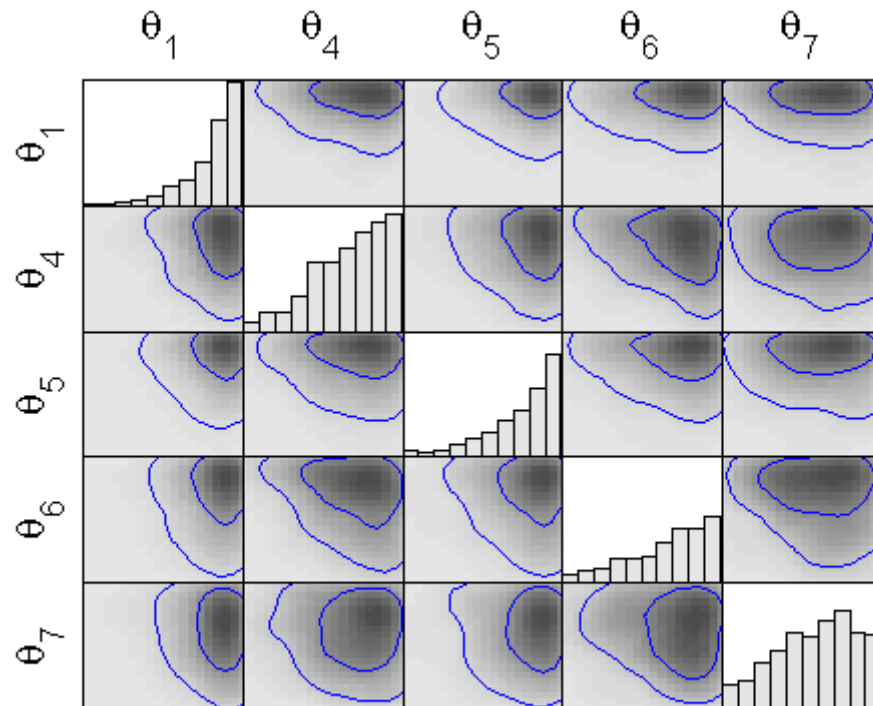

Figure 4-18: The bivariate joint distribution of the five calibration parameters.

The posterior distribution function is estimated by 500,000 MCMC-accepted random walks in a five-dimensional parameter domain. Figure 4-18 shows marginal probabilities of each parameter on the main diagonal and the bivariate distributions in the

off-diagonal boxes (θp; θq). As suggested by Wilson and Boyack (1998) and reiterated by Trucano et al. (2006), a proper means of representing the calibrated model should take the form of a best estimate with uncertainty bounds. Accordingly, Table 4-7 lists the mean and standard deviation inferred from the posterior distributions of Figure 4-18. Readers are warned against taking the values in Table 4-7 as true values for the five calibration parameters, but instead encouraged to consider Table 4-7 as an improvement in the existing knowledge (or as a reduction in the "lack of knowledge") about these parameter values.

Table 4-7: The Mean and Variance of Posterior Distributions of the Calibrated Parameters

FE Model Parameter		Mean	Standard Deviation	Coefficient of Variation
($\theta 1$)	Young's modulus of ribs	4.9×10^9 N/m^2	0.4×10^9 N/m^2	0.08
($\theta 4$)	Young's modulus of piers	11.4×10^9 N/m^2	1.4×10^9 N/m^2	0.12
($\theta 5$)	Young's modulus of webbing	2.8×10^9 N/m^2	0.4×10^9 N/m^2	0.13
($\theta 6$)	Stiffness constants of springs at the springing level	5.4×10^7 N/m	0.9×10^7 N/m	0.16
($\theta 7$)	Stiffness constants of springs at the buttress level	11.8×10^7 N/m	1.2×10^7 N/m	0.10

This propagation of uncertainty has been completed based on the premise that the calibration parameters are uncorrelated. When there is such a relation present between any of the parameters, however, the model calibration can easily converge to a numerically viable but physically incorrect solution. The bivariate distributions in Figure 4-18 can also help us observe the hidden dependencies or correlations between the parameters. Figure 4-18 depicts that there is no strong correlation or dependency between any components.

4.9 Discussions and Results

This section discusses the results obtained from stochastic calibration. In Section 4.9.1, based on the calibration results, inferences will be made on the calibrated parameter values of the FE model. In Section 4.9.2, a rudimentary check will be made to validate the calibration results. Stability of the calibration as the number of experimental information used in calibration increases will be investigated in Section 4.9.3.

4.9.1 Posterior Distributions of Calibration Parameters

The posterior distributions show that material properties for limestone are in fact variable for piers, ribs, and webbing. Generally, the piers are observed to be considerably stiffer than the ribs and the webbing. This can be explained by the lower percentage of mortar in the assembly due to the larger masonry units and less frequent mortar joints. Also, piers are also expected to have lower stresses because of their larger cross-sectional area, and as a result, the nonlinear stress-strain relationship of masonry would yield a higher Young's modulus for low stress levels. Piers, being primarily under compression, are expected to have minimal cracks compared to the ribs and webbing of the vaults. It is quite plausible that the webbing has the least Young's modulus among all three components built out of limestone. Webbing, because of its double curvature and difficulty of construction, has the greatest proportion of mortar and the greatest propensity to crack.

Posterior distributions are also obtained for the spring constants used to represent the semiflexible boundary conditions between the substructure FE model and the unmodeled components of the church. The mean estimates of these posterior distributions can now be used to investigate the load paths within the vault system and the structural roles of each component. For instance, with the estimated values of the stiffness constants of the buttress level springs, the horizontal restraining forces exerted by the buttresses can be estimated.

Overall, the coefficient of variance seems relatively low for a random, hand-assembled material. This can be explained by the low-amplitude vibration experiments which only excite the masonry behavior with impact forces varying between 500–700 lb.

With these refined-input parameter values, the FE model will predict the natural frequencies with close fidelity (Table 4-8). However, even at the best-calibrated parameter values, some discrepancy remains between the measurements and FE solutions. The "bias," described in Chapter 3, is due to the many potential sources of error in the model that cannot be remedied by solely calibrating the selected five parameters. It is always possible that parameters that are in need of calibration are overlooked. For instance, the symmetry assumption and assigning a single variable for all spring constants is perhaps too strict an assumption and relaxing this assumption by assigning a separate parameter for each spring may yield improved agreement between the FE model and physical evidence.

**Table 4-8: Improved Correlation of Natural Frequencies
of the Calibrated FE Model**

Experiment		Finite Element		
Mode	Frequency (mean)	Mode	Frequency (mean)	Within
1	4.94 Hz ± 0.4 Hz	1	5.1 Hz	1- σ
2	9.61 Hz ± 0.3 Hz	2	8.8 Hz	3- σ
3	12.3 Hz ± 0.25 Hz	3	13.5 Hz	3- σ
4	13.9 Hz ± 0.6 Hz	4	14.0 Hz	1- σ
5	14.5 Hz ± 0.7 Hz	5	14.3 Hz	1- σ

If further improvement and refinement in the calibration is needed, the posterior distributions, provided in Table 4-7, can now be used in a refined, follow-up calibration study, perhaps with a larger amount of experimental information. Also, including higher-order modes may enable us to better define the probability distributions of the calibration parameters.

4.9.2 Validation of the Calibrated FE Model

Calibration, discussed in the previous section, only illustrated that the fidelity of the FE model to physical evidence can be improved by calibrating certain model parameters. The model obtained with calibrated parameter values is conditioned to the physical evidence; therefore, the same physical evidence cannot be used to validate this calibrated FE model. The last objective of this chapter is to confirm that the calibration's results are in **acceptable agreement** with an independent set of evidence. Once again, definition of the acceptable agreement is subjective and requires engineering judgment.

An independent set of information related to the material properties that will enable us to confirm the calibrated material property values is missing. Therefore, the validation cannot be completed based on material properties. However, an independent set of information to validate the calibrated model can be obtained for the spring constants.

For this, an FE model of the remaining components of the choir of Washington National Cathedral must be built (Figure 4-19), which will be referred to as the base FE model. The material property of the structure is assumed to be uniform and identical to the calibrated values of the Young's modulus of the piers ($\theta4$) with a mean value of 10.7 GPa. This assumption is clearly very crude, as a typical masonry wall and buttress construction constitute voids and empty volumes in between the exterior wythes; however, within the scope of this study, a correct evaluation of these structural aspects is

practically impossible. Therefore, the base FE model is expected to overestimate the stiffness of the lower part of the structure.

To incorporate the uncertainty remaining in the calibrated Young's modulus value of the piers, this parameter is treated within a range with first standard deviation; therefore, a minimum of 8.2×10^9 N/m^2 and a maximum of 13.2×10^9 N/m^2 are used while calculating the spring constants.

The soil-structure interaction is poorly known, therefore, another aspect of the base FE model is in the determination of the support conditions of piers and buttresses, which is where judgment is necessary. Because of the high mass of the structure, friction forces are first assumed to provide sufficient translational resistance. Therefore, the pier base is restrained for translation in all three directions at the base of the piers. This assumption effectively provides a rotation restraint and is therefore a fixed boundary condition. This assumption is very crude and is anticipated to result in an overestimation of the stiffness of the lower part of the structure. Therefore, the procedure is repeated considering a rotation free hinge connection at the base of the piers instead of a fixed connection.
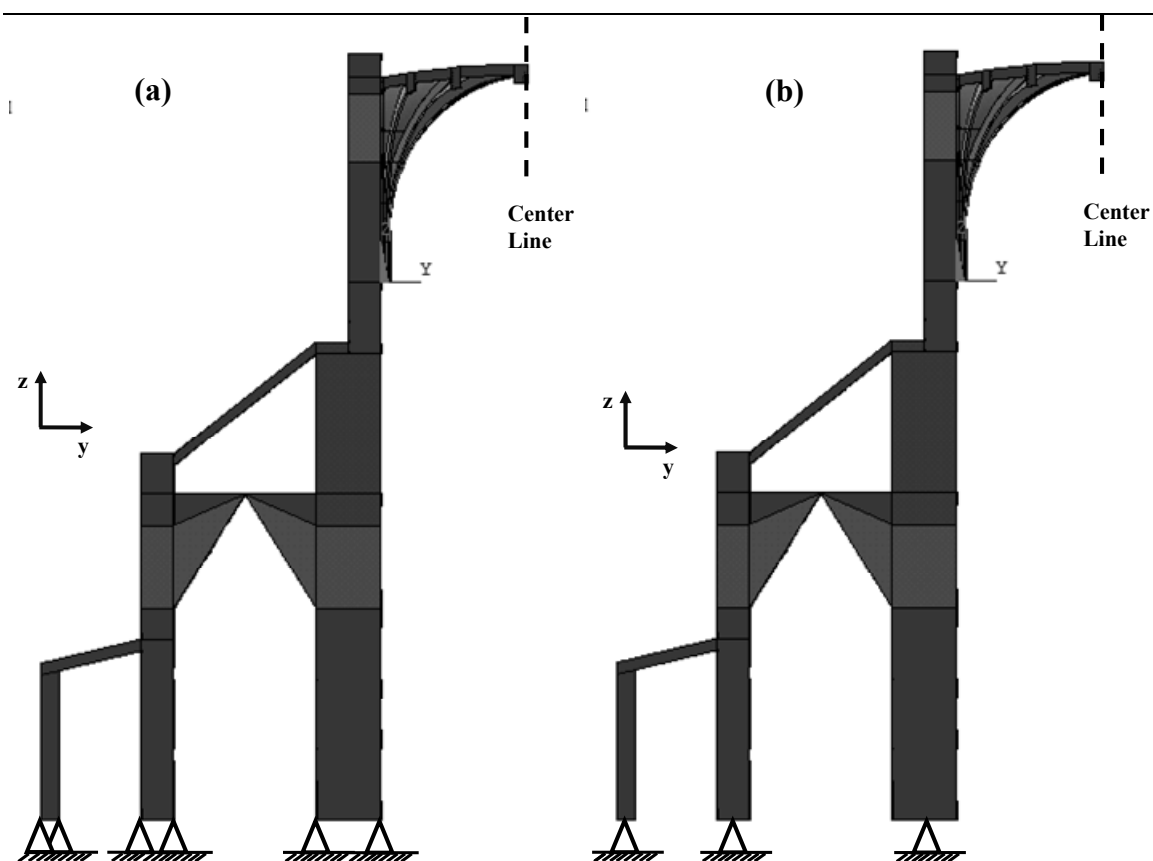

Figure 4-19: The FE model of the remaining of the structure, referred to as base FE model in the text: (a) the fix boundary condition, (b) hinge boundary condition.

A 1000 N horizontal force is applied at the top of the base FE model, precisely where the springs are located on the actual FE model (Figure 4-20). When the base supports are fixed with both rotational and translational restraints, the resulting displacements are observed to be between 0.6210^{-4} m and $0.38 \ 10^{-4}$ m, depending on the Young's modulus of the piers. Assuming that the loads are shared equally by the two springs at each pier, an approximate spring constant varying between 8.1×10^{6} N/m and 13×10^{6} N/m is obtained for each of the two springs. The parameter value obtained for $\theta 4$ by calibration, meanwhile, is 5.4×10^{6} N/m $\pm \ 1 \times 10^{6}$ N/m with one standard deviation. Although a disagreement is evident between the spring constant values obtained by two methods, with two standard deviation statistics, they show a level of agreement as seen in Figure 4-20. In Figure 4-20, the probability distribution obtained by the base FE model is denoted with the solid red line, while the probability distribution obtained by the calibration of the original FE model is denoted with the blue line. When the base supports are assumed to be hinge with only translational restraints, the horizontal displacements are observed to vary between $1.07 \ 10^{-4}$ m and $0.67 \ 10^{-4}$ m, depending on the Young's modulus of the piers when the bottom of the piers are hinged supported. In turn, the stiffness constant ($\theta 4$) is obtained to vary between 4.7×10^{6} N/m and 7.5×10^{6} N/m. In Figure 4-20, the probability distribution obtained by the base FE model with hinge connections at the bottom of the piers is denoted with the dashed red line.

As evidenced in Figure 4-20, the results of the FE model calibration yield better agreement with the base FE model solution when the supports are represented with hinge connections. The observed discrepancy between the calibrated spring constant and that predicted by the base FE model can be attributed to various imprecise model parameters in the base FE model. These include absence of knowledge about the interior composition of the piers and buttresses, the difficulty in representing the soil-structure interaction, and the limitations of the available documentation about the physical geometry of the buttresses and aisle vaults.

Oberkampf et al. (2002) effectively argue that the validation process of a postcalibrated model is a systematic process of evidence accumulation. The present study acknowledges that as additional evidence becomes available, the validation discussed herein will gain more credibility. However, due to the practical limitations in obtaining this evidence, this study is not in a position to claim that a perfect credibility in the FE model is reached for solving static or quasistatic analysis. Instead, a more realistic statement about the contribution of this study would be the fact that the FE model is improved because the uncertainty in the postcalibrated model is significantly reduced. Considering the complexity of the studied structure, this task should be considered as a significant achievement.

The Statistical Comparison of Estimated and Calibrated Spring Constant Value

Calibration of the original FE model

Base FE model with hinged pier bases

Base FE model with fixed pier bases
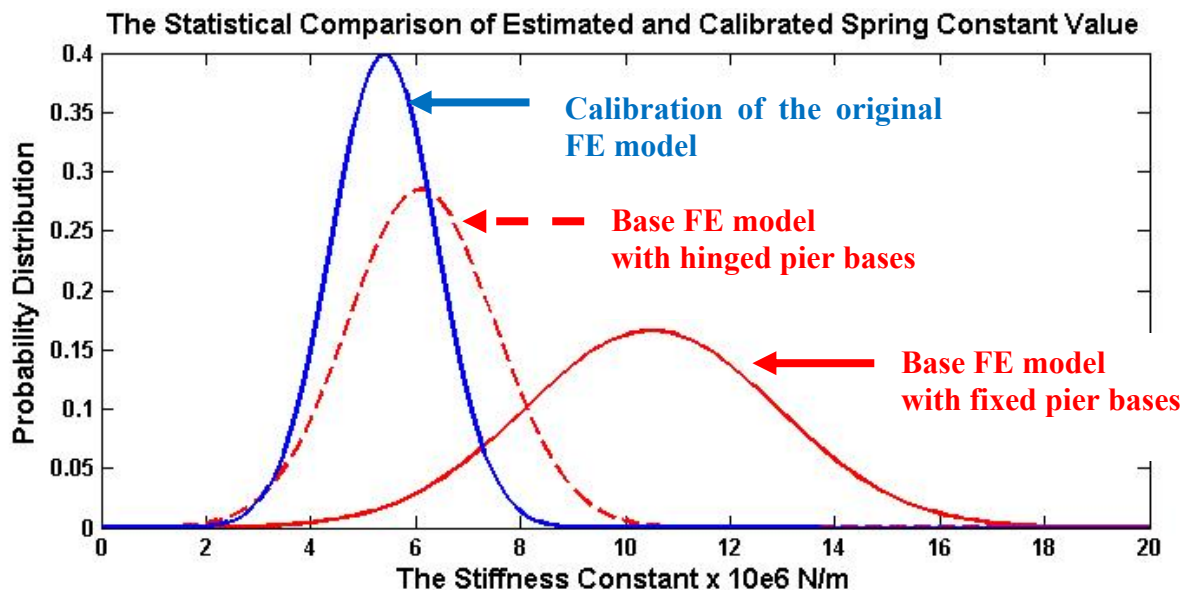
Figure 4-20: The statistical comparison of the values for the spring constant.

4.9.3 Stability of Calibration

In Atamturktur et al. (2008), the importance of the calibration parameters to maintain stability during calibration is stressed. Stability herein means that as higher-order natural frequencies are added to the calibration, the calibrated parameters should converge to their true values, rather than fluctuating within the ranges of the parameter.

In this study, the calibration process has been repeated five times with increasing number of natural frequencies used as comparative features. The first probability distribution estimate is obtained by calibrating the model with respect to the first natural frequency; the next probability distribution estimate is obtained by calibrating the model with the first two natural frequencies, and so on. Figure 4-21 provides the representation of posterior distributions of the first calibration parameter as a function of the number of natural frequencies used in calibration.

Figure 4-21: The Young's modulus of limestone ribs obtained by successive calibration studies with increasing number of experimental modes.
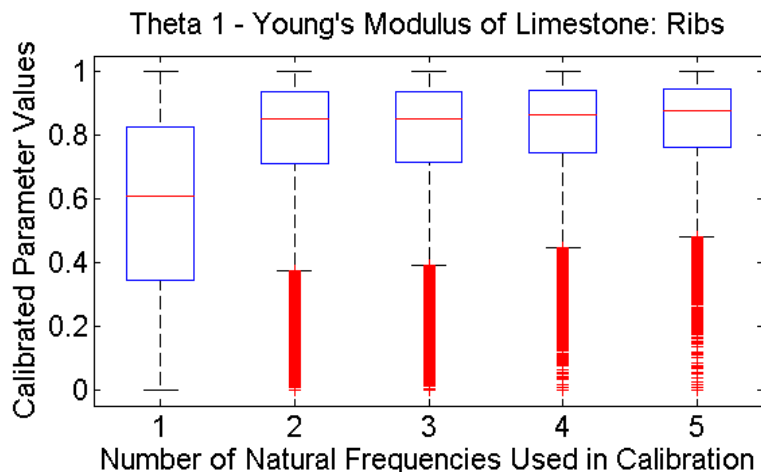
In Figure 4-21, y axis denotes the normalized range of the parameters. Thus, 0 on the y axis means that the parameter value is expected to be at the minimum value as defined in Table 4-5, while 1.0 on the y axis means that the parameter value is expected to be at the maximum value as defined in Table 4-5. In Figure 4-21, when the Young's modulus of limestone ribs are calibrated using only the first natural frequency, the mean value is around 0.6. However, adding the second natural frequency in the calibration changes the mean value for Theta 1 to 0.8. After this point, adding third, fourth, or fifth natural frequencies do not affect the posterior distributions of the Young's modulus of limestone ribs. A very similar observation can be made for Theta 7, the spring constant of buttresses.

Figure 4-21 and Figure 4-22 illustrate the stable behavior of the posterior distributions of Theta 1 and Theta 7. The other three calibration parameters also exhibit similar behavior with less change in the mean values, which can be attributed to the lower sensitivity of these parameters to the natural frequencies (see Figure 4-14). Neither Figure 4-21 nor Figure 4-22 indicate insensible fluctuations of mean values. This observation increases the confidence in calibration results.
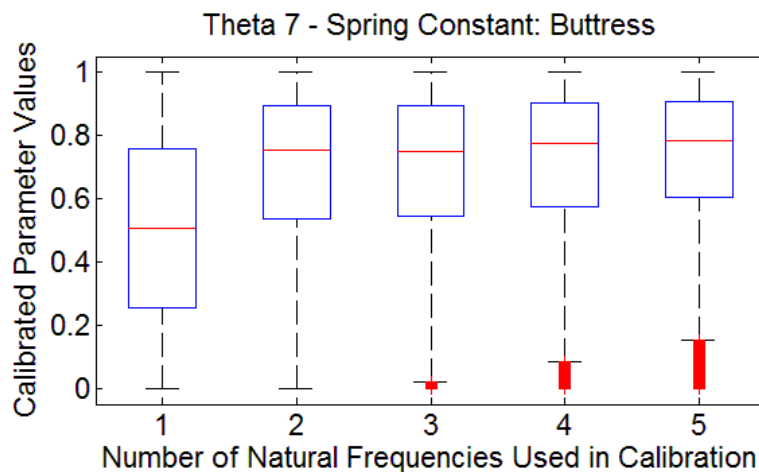
Figure 4-22: The stable behavior of the posterior distribution of Theta 7.

4.10 Concluding Remarks

Considering all potential sources for uncertainty in a masonry construction, implementing a stochastic approach is natural. Stochastic model calibration is a very specialized process that responds to the need to implement FE models to predict phenomena for which physical measurements are not available.

The goal of this chapter was to take a step towards illustrating the application of tools collectively referred to as stochastic model calibration to improve the predictive accuracy of large-scale FE simulations of the Washington National Cathedral, DC. For this purpose, large amounts of experimental and computational information collected from the choir vaults of the Cathedral were integrated in the context of Bayesian inference. Both from the physical measurements and computer experiments, modal parameters were extracted probabilistically as mean and variance statistics. After effect screening, the uncertain parameters that are candidates for calibration were ranked based on their effect on numerical model output. Three material properties and two spring constants, which represent the inter-element connectivity, were selected as comparative features. Once the comparative features and calibration parameters were defined, Bayesian inference was used to compound the prior knowledge about the calibration parameters, together with experimental observations collected from vibration testing. Bayesian inference, then, resulted in updated knowledge of the calibration parameters in the form of a posterior probability distribution. The posterior distributions of the spring constants can be articulated further to make inference about load paths in masonry structures. An improved understanding of the load paths has practical impacts in the preservation and rehabilitation of historic structures. The point of this exercise was to better understand where modeling uncertainty originates from and to obtain model predictions that are statistically consistent with the measurements and their uncertainty.

Chapter 5

DISCUSSION AND CONCLUSIONS

5.1 Summary of the Research Program

When building finite element (FE) models of masonry structures, uncertainties and errors arise from many different sources. Appropriate constitutive laws and parameters of these laws are implemented with great difficulty for masonry structures due both to the lack of precise engineering understanding of the masonry material behavior and to the significant variations in masonry quarried from different geographic locations and in mortar mixed by different workmen. The variability is multiplied when the properties of masonry units and mortar joints are homogenized to obtain effective material properties. These effective material properties vary depending on the dimensions of the masonry units and joint thickness, orientation of the masonry units, the voids within the masonry assembly, and the quality of workmanship, as well as the development of various forms of damage, such as cracks, hinges, and material deterioration in the structure. These factors cause high uncertainties while defining the masonry material properties.

The masonry material behavior varies from unit to unit, and has a variation within a structural component, for instance, within a masonry pier. However, it is often desirable to ignore this internal variability within a structural component and assume a constant averaged material property value for large portions of a building structure. This approach, although it is very convenient for modeling purposes, adds to the uncertainties while defining the masonry material properties in FE models.

Similarly, uncertainties arise when determining the interaction between adjacent structural components. This is needed when (1) defining the connectivity conditions at contact locations with unmodeled structural members or (2) defining soil-structure interaction. In several previous studies, these boundary conditions have been approximated by using the three common types of boundary conditions: fixed, pinned, or free. Although these boundary conditions may be applied with satisfactory results to steel structures, in which connections are deliberately designed to be one of these three types, their applicability when defining the connections between masonry members is often limited. Where masonry structures are concerned, the connectivity between two structural members relies on various factors, which include the elastic properties of the materials, surface friction, and the amplitude of the load. Thus, masonry connections practically never fall under the categories of fixed or pinned restraint. This elastic connectivity between the members included in the FE model and those that are excluded can be **partially** represented by linearly elastic springs with constant stiffness properties. However, the stiffness constants of these springs are obviously highly uncertain.

As the complexity of the problem increases, especially with historic masonry structures, the ability to appropriately incorporate the physical reality in the FE model decreases. Several strong assumptions become necessary and the FE solutions become a rough approximation of reality. The difficulties in structural analysis of historic masonry monuments can be mitigated by treating the FE input parameters probabilistically. When the FE model input parameters are defined probabilistically, the output response is obtained probabilistically as well. As far as masonry structures are concerned, this is a desirable way of developing credible FE models for structural analysis.

In the present study, the material property values are defined as ranges with lower and upper bounds instead of deterministic, averaged values. The information to determine these bounds is compiled from published experimental studies and later refined through test and analysis correlation. In regards to boundary conditions, the stiffness constants are varied from very low values to very high values to investigate their asymptotic effect on the response feature. This task is completed separately for each spring constant and the ranges within which the springs provide the desired semiflexible restraint are obtained.

There are several modeling parameters that are uncertain in the analysis of masonry structures. However, not all of them are influential on the desired results. Some of these parameters can be kept constant at their nominal values, and effect screening can be used to detect these low-sensitivity parameters. In this study, a specific type of effect screening, analysis of variance, is used to select the calibration parameters from the list of FE model input parameters. In effect screening, the parameter sensitivity is evaluated relative to the sensitivity of other parameters. Therefore, this is another instance when engineering judgment becomes necessary. The goal must be to reduce the number of calibration parameters as much as possible while including the parameters that have a significant influence on the accuracy of the solutions.

The deterministic calibration approach relies on an assumption that experimentally identified modal parameters are known with certainty. However, there are several reasons for the identified modal parameters to deviate from reality during both experimentation and data processing. The uncertainty in the measured modal parameters can be characterized by mean and standard deviation statistics. Once these statistical properties are known, measurement uncertainties can be implemented in the FE calibration process.

To determine the mean and standard deviation statistics of measured data, repeated tests must be conducted. A large number of repeated tests were in fact collected during the tests on Washington National Cathedral. The feature extraction is completed for all datasets and the modal parameter variability is computed accordingly.

After the experiments are conducted and the FE model is built and parameterized, the next step is the calibration through which selected parameters are improved in a systematic way. When considering all potential sources for uncertainty in a masonry construction, implementing a stochastic calibration approach is a natural choice. In this study, the scope of model calibration is expanded from one that ignores the presence of uncertainty to one that fundamentally relies on the definition and propagation of parameter uncertainty. Bayesian inference is used to compound the prior knowledge about the calibration parameters with experimental observations collected from vibration testing. Bayesian inference, then, results in updated knowledge of the calibration

parameters in the form of a posterior probability distribution. The goal herein was to better understand from where modeling uncertainty originates and to obtain model predictions that are statistically consistent with the measurements and their uncertainty.

The framework discussed in this thesis was illustrated for two Gothic churches. However, this theoretical framework can be extended to masonry structures in different typologies: isolated residential buildings, row buildings, complex public buildings, towers, palaces, and arenas.

5.2 Findings of the Presented Research

As a result of the summarized work, the following findings are concluded:

1. Model calibration is a procedure of determining the appropriate parameters in an FE model to give an improved representation of a prototype structure. In load-bearing masonry subjected to linear elastic analysis, the parameters representing stiffness constants, densities, and support restraints can be successfully calibrated. In this study, it is concluded that calibrating the geometric properties of the structure is not a feasible solution for the masonry vaulted structures due to their complex geometry, because at each iteration, the FE mesh must be redone.

2. Based on solution verification studies, a FE mesh size around 30 cm is found to be suitable for the dynamic analysis of these structures.

3. An FE model that is to be calibrated must be parameterized appropriately. In this study, it is found that different structural components, such as piers, walls, and vault ribs, built out of the same type of stone may exhibit different material properties due to the variations in workmanship, the material source, the mortar thickness, and the loads they are subjected to. Therefore, these structural members must be parameterized individually.

4. This study shows that for linear elastic FE models of historic masonry monuments, linear springs can be implemented with success to represent semiflexible connections in masonry structures. Although this study illustrated only the application of translational springs, the same concept can be applied to rotational restraints with equal success using rotational springs.

5. Assuming symmetrical geometry for the structure is found to yield acceptable results. However, when the requirements on the model accuracy are higher, irregularities that may be present in the structure may be implemented in the FE model to incorporate the unsymmetrical behavior. Relaxing this assumption by assigning a separate parameter for each spring may ultimately yield improved agreement between the FE model and physical evidence.

6. In literature, the most commonly employed comparatives are modal parameters such as frequencies and mode shapes. In this study, modal parameters are

observed to yield satisfactory results when applied to historic unreinforced masonry buildings.

7. When modal parameters are selected as comparative features, attention must be paid to distinguish the global modes from the local modes. Typically, local modes have lower amplitudes and are dominated by the global modes in the frequency response functions (FRFs).

8. When modal parameters are selected for the comparative features, attention must be paid to the spatial aliasing. Number of modes that can be identified are related to the number and placement of measurement points. After the point when the higher-order modes are observed to alias the lower-order modes, the mode shape vectors should not be implemented in test-analysis correlation.

9. Determining the experimental uncertainty invariably requires repeated experiments. When the available time or resources do not allow the replication of the entire test campaign, a portion of the test can be replicated to assess the experimental uncertainty. In cases when this option is not available, the experimental uncertainty can be derived from the coherence functions.

10. The spring boundary conditions typically present an asymptotic behavior at very low and very high values. By investigating this asymptotic response separately for spring stiffness constant, the lower and upper bounds within which the linear spring provides a semiflexible boundary condition can be obtained.

11. In literature, attempts were made to uncouple the calibration of material properties and boundary conditions. In these studies, after the boundary conditions are calibrated according to the mode shapes, the material properties are tuned according to the natural frequencies. However, during the present research, it is observed that such an approach is not suitable. Changes in the relative ratios of the properties of different materials can easily alter the mode shapes. It is suggested that all the calibration parameters are compiled together and the effect screening analysis and stochastic calibration studies are conducted while operating on all of the calibration parameters simultaneously.

12. Model calibration is a decision-based process, and regardless of how sophisticated its algorithms are, its success strictly relies on the quality of the decisions made during the process. For instance, analysis of variance yields the relative effects of the calibration parameters on the selected response feature, however, it is up to the analyst to decide whether to include or exclude an input parameter. Therefore, these tools can only be considered as aids in the decision making process.

13. Replacing the computationally expensive FE model with a fast running surrogate significantly reduces the demands on the resources, in the case of the National Cathedral FE models, this reduction was 10 times. Therefore, surrogate models enable one to explore the calibration parameter domain

with high resolution, in the case of the National Cathedral, 128 computer runs were performed using the surrogate model.

14. When modal parameters are used as comparative features during test-analysis correlation, three main problems are faced. As the FE model input parameters are varied, the modes may disappear/reappear, modes may swap order, or modes may become linear combinations of each other. A careful tracking of modes is a crucial task during the training of the surrogate model. If the surrogate model is trained without taking these factors into account, the calibration results would have no meaning.

15. Typically, automated calibration studies rely on the assumption that the calibration parameters are independent and uncorrelated. However, certain modeling parameters may have correlations and dependencies that may not be obvious at the inception of the study. It is suggested that the bi-variate posterior distributions be calculated to confirm this *a priori* assumption.

16. The proposed method is observed to yield satisfactory results for up to five calibration parameters. Generally, it is advisable to keep the number of calibration parameters low. The Phenomenon Identification and Ranking Table is an effective means of reducing the size of the parameter space for analysis.

17. It is observed, through the calibration exercises conducted in the present research, that defining uninformative prior distributions for the calibration parameters is an acceptable approach.

18. The posterior distributions obtained in this study show that the piers are stiffer than the ribs and the webbing, even though they all are built out of the same material. This can be explained by the fact that piers being under compression are not expected to crack, while the webbing and ribs may develop cracks which would ultimately yield severe stiffness reductions.

19. The published values for limestone in pertinent literature are found to be high, and it is an endorsement of this procedure that it brought them down to sensible levels. The posterior distributions obtained for the Young's modulus of the stone fell into the lower end of the initially defined ranges indicating that a lower initial choice of E would be more appropriate.

20. Repeating the calibration exercise with an increasing number of experiments allows one to monitor the stability of the calibration exercise. As new experimental information becomes available, the mean values should converge to a stable value. Also, additional experimental information should consistently reduce the uncertainty in the calibration parameters.

21. The model obtained with calibrated parameter values is conditioned to the physical evidence; therefore, the same physical evidence cannot be used to validate this calibrated FE model. The replacement of the nonmodeled parts of the structure to verify the spring constant shows the effectiveness of this procedure and highlights the difficulty in determining parameters for an element, such as the pier, without implementing a calibration scheme.

5.3 Remaining Technical Issues

This study uncovered several issues that have yet to be addressed. The most important of these issues are summarized in this section.

Although defining linear springs can be considered suitable for static analysis, where dynamic analysis is concerned, dynamic impedance must be considered. In other words, the stiffness of the linear springs (substituting for the remainder of the structure) should be variable, based on the frequency of vibration. This would, however, increase the number of calibration parameters and require larger amounts of experimental data to be collected.

During the tests on Washington National Cathedral, the practical limitations of the equipment mandated the acceleration measurements be limited to the vertical axis. Future applications of modal testing on vaults should not limit the measurements to a single axis, but instead explore the horizontal movements of the vaults in the transverse direction.

In this study, effect screening is performed considering the modal parameters, specifically the natural frequencies. An FE model input parameter, which is not influential on modal parameters, is assumed to also be ineffective on other response features; however, this assumption is not validated in this study. In practical applications effect screening should be completed considering all of the possible output solutions of the FE model.

If effect screening depicts some parameters as having negligible importance on the modal parameters, it means that natural frequencies and mode shapes do not contain sufficient information to infer the values of these parameters. If refined information is specifically needed for one or more of these insensitive parameters, alternative comparative features can be sought. Alternative comparative features in linear dynamics are FRF amplitudes, Root Mean Square response, statistical moments, etc. A list of these alternative comparative features that can be extracted from raw time domain acceleration measurements is provided in Section 3. Also, it is possible to combine different types of features during calibration—such as displacement and mode shape vector. Having a larger variety of comparative features would enable one to update a larger variety of parameters.

To validate and quantify the accuracy of an FE model, an independent set of experimentally derived information other than that used in the calibration is necessary. This step is critical to the validation of the calibrated FE solutions (Trucano et al. 2006). Insistence on such a validation experiment increases the already high demands on resources; however, it is important to distinguish between a calibrated model and a validated model. In this study, in the absence of additional information against which the calibrated FE solutions can be validated, a procedure using existing data is determined to increase the credibility of the results. The unmodeled portions of the Cathedral are separately modeled to investigate the elastic restraints that the remaining structure would impose on the vaults. This enabled a simple validation of the calibrated spring constant values. Therefore, this study is not in a position to state a validated FE model for the calibrated models.

5.4 Recommendations for Future Work

Most masonry structures exhibit very complex inelastic and nonlinear dynamic behavior, which makes the experimentation and comparative feature selection very difficult. Features with strong linearity assumptions, such as those derived in linear dynamics, tend to smear the effects of inelastic nonlinear behavior, degrading the quality of the calibration studies. Features that are not deeply rooted in strong linearity assumptions, unlike modal parameters, FRF, and their derivatives, warrant particular attention for future research.

Subcomponent testing, commonly implemented in mechanical and nuclear engineering applications, is another avenue for authentic contribution. Subcomponent testing evaluates components individually (such as piers or walls) and later integrates the results into the global structure model. Subcomponent testing can also supply information about local phenomena that may not have a strong effect on the global response of the structure. It must be noted that calibrating a model with global response measurements of the structure can only be used for phenomena that have a substantial influence on the global behavior of the structure.

Obviously, the credibility of a calibrated model is increased as the amounts of experimental information accurately reproduced by the calibrated model increases. Pertinent literature does not discuss how the decision about the completion of calibration is reached. There is a need to develop a measure of sufficiency for experimental information and an indicator of completion for the calibration exercise. For this purpose, a stability criterion is discussed in Section 4.7. This stability criterion monitors the calibrated parameters' mean and standard deviation statistics as the amount of experimental information used in calibration is consistently increased. If the mean values are relatively stable and if the standard deviation is consistently reduced, it can be considered as a sign of stable calibration. However, if the mean values are fluctuating as new experimental information becomes available, then one would have little confidence in the calibration exercise.

The tasks for stochastic model calibration discussed in this study require extensive resources and expertise and are therefore not currently practical as routine. However, the stochastic approach is a first necessary step to bring calibration of analytical models into the engineering mainstream. This procedure is in need of being demystified for practicing engineers. With the ever-increasing popularity of FE model calibration and its byproducts, structural health monitoring and damage detection, the field of civil engineering will soon be able to use this proposed method on a diverse group of structures.

5.5 Concluding Remarks

Although the demand to assess historic unreinforced masonry buildings has been consistently increasing, structural analysis guidelines consistent with the principles of

unreinforced masonry systems are still unavailable in literature. As engineers involved in maintenance, rehabilitation, and strengthening campaigns for historic structures seek to use FE model predictions for more and more ambitious applications, the probabilistic-based calibration methods to these structures will gain importance. This research program proposed an approach to obtain calibrated FE models for civil engineering systems.

The testing of an existing building yields very useful information about the characteristics per se. However, only by integrating these experimental measurements with computerized FE tools is it possible to gain a thorough understanding of the structural behavior of the building. Although experimental measurements are always incomplete in the sense of their spatial resolution, they play an instrumental role in model calibration. This ultimately yields mathematical representation of the structural behavior in a much finer spatial resolution. The proposed integrated analytical and experimental procedure makes use of the techniques of FE analysis and experimental modal analysis. The concept of model calibration should not be considered as a mere tuning of the variables of the model but instead as an attempt to genuinely improve the predictive ability of the analytical model through comparison with the experimental measurements. Model validation ultimately offers tools through which engineers can defend the credibility of computer models and their model-based decisions.

Although the immediate benefits of model calibration are not as obvious in civil engineering as they are in fields where prototyping and mass production are common, the determination of the modeling strategies learned through model calibration can ultimately serve the civil engineering community with an improved understanding of computer modeling. Calibrated FE models can help engineers to better understand the behavior of historic monuments and ultimately pursue successful repair and retrofit schemes.

Acknowledgments

Bibliography

Allemang, R. J. and Brown, D. L. 1982, "Correlation Coefficient for Modal Vector Analysis," *Proceedings of 1st International Modal Analysis Conference*, Orlando, Florida, USA, pp. 110–116.

ANSYS, Inc. 2009, ANSYS v. 11.0, *Structural Guides*.

Antonacci, E., Sortis, A. D., and Vestroni, F. 2000, "Dynamic Identification of Masonry Buildings by Forced Vibration Tests," *Proceedings of International Conference on Noise and Vibration Engineering*, Leuven, Belgium, pp. 1691–1698.

Antonacci, E. 2001, "Retrofitting Effects on the Dynamic Behaviour of Basilica S. Maria Di Collemaggio," *Computational Methods and Experimental Measurements*, Vol. 10, pp. 479–488.

Aoki, T., Sabia, D., Rivella, D., and Muto, H. 2005, "Dynamic Identification and Model Updating of the Howa Brick Chimney, Tokoname, Japan," *Structural Studies, Repairs, and Maintenance of Heritage Architecture*, IX, Vol. 83, pp. 265–275.

Arêdê, A., Almeida, C., Costa, A., Rodrigues, J., and Costa, A. C. 2001, "Dynamic Identification and Seismic Analysis of the 'Serra Do Pillar' Monastery Church," *Proceedings of SPIE*, Vol. 4753, No. 2, pp. 1237–1243.

Armstrong, D. M., Sibbald, A., Fairfield, C. A., and Forde, M. C. 1995a, "Modal Analysis for Masonry Arch Bridge Spandrel Wall Separation Identification," *NDT&E International*, Vol. 28, No. 6, pp. 377–386.

Armstrong, D. M., Sibbald, A., and Forde, M. C. 1995b, "Integrity Assessment of Masonry Arch Bridges Using the Dynamic Stiffness Technique," *NDT&E International*, Vol. 28, No. 6, pp. 367–375.

Atamturktur, S. 2006, "Structural Assessment of Guastavino Domes," M.S. Thesis, The Pennsylvania State University, PA, May 2006.

Atamturktur, S. 2009, "Validation and Verification Under Uncertainty Applied to Finite Element Models of Historic Masonry Monuments," *Proceedings of 27th Society of Experimental Mechanics (SEM) International Modal Analysis Conference (IMAC-XXVII),* Orlando, Florida, USA.

Atamturktur, S. and Boothby, T. 2007, "Finite Element Modeling of Guastavino Domes," *Bulletin of Association for Preservation Technology*, Vol. 28, No. 4, pp. 21–29.

Atamturktur, S., Fanning, P., and Boothby, T. 2007, "Traditional and Operational Modal Testing of the Washington National Cathedral," *Proceedings of the International Operational Modal Analysis Conference*, Copenhagen, Denmark.

Atamturktur, S., Pavic, A., and Reynolds, P. 2008, "Sensitivity of Modal Parameters of Historic Monuments to Geometric Distortion," *Proceedings of 26th International Modal Analysis Conference*, Orlando, Florida, USA.

Atamturktur, S., Pavic, A., Reynolds, P., and Boothby, T. 2009a, "Full-Scale Modal Testing of Vaulted Gothic Churches: Lessons Learned," *Journal of Experimental Techniques*.

Atamturktur, S., Bornn, L., and Hemez, F. 2009b, "Damage Detection in Masonry Vaults by Time-Domain Vibration Measurements," to appear in the *Journal of Engineering Structures*.

Avitabile, P., O'Callahan, L., and Milani, J. 1989, "Comparison of System Characteristics Using Various Model Reduction Techniques," *7th International Modal Analysis Conference*, Las Vegas, Nevada, pp. 1109–1115.

Avitabile, P., Pechinsky, F., and O'Callahan, L. 1992, "Study of Vector Correlation Using Various Techniques for Model Reduction," *10thInternational Modal Analysis Conference*, San Diego, California, pp. 572–583.

Avitabile, P. 2001, "Experimental Modal Analysis," *Sound and Vibration*, January 2001.

Bagchi, A. 2005, "Updating the Mathematical Model of a Structure Using Vibration Data," *Journal of Vibration and Control*, Vol. 11, No. 12, pp. 1469–1486.

Bathe, K. J. and Wilson, E. L. 1972, "Solution Methods for Eigenvalue Problems in Structural Mechanics," *International Journal of Numerical Methods in Engineering*, Vol. 6, pp. 213-–226.

Bathe, K. J. 1982, *Finite Element Procedures in Engineering Analysis*, City Prentice-Hall, Inc., NJ.

Bayraktar, A., Altunışık, A. C., Sevim, B., Türker, T., Akköse, M., and Coşkun, N. 2008, "Modal Analysis, Experimental Validation and Calibration of a Historical Masonry Minaret," *Journal of Testing and Evaluation*, Vol.36, No.6, pp. 516–524.

Bensalem, A., Fairfield, C. A., and Sibbald, A. 1995, "NDT for Condition Based Maintenance of Arch Bridges," *Proc. 8th Int. Conf. Condition Monitoring*, 2, Kingston, Canada 1995, pp. 503–509.

Bensalem, A., Fairfield, C. A., and Sibbald, A. 1997, "Non-destructive Evaluation of the Dynamic Response of a Brickwork Arch," *Proceedings of the Institution of Civil Engineers, Structures, and Buildings,* Vol. 122, No. 1, pp. 69–82.

Bensalem, A., Ali-Ahmed, H., Fairfield, C. A., and Sibbald, A. 1999, "Non-destructive Testing to Detect Voids Hidden Behind the Extrados of an Arch Bridge," *NDT and E International*, Vol. 32, No. 6, pp. 343–353.

Biemiller, L. 2006, "Catocton Creek Aqueduct Restoration," *Society for Industrial Archeology*, Vol. 35, No. 2, pp. 8–9.

Binda, L. and Saisi, A. 2002, "State of the Art of Research on Historic Structures in Italy," *Proceedings of 11th Advanced Research Initiation Assisting and Developing Networks in Europe (ARIADNE) Workshop*, May 20–26, 2002.

Bishop, R. and Gladwell, G. 1963, "An Investigation Into the Theory of Resonance Testing," *Philosophycal Transactions of the Royal Society of London*. Vol. 255A, No. 1055, pp. 241–280.

Boothby, T. E., Yurianto, Y., and Erdogmus, E. 2005, "Experimental Replication of Masonry Arch Spandrel Wall Collapse," *The Masonry Society Journal*, Vol. 23, No. 1, pp. 37–46.

Boothby, T. and Atamturktur, S. 2007, "A Guide for the Finite Element Analysis of Historic Load Bearing Masonry Structures," *Proceedings of 10th North American Masonry Conference*, St. Louis, Missouri, USA.

Brencich, A. and Sabia, D. 2008, "Experimental Identification of a Multi-Span Masonry Bridge: The Tanaro Bridge," *Construction and Building Materials*, Vol. 22, No. 10, pp. 2087–2099.

Brown, D., Allemang, R., Zimmerman, R., and Mergeay, M. 1979, "Parameter Estimation Techniques for Modal Analysis," *SAE Paper*, *Automotive Engineering*, Vol. 790221, pp. 828–846.

Brownjohn, J. M. W. and Xia, P. Q. 2000, "Dynamic Assessment of Curved Cable-Stayed Bridge by Model Updating," *Journal of Structural Engineering*, Vol. 126, No. 2, pp. 252–260.

Bruel and Kjaer, 1982, "Measuring Vibration," Technical notes (http://www.bksv.com).

Coleman, H. W. and Steele, W. G., Jr. 1999, *Experimentation and Uncertainty Analysis for Engineers*, 2nd Edition, John Wiley & Sons, Inc., New York.

Cook, R. D., Malkus, D. S., Plesha, M. E., and Witt, R. J. 2002, *Concepts and Applications of Finite Element Analysis*, 4th Edition, Wiley, NY.

Creazza, G., Saetta, A. V., and Matteazi, R. 2001, "Analysis of Masonry Structures Reinforced by FRP," *Historical Constructions,* Guimarães, pp. 539–546.

Creazza, G., Matteazzi, R., Saetta, A., and Vitaliani, R. 2002, "Analyses of Masonry Vaults: A Macro Approach Based on Three-Dimensional Damage Model," *Journal of Structural Engineering*, Vol. 128, No. 5, pp. 646–654.

Cukier, R. I., Levine, H. B., and Schuler, K. E. 1978, "Nonlinear Sensitivity Analysis of Multiparameter Model Systems," *Journal of Computational Physics*, Vol. 26, pp. 1–42.

Dascotte, E. 2004, "Linking FEA with Test," *Journal of Sound and Vibration*, Vol. 20, pp. 12–16.

De Stefano, 2007, "Structural Identification and Health Monitoring on the Historical Architectural Heritage," *Key Engineering Materials*, Vol. 347, pp. 37–54.

Denoyer, K. K. and Peterson, L. D. 1996, "Structural Model Update Using Dynamically Measured Static Flexibility Matrices," Centre for Aerospace Studies report CU-CAS-96-27, College of Engineering, University of Colorado, Boulder, CO.

Ellis, B. R. 1998, "Nondestructive Dynamic Testing of Stone Pinnacles of the Palace of Westminster," *Proceedings of the Institution of Civil Engineers*, Structures and Buildings, UK.

Erdogmus, E. 2004, "Structural Appraisal of the Florentine Gothic Construction System," Ph.D. Thesis, The Pennsylvania State University, PA.

Erdogmus, E. 2008, "Timbrel Domes of Guastavino Construction: Non-destructive Assessments on a Half Scale Model," *International Journal of Architectural Heritage*, Vol. 2, No. 4, pp. 330–352.

Ewins, D. J. 2000, "Basics and State-of-the-Art Modal Testing," Sadhana Academy Proceedings in Engineering Sciences, Vol. 25, No. 3, pp. 207–220.

Fanning, P. and Boothby, T. 2001, "Three Dimensional Modeling and Full-scale Testing of Stone Arch Bridges," *Computers and Structures*, Vol. 79, pp. 2645–2662.

Fanning, P. J., Szobak, L., Boothby, T. E., and Salamoni, V. 2005, "Load Testing and Model Simulations for a Stone Arch Bridge," *Bridge Structures*, Vol. 1, No. 4, pp. 367–378.

Farrar, C. R., Worden, K., Todd, M. D., Park, G., Nichols, J., Adams, D. E., Bement, M. T., and Farinholt, K. 2007, "Nonlinear System Identification for Damage Detection," Los Alamos National Laboratory report LA-14353.

FEMtools, User Manual 2007, Dynamic Design Solutions (DDS) NV.

Friswell, M. I. and Mottershead, J. E. 1995, *Finite Element Model Updating in Structural Dynamics*, Kluwer Academic Publishers, Dordrecht, The Netherlands.

Genovese, F. and Vestroni, F. 1998, "Identification of Dynamic Characteristics of a Masonry Building," *Proceedings of the 11th European Conference on Earthquake Engineering*, Paris la Défense, France.

Gentile, C. and Saisi, A. 2007, "Ambient Vibration Testing of Historic Masonry Tower for Structural Identification and Damage Assessment," *Construction and Building Materials*, Vol. 21, No. 6, pp. 1311–1321.

Guyan, R. J. 1965, "Reduction of Stiffness and Mass Matrices," *AIAA Journal*, Vol. 3, No. 2, pp. 380.

Hatch, M. R. 2000, *Vibration Simulation Using Matlab and Ansys*, Chapman & Hall/CRC, NY.

Hanagan, L. M., Raebel, C. H., and Trethewey, M. W. 2003, "Dynamic Measurements of In-Place Steel Floors to Assess Vibration Performance," *The Journal of Performance of Constructed Facilities*, Vol. 17, No. 3, pp. 126–135.

Helton, J. C., Garner, J. W., McCurley, R. D., and Rudeen, D. K. 1991, "Sensitivity Analysis Techniques and Results for the Performance Assessment at the Waste Isolation Pilot Plant," Sandia National Laboratories report SAND90-7103.

Hemez, F. M. 2007, "Lecture Notes: A Course on Verification and Validation of Computer Models," Los Alamos National Laboratory.

Heyman, J. 1966, "The Stone Skeleton," *International Journal of Solids and Structures*, 2nd Edition, pp. 249–279.

Heyman, J. 1995, *The Stone Skeleton*, Cambridge University Press, UK

Higdon, D., Gattiker, J., Williams, B., and Rightley, M. 2008, "Computer Model Calibration Using High-dimensional Output," *Journal of the American Statistical Association*, Vol. 103, No. 482, pp. 570–583.

Hills, R. G. 2006, "Model Validation: Model Parameter and Measurement Uncertainty," Journal of Heat Transfer, April 2006, Vol. 128, pp. 339–351.

Hogg, R. V. and Craig, A. T. 1978, *Introduction to Mathematical Statistics*, Macmillan.

Ibrahim, S. 1977, "Modal Confidence Factor in Vibration Testing," *The Shock and Vibration Bulletin*, Vol. 48, No. 1, pp. 65–75.

Jaishi, B., Ren, W. X, Zong, Z. H., and Maskey, P. N. 2003, "Dynamic and Seismic Performance of Old Multi-Tiered Temples in Nepal," *Engineering Structures*, Vol. 25, pp.1827–1839.

Juang, J. N. and Pappa, R. S. 1985, "An Eigensystem Realization Algorithm for Modal Parameter Identification and Model Reduction," *Journal of Guidance, Control, and Dynamics*, Vol. 8, No. 5, pp. 620–627.

Juang, J. N. and Pappa, R. S. 1986, "Effects of Noise on Modal Parameters Identified by the Eignsystem Realization Algorithm," *Journal of Guidance, Control, and Dynamics*, Vol. 9, No. 3, pp. 294–303.

Juang, J. N. and Suzuki, H. 1988, "An Eigensystem Realization Algorithm in Frequency Domain," *ASME Transactions on Vibrations, Acoustics, and Stress*, Vol. 110, No. 24, pp. 24–29.

Júlio, E., Rebelo, C., and Dias Da Costa, D. 2008, "Structural Diagnosis of the Tower of the University of Coimbra by Modal Identification," *Engineering Structures*, Vol. 30, No. 12, pp. 3468–3477.

Kennedy, C. C. and Pancu, C. D. 1947, "Use of Vectors in Vibration Measurement and Analysis," *Journal of Aeronautical Sciences*, Vol. 14, No. 11, pp. 603–625.

Kennedy, M. and O'Hagan, A. 2000, "Predicting the Output from a Complex Computer Code When Fast Approximations are Available," *Biometrika*, Vol. 87, pp. 1–13.

Lanczos, C. 1950, "An Iteration Method for the Solution of the Eigenvalue Problem of Linear Differential and Integral Operators," *Journal of Research of the National Bureau of Standards*, Vol. 45, pp. 255–282.

Li, S., Brown, D. L., and Vold, H. 1994, "A Scaled Total Least Squares Method for Modal Parameter Testing Using the Unified Matrix Polynomial Approach," *Proceedings of the 12th International Modal Analysis Conference*, Honolulu, Hawaii, USA.

Ljung, L. 1999, *System Identification: Theory for the User*, 2nd Edition, Prentice Hall, Englewood.

Mace, B. R., Worden, K., and Mansom, G. 2005, "Uncertainty in Structural Dynamics," *Journal of Sound and Vibration*, Vol. 288, No. 3, pp. 423–429.

Maia, N. and Silva, J. 1997, "Theoretical and Experimental Modal Analysis," RSP, NY.

Mark, R. 1982, *Experiments in Gothic Structure*, The MIT Press, London, pp. 102–117.

Mark, R. 1984, *Architectural Technology up to the Science Revolution: The Art and Structure of Large-Scale Buildings*, The MIT Press, London.

Mark, R. and Hutchinson, P. 1986, "On the Structure of Roman Pantheon," *The Art Bulletin*, Vol. 68, No. 1, pp. 24–34.

Mergeay, M. 1983, "Least Squares Complex Exponential Method and Global System Parameter," *Proceedings of the 8th International Seminar on Modal Analysis*, Leuven, Belgium.

McConnel, 2008, *Vibration Testing*, John Wiley and Sons, Inc., New York.

Montgomery, D. G. 1997, *Design and Analysis of Experiments*, 2nd edition, John Wiley and Sons, Inc., New York.

Montgomery, D. G. 2000, *Design and Analysis of Experiments*, 3rd edition, John Wiley and Sons, Inc., New York.

Myers, H. M. and Montgomery, D. C. 2002, "Response Surface Methodology," 2nd Edition, Wiley Series in Probability and Statistics, John Wiley and Sons, Inc., New York.

National Research Council, Commission on Engineering and Technical Systems (CETS) Committee on Conservation of Historic Stone Buildings and Monuments, National Materials Advisory Board, 1982, *Conservation of Historic Stone Buildings and Monuments*.

Oberkampf, W. L., Trucano, T. G., and Hirsch, C. 2002, "Verification, Validation, and Predictive Capability in Computational Engineering and Physics," *Foundations for Verification and Validation in the 21st Century Workshop*, John Hopkins University, Laurel, Maryland, USA.

O'Callahan, J., Avitabile, P., and Riemer, R. 1989, "System Equivalent Reduction Expansion Process," *7th International Modal Analysis Conference*, Las Vegas, Nevada, 1109–1115.

Pavic, A., Reynolds, P., and Waldron, P. 2002, "Modal Testing and FE Model Correlation of a Long-Span Prestressed Concrete Floor," *Journal of Structures & Buildings*, Vol. 152, No. 2, pp. 97–109.

Pavic, A., Miskovic, Z., and Reynolds, P. 2007, "Modal Testing and Finite-Element Model Updating of a Lively Open-Plan Composite Building Floor," *Journal of Structural Engineering*, Vol. 133, No. 4, pp. 550–558.

Parker, J. 2009, Lecture Notes, University of Alabama, (http://www.me.ua.edu/me360/PDF/Wilcoxon_Research_Vibration_Notes.pdf.)

Pendered, W. 1965, "Theoretical Investigation Into the Effects of Close Natural Frequencies in Resonance Testing," *Journal of Mechanical Engineering Science*, Vol. 7, No. 4, pp. 372–379.

Pilch, M., Trucano, T., Peercy, D., Hodges, A., Young, E., and Moya, J. 2001, "Guidelines for Sandia ASCI Verification and Validation Plans – Content and Format: Version 2.0," Sandia National Laboratory report SAND2000-3101.

Rabits, H. 1989, "System Analysis at Molecular Scale," *Science*, Vol. 246, pp. 221–226.

Ramos, L. F., Lourenço, P. B., and Costa, A. C. 2005, "Operational Modal Analysis for Damage Detection of a Masonry Construction," *Proceedings of the 1st Int. Operational Modal Analysis Conference*, Copenhagen, Denmark, pp. 495–502.

Ramos, L. F. 2007, "Damage Identification on Masonry Structures Based on Vibration Signatures," Ph.D. Thesis, University of Minho.

Ricart-Nouel, A. 1991, "Structural Repair and Maintenance of Historical Buildings II," *Proceedings of the Second International Conference,* Seville, Spain, pp. 37–52.

Roache, P.J. 1998, *Verification and Validation in Computational Science and Engineering*, Hermosa Publishers, New Mexico.

Saltelli, A., Chan, K., and Scott, E. M. 2004, *Sensitivity Analysis*, Wiley Series in Probability and Statistics, John Wiley and Sons, Inc., New York.

Sansalone, M. 1997, "Impact-Echo: The Complete Story," *ACI Structural Journal*, Vol. 94, No. 6, pp. 777–786.

Santner, J. T., Williams, B., and Notz, W. I. 2003, *The Design and Analysis of Computer Experiments*, Springer Series in Statistics, Springer, New York.

Sigmund, V. A. and Herman, K. 1998, "Dynamic Characteristics as Indicators of Structural Integrity," *Proceedings of the Conference on Saving Buildings in Central and Eastern Europe*.

Silva, C. 2009, *Vibration Monitoring, Testing, and Instrumentation*, CRC Press, New York.

Slastan, J. A. and Foissnerr, P. 1995, "Masonry Building Dynamic Characteristics Evaluation by Means of Ambient Vibration," *Proceedings of the 10th European Conference on Earthquake Engineerin*g, Vienna, Austria.

Sortis, A. D., Antonacci, E., and Vestroni, F. 2005, "Dynamic Identification of a Masonry Building Using Forced Vibration Tests," *Engineering Structures*, Vol. 27, pp. 155–165.

Steenackers, G. and Guillaume, P. 2006, "Finite Element Model Updating Taking into Account the Uncertainty on the Modal Parameters Estimates," *Journal of Sound and Vibration*, Vol. 296, No. 4–5, pp. 919–934.

Theodossopoulos, D., Sinha, B. P., and Usmani, A. S. 2003, "Case Study of the Failure of a Cross Vault: Church of Holyrood Abbey," *Journal of Architectural Engineering*, Vol. 9, No. 3, pp. 119–127.

Trucano, T. G., Swiler, L. P., Igusa, T., Oberkamp, W. L., and Pilch, M. 2006, "Calibration, Validation, and Sensitivity Analysis: What's What," *Reliability Engineering and System Safety*, Vol. 91, pp. 1331–1357.

Turek, M., Ventura, C. E., and Placencia, P. 2002, "Dynamic Characteristics of a 17th Century Church in Quito," *Proceedings of the International Society of Optical Engineering*, Vol. 4753, No. 2, pp. 1259–1264.

Verboven, P. 2002, "Frequency Domain System Identification for Modal Analysis," Ph.D. Thesis, Vrije Universiteit Brussel.

Vestroni, F., Beolchini, G. C., Antonacci, E., and Modena, C. 1996, "Identification of Dynamic Characteristics of Masonry Buildings from Forced Vibration Tests," *Proceedings of the 11th World Conference on Earthquake Engineering*, Acapulco, México.

Washington National Cathedral, 2004, *Washington National Cathedral Guide Book*, Washington, DC.

Williams, B. 2008a, Phone conversation with Brian Williams from Los Alamos National Laboratory.

Williams, B. 2008b, Email exchange with Brian Williams from Los Alamos National Laboratory.

Wilson, G. E. and Boyack, B. E. 1998, "The Role of the PIRT Process in Experiments, Code Development, and Code Applications Associated with Reactor Safety Analysis," *Nuclear Engineering and Design*, Vol. 186, pp. 23–37.

Zembaty, Z. and Kowalski, M. 2000, "Dynamic Identification of a Brick Masonry Building," *Archives of Civil Engineering*, Vol. 46, No. 1, pp. 106–136.

Zienkiewicz, O. C. 1977, *The Finite Element Method*, McGraw-Hill, New York.

Zonta, D. 2000, "Structural Damage Detection and Localization by Using Vibrational Measurements," Ph.D. Thesis, University of Bologna, Italy.